SIMULATION OF A

MICRO HEAT PUMP CYCLE

Martin van Eldik, B ENG.

Dissertation submitted in partial fulfilment of the degree

Master of Engineering

in the

School of Mechanical and Materials Engineering,

Faculty of Engineering

at the

Potchefstroom University for Christian Higher Education

Promoter: Prof. P.G. Rousseau

POTCHEFSTROOM

1998

ACKNOWLEDGEMENTS

Philippians 4:13, "I can do all things through Christ which strengtheneth me."

I would like to thank Prof. P.G. Rousseau for his excellent guidance and advice. Thank you for the enthusiasm and interest shown during the two years of my study. I will never forget it.

Thank you to Pieter Coetzer, who was responsible for building the micro heat pump. We spent long hours obtaining valid experimental results, but it was worth it.

Thank you to Robbie Arrow for all his assistance and advice during the experimental phase of this dissertation and for always making time to help.

Thank you to my parents for the opportunity they gave me to study; for trusting me and believing in me.

Last but the most important, my wife Elize, for her love, support and patience during the past two years and for always being there for me.

ABSTRACT

Title	:	Simulation of a micro heat pump cycle.
Author	:	Martin van Eldik
Promoter	:	Prof. P.G. Rousseau
School	:	Mechanical and Materials Engineering
Degree	:	Master of Engineering

The purpose of this study was to develop a thermal cycle simulation for a micro heat pump. A feature of the simulation is that it can simulate the four basic components in detail, based on fundamental principles. The product of this study is a simulation routine which can be used as a design tool for micro heat pumps as well as its individual components. Experimental tests were conducted on an existing R-134a micro heat pump and the results were successfully used to verify the simulation routines. An extensive literature survey was conducted on heat pump component models as well as heat transfer correlations.

In this study models were developed for each of the four basic components used in the micro heat pump, i.e. fluted tube water heating condenser, air-cooled evaporator, reciprocating compressor and capillary tube. The theory on which each model is based, was derived from first principles and the relevant model algorithms were developed and implemented in C++ computer routines. The component models were also integrated to allow a complete cycle simulation at different operating conditions.

An advantage of the fluted tube condenser model is that it allows the surface area to be divided into any number of sections over which the change in refrigerant and water properties can be evaluated. The evaporator model calculates the change in refrigerant properties along the length of each tube in the coil. It can also predict in detail the state of the air across the coil face and along the depth of the coil. A model for simulating the compressor was derived which solves for both the mass flow rate and the refrigerant outlet conditions. Two capillary tube models were implemented. The first was based on a theoretical model obtained in the literature. This model did not provide sufficiently accurate results, however the second capillary tube model was based on a dimensional analysis providing a non-dimensional correlation for the mass flow rate. The coefficients of the correlation had to be modified for this application. The individual component models as well as the integrated cycle were both verified by means of the experimental data.

The verification study showed that for the integrated cycle the condenser and evaporator heat transfer rates were predicted with average accuracies of 97% and 96% respectively. The refrigerant mass flow rates predicted by the compressor and the capillary tube models resulted in an average accuracy of 95%.

The high degree of accuracy obtained with the individual models as well as with the integrated cycle provides confidence in the simulation results. The simulation can therefore be applied as a design tool for micro heat pumps and its individual components.

OPSOMMING

Titel	:	Simulasie van 'n mikro hittepomp siklus.
Outeur	:	Martin van Eldik
Promotor	:	Prof. P.G. Rousseau
Skool	:	Meganiese en Materiaal Ingenieurswese
Graad	:	Meestersgraad in Ingenieurswese

Die doel van hierdie studie was die ontwikkeling van 'n termiese siklussimulasie vir 'n mikrohittepomp. 'n Kenmerk van die simulasie is dat dit die vier basiese komponente in detail kan simuleer, gebaseer op fundamentele beginsels. Die produk van hierdie studie is 'n simulasieroetine wat as 'n ontwerphulpmiddel vir mikrohittepompe asook individuele komponente gebruik kan word. Eksperimentele toetse is gedoen op 'n bestaande R-134a mikrohittepomp en die resultate is suksesvol gebruik om die simulasieroetine te verifieer. 'n Uitgebreide literatuurstudie is onderneem in verband met hittepompkomponentmodelle asook hitte-oordragkorrelasies.

Gedurende hierdie studie is modelle ontwikkel vir elk van die vier basiese komponente wat gebruik is in die mikrohittepomp. Die komponente is 'n gedraaide buiskondensator, lugverkoelingsverdamper, resiprokerende kompressor en 'n kapillêre buis. Die teorie waarop elke model gebaseer is, is afgelei vanuit eerste beginsels en die relevante modelalgoritmes is ontwikkel en geïmplementeer in C++ rekenaarroetines. Die komponentmodelle is geïntegreer in 'n siklussimulasie .

'n Voordeel van die gedraaide buis kondensatormodel is dat die oppervlakarea in enige aantal seksies verdeel kan word, en die verandering in koelmiddel- en watereienskappe geëvalueer kan word. Die verdampermodel bepaal die verandering in koelmiddeleienskappe langs die lengte van elke buis af in die klos. Die model kan ook die verandering in lugtoestande oor die sigarea en die diepte van die klos voorspel. 'n Model om die kompressor te simuleer, is afgelei wat vir beide die massavloeitempo en die koelmiddel se uitlaattoestand oplos. Twee kapillêre buismodelle is geïmplementeer, met die eerste model gebaseer op 'n teoretiese model gevind in die literatuur. Hierdie model het egter nie voldoende akkurate resultate opgelewer nie. Die tweede kapillêre buismodel is gebaseer op 'n dimensionele analise wat 'n nie-dimensionele korrelasie vir die massavloeitempo lewer. Die koëffisiënte van die korrelasie moes egter

aangepas word vir die huidige toepassing. Die individuele komponentmodelle asook die geïntegreerde siklussimulasie is geverifieer met behulp van eksperimentele data.

Die verifikasiestudie het getoon dat vir die geïntegreerde siklus beide die kondensator en die verdamper die hitte-oordragtempo voorspel het met 'n gemiddelde akkuraatheid van 97% en 96% onderskeidelik. Die koelmiddelmassavloeitempo wat voorspel is deur die kompressormodel en die kapillêre buismodel toon 'n gemiddelde akkuraatheid van 95%.

Die graad van akkuraatheid verkry met die individuele modelle asook die geïntegreerde siklus verleen vertroue in die simulasieresultate. Die simulasie kan daarom geïmplementeer word as 'n ontwerphulpmiddel vir mikrohittepompe asook individuele komponente.

CONTRIBUTIONS OF THIS STUDY

- An extensive literature survey was conducted on existing component simulation models
- A micro heat pump simulation routine was developed, simulating the following components:
  - Fluted tube condenser.
  - Air-cooled evaporator.
  - Reciprocating compressor.
  - Capillary tube.
- The component models were derived from first principles, minimising the use of empirical data.
- The component models were successfully verified against experimentally generated data on a micro heat pump.

NOMENCLATURE

A	:	Inside surface area	m^2
b	:	Transform variable in dimensionless correlation	-
B	:	Coefficient in dimensionless capillary correlation	-
Bo	:	Boiling number	-
Co	:	Convection number	-
c_p	:	Specific heat	kJ/(kg.K)
d	:	Diameter	m
d_c	:	Capillary tube inside diameter	m
dT_{sub}	:	Degree of subcool	°C
dT_{sup}	:	Degree of superheat	°C
D'	:	Reference length	m
D_h	:	Hydraulic diameter	m
D_o	:	Inner diameter of outer jacket	m
D_{vi}	:	Volume-based inside diameter	m
D_{vo}	:	Volume-based outside diameter	m
e	:	Specific energy	kJ/kg
e	:	Flute depth	m
e^*	:	Non-dimensional flute depth	-
f	:	Internal friction factor	-
ff	:	Friction factor	-
fsc	:	Friction factor	-
F	:	Force	N
F	:	Factor in Shah's evaporation correlation	-
Fpi	:	Fins per inch	-
g	:	Acceleration due to gravity	m/s^2
G	:	Mass flux	$kg/(s.m^2)$
h	:	Enthalpy	J/kg
hc	:	Convection heat transfer coefficient	$W/(m^2.K)$
h_i	:	Inside heat transfer coefficient	$W/(m^2.K)$
h_o	:	Outside heat transfer coefficient	$W/(m^2.K)$
k	:	Boltzmann constant	J/K

k	:	Thermal conductivity	W/(m.K)
ΔL	:	Length increment	m
L	:	Length	m
m	:	Coefficient in dimensionless capillary correlation	-
$\dot{m}$	:	Mass flow rate	kg/s
m_f	:	Factor in determining fin efficiency	-
N	:	Factor in Shah's evaporation correlation	-
Ntu	:	Number of transfer units	-
Nu	:	Nusselt number	
Δp	:	Pressure drop	Pa
p	:	Pressure	Pa
p	:	Flute pitch	m
p^*	:	Non-dimensional flute pitch	-
pr	:	Reduced pressure	-
P	:	Pressure	Pa
Pr	:	Prandtl number	-
P_{sat}	:	Saturated pressure	Pa
q	:	Heat transfer	W
q_{max}	:	Maximum heat transfer	W
$\dot{Q}$	:	Heat transfer rate	W
r^*	:	Fluted tube annulus radius ratio	-
Rey	:	Reynolds number	-
s	:	Entropy	J/kg.K
t	:	Tube wall thickness	m
T	:	Temperature	K
T_{crit}	:	Absolute critical temperature	K
T_s	:	Absolute liquid temperature	K
u	:	Velocity component in the axial direction	m/s
U	:	Overall heat transfer coefficient	W/(m^{2}K)
V	:	Velocity	m/s
$\bar{V}$	:	Average velocity	m/s
$\vec{V}$	:	Velocity vector	m/s

Vc	:	Constant volume	m^3
Ve	:	Expansion volume	m^3
Vsu	:	Supply volume	m^3
Vsw	:	Sweep volume	m^3
Vol	:	Volume	m^3
W	:	Work	J
$\dot{W}$	:	Work rate	W
Wcp	:	Compressor work rate	W
Ws	:	Isentropic work rate	W
x	:	Quality	-
X	:	Transform variable in dimensionless correlation	-
y	:	Factor in determining friction factor	-
z	:	Elevation	m

SUBSCRIPTS

a	:	Air
c	:	Capillary tube
crit	:	Critical
e	:	Exit
ex	:	Exhaust, outlet
f	:	Fluid
f	:	Fin
g	:	Gas, vapour
i	:	Entrance
i	:	In
i	:	Inside
liq	:	Liquid
m	:	Average
max	:	Maximum
min	:	Minimum
o	:	Outside
r	:	Refrigerant
s	:	Surface
s	:	Isentropic
sc	:	Subcool
su	:	Supply
sub	:	Subcool
sup	:	Superheat
tot	:	Total
tp	:	Two-phase
tpc	:	Two-phase condenser
tpe	:	Two-phase evaporator
v	:	Vapour
w	:	Water
x	:	Quality

GREEK SYMBOLS

ε	:	Effectiveness	-
μ	:	Viscosity	kg/(s.m)
σ	:	Liquid surface tension	N/m
σ_A	:	Flow area ratio	-
Π	:	Buckingham Pi parameter	-
η	:	Effectiveness	-
η	:	Fin efficiency	-
ρ	:	Density	kg/m^3
θ	:	Helix angle	°
θ^*	:	Non-dimensional helix angle	-
ν	:	Specific volume	m^3/kg
Ψ	:	Two-phase heat transfer multiplier	-

TABLE OF CONTENTS PAGE

CHAPTER 1: INTRODUCTION

CHAPTER 2: LITERATURE SURVEY

CHAPTER 3: THEORETICAL BACKGROUND

CHAPTER 4: MODEL IMPLEMENTATION

CHAPTER 5: VERIFICATION

CHAPTER 6: CONCLUSION

APPENDICES

LIST OF FIGURES PAGE

LIST OF TABLES PAGE

CHAPTER 1

INTRODUCTION

CHAPTER 1
INTRODUCTION

'Earth is not a gift we inherited from our forefathers,
it is a place we're borrowing from our children.'

1.1 The problem and its setting

In a country such as South Africa with a population of more than forty million people, there is a huge demand for energy (1.12×10^{12} kWh in 1993). Due to the increasing energy demand each year, not only in South Africa but all over the world, the following three problems are facing us:

- The exhaustion of natural resources (coal, oil, etc.) in the near future.
- The wasteful use of our limited fresh water supply in power plants.
- Last, but not least the devastation of the earth by means of pollution and heat emission to the atmosphere.

Mankind must decide whether it wants to continue its destruction at the current pace, or start thinking about how a change could be brought about. Change does not come overnight, however, when starting on a small scale a global change could be reached. One of the areas which has an impact on all our lives and the total energy demand, is the heating of water in the industrial, commercial (Greyvenstein & Rousseau, 1998) and domestic sector. In the rest of this chapter only the domestic sector of water heating will be looked at, as it forms the focus point of this dissertation.

In the following sections the impact of domestic hot water use on the energy demand will be illustrated by looking at the problem from the viewpoint of the consumer as well as the supplier of electricity namely the Electricity Supply Commission (ESKOM).

1.1.1 Energy use of the domestic sector

A useful example to illustrate the impact of domestic water heating on the energy demand and the environment is given by Rousseau (1996:4). In order for ESKOM to deliver 100 kWh electricity to our homes, which will be used for 100 kWh heating, approximately 50 kg coal and 200 litres water are required. Also, 100 kg harmful CO_2 gas is released into the atmosphere. One way of reducing the problem is by using hot water more economically. This cannot always be achieved because people are not yet conscious of the problem and like to have hot water when required. Another way of overcoming the problem is by making the water heating process more effective. For example, if the same water heating could be achieved with only 80 kWh of electricity, the amount of coal required could be reduced to 40 kg and the water used to 160 litres. The CO_2 emission could also be reduced to 80 kg.

The above example clearly illustrates that engineers should pay attention to the design and implementation of technology for the effective use of energy.

Rousseau (1996:6) points out that electricity generation is responsible for 40.68% of the total primary energy use each year. As stated earlier, the total energy use for 1993 was 1.12×10^{12} kWh. Electricity use is further divided into the following sectors:

Trade & industry	52.45 %
Mining	25.85 %
Domestic	14.76 %
Transport	4.52 %
Agriculture	2.42 %

Table 1.1: Electrical energy use in South Africa

As can be seen from Table 1.1, 14.76 % of the electrical energy goes to the domestic sector, forming about 6 % of the total primary energy use of South Africa. Due to power station inefficiency, the end use energy is equal to 2.33×10^{10} kWh each year.

It must be noted that any electrical energy saving will have a significant impact on the total energy use of this country because of the ineffective process by means of which electricity is generated in steam turbines. Its effectiveness is only 35 %.

The effect of any saving in electricity use in the domestic sector could by multiplied by a factor of 2.89 (Rousseau, 1996:7) to obtain the effect on the total energy use in South Africa.

1.1.2 Domestic water heating

In the domestic sector the above-mentioned 2.33×10^{10} kWh can further be divided among approximately 2.3 million households, i.e. 9300 kWh each year per household. Figure 1.1 illustrates how this electricity is further divided for use in homes.

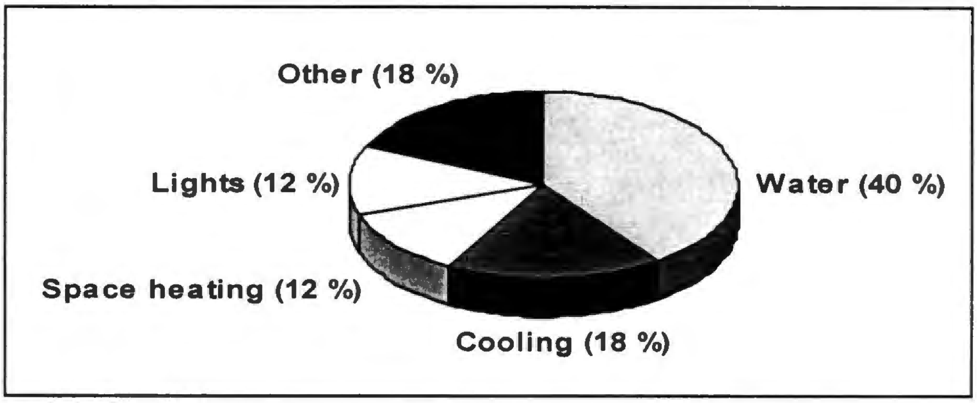

Figure 1.1: Electricity use in the domestic sector.

The distribution in Figure 1.1 is valid for high income and middle income homes. Rousseau (1996) states that for low income houses only 12 % of the electricity is used for heating water. Therefore the focus will only fall on high and middle income homes. The 40 % being used for the heating of water constitutes about 0.75 % of the total primary energy use of South Africa.

About 88 % of these households use direct electrical resistance water heaters, such as those used in hot water cylinders. This means that about 7.73×10^9 kWh of the electricity is used annually for water heating by means of direct resistance heaters. This is about 0.64% of the country's primary energy use each year. If 1 kWh costs 22 cents, the total cost for the consumer is about 1700 million rand each year, which amounts to R 740 per household. Because of the ineffective way electrical energy is generated, the impact on the total energy use of the country is 1.86 %.

A major contributor to the amount of electricity being used in the domestic sector is the peak electrical demand which occurs during the day. The peak demand will be discussed in the next section.

1.1.3 Peak electrical demand

A major concern for energy suppliers such as ESKOM is the issue of peak electrical demand. Peak demand is the total electricity load required at any given moment, which has to be supplied by ESKOM. In a study conducted (Lane, 1996) on the daily load profiles, it was found that the commercial and domestic sectors are the main contributors to the peak electrical demand. The heating of sanitary water in the domestic sector contributes to 32 % of the domestic peak demand and forms an important part of the total peak demand each day. Direct resistance electrical water heaters therefore contribute 28 % of the domestic peak demand.

Figure 1.2 shows the demand profile of domestic water heaters as reported by Lane (1996). It can clearly be seen that there are two periods of high demand during the day. The first is in the mornings between 06:00 and 09:00, and again in the evenings between 18:00 and 20:00.

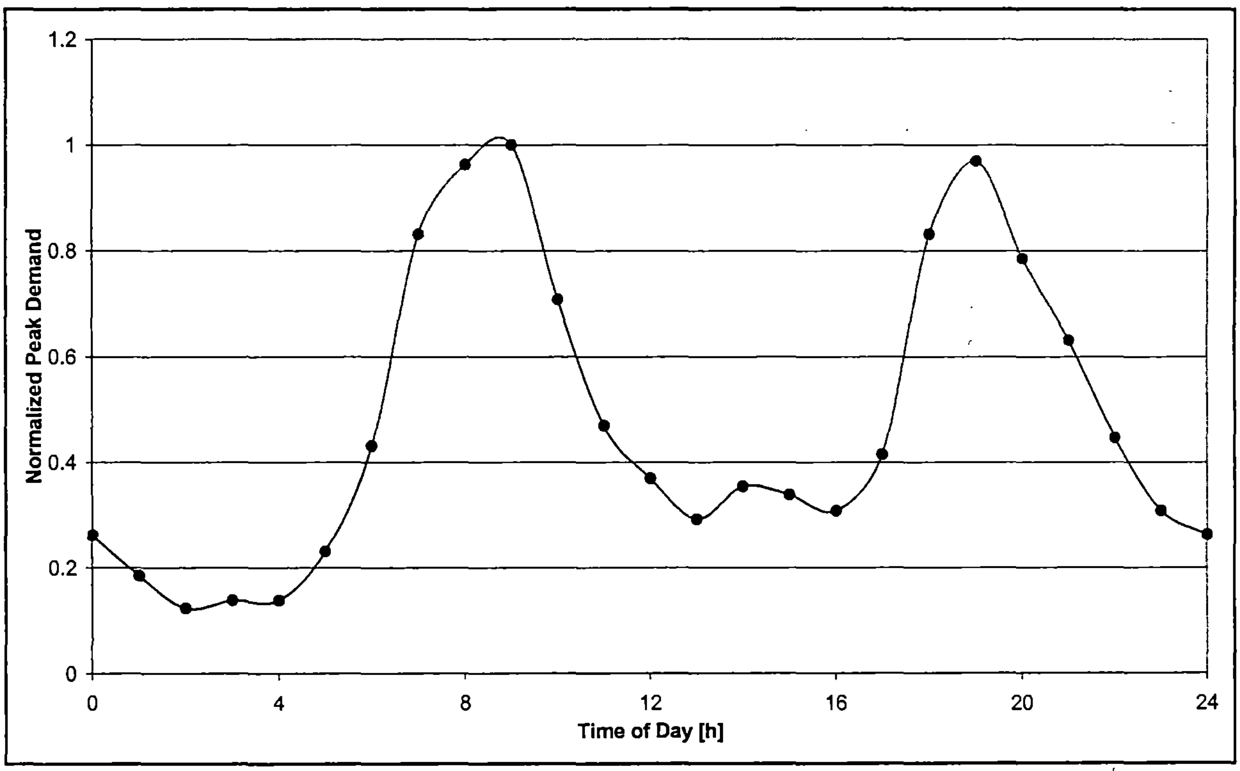

Figure 1.2: Domestic water heater demand profile

The ideal situation for suppliers of electricity is a lower but constant demand throughout the day instead of the two high demands in the morning and evening. The reason is that to enable ESKOM to cope with the peak demand, the total generation capacity of its power stations has to be higher than the peak load. This usually implies that more power plants have to be built just to cope with the short peak demand. An alternative is to store energy in off-peak hours, which is an expensive operation.

The consumer on the other hand, wants hot water at any time of the day, and especially during the two peak zones. These peak loads may lead to the point where the consumer will start paying extra for electricity during peak hours. A compromise between the supplier and the consumer is therefore needed. A possible solution is the implementation of heat pumps for the heating of sanitary hot water instead of the existing direct resistance electrical water heaters. The efficiency of heat pumps will be discussed in the next section.

1.1.4 Energy efficiency of heat pump water heaters

A heat pump is a mechanical device which uses a refrigerant, such as freon, to transfer heat from a low temperature source to a high temperature sink via a vapour compression cycle which requires power input via a compressor. Heat pumps are already widely used in the South African commercial sector, mainly in the form of water chillers and air-conditioners. For both chillers and air-conditioners the emphasis falls on cooling with heating as a by-product.

For the heating of sanitary hot water in the commercial sector the emphasis of the heat pump falls on heating with cooling as a by-product. In the domestic sector heat pumps have not yet been implemented on such a wide scale as in the commercial sector, accordingly leaving room for improvement on direct electrical resistance heaters.

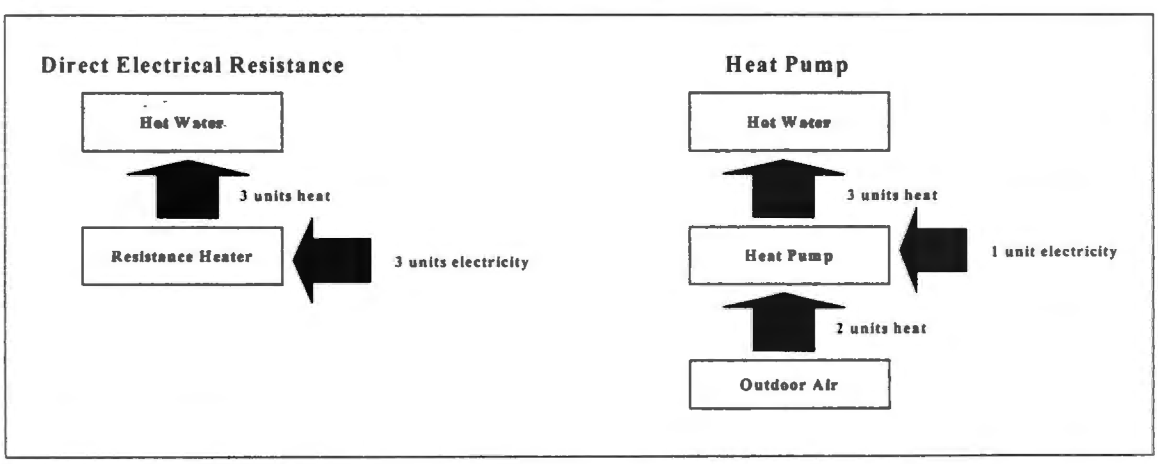

Figure 1.3: Basic operation of the direct electrical resistance heater and the heat pump

In Figure 1.3 the difference between the basic operation of the resistance heater and the heat pump is illustrated. The resistance heater delivers one unit of heating for each unit of electrical input. The heat pump also has one unit of electrical input but withdraws two additional units of energy from the environment, supplying three units of heating for every unit of electrical input. The ratio of three units heating for every unit electrical input is referred to as the 'Coefficient of Performance' or COP of the heat pump. The COP varies for different environmental conditions and type of heat pump configuration but is generally in the order of 3.

If the outside air were to be used as the low temperature source and the domestic hot water as the high temperature sink, 100 kWh heating could be achieved with an electrical input of only 33 kWh. A heat pump therefore provides a saving of approximately 67 % compared to a direct resistance electrical heater. The impact on the environment as well as the natural resources could therefore be reduced drastically. Table 1.2 provides a comparison between the impact of heat pumps and direct electrical heating.

Category	Direct electrical resistance	Heat pump
1. Water heating	100 kWh	100 kWh
2. Electricity supplied	100 kWh	33 kWh
2.1 Coal	50 kg	16 kg
2.2 Water	200 litre	67 litre
2.3 CO_2	100 kg	33 kg

Table 1.2: Comparison between direct electrical heating and heat pumps

The 66 % saving on electricity for the heating of water compared to direct electrical resistance heating means that 1.26 % of the total energy use of South Africa could be saved. This is about 1122 million rand each year, i.e. about R 500 per household. Another component that should be considered is the investment the consumer has to make to change from direct electrical heating to a heat pump. In the next section the cost-effectiveness of heat pumps will be discussed to indicate that it could be worthwhile for the consumer.

1.1.5 Cost-effectiveness of heat pump water heaters

There are two factors that are decisive for the cost-effectiveness of heat pumps for heating sanitary hot water, namely:

- The number of hours each day for which the heat pump was designed to heat water.
- The normalised cost of the heat pump installation per nominal kilowatt heating capacity.

Greyvenstein (1992) indicated that the cost-effectiveness of heat pumps might be improved by maximising the daily runtime of the heat pump for a given daily hot water consumption. Rousseau (1996:11) also stated that the cost-effectiveness of the heat pump increases as the daily runtime is increased. The reason is that if the runtime were to be increased, the same amount of water could be heated over a longer period, meaning that a lower capacity heat pump could be used, decreasing the cost of the unit. The cost-effectiveness also increases if the cost of the heat pump were decreased.

For this reason a micro heat pump with a nominal capacity of 1.2 kW is currently being developed. This heat pump could also have a positive impact on the peak demand. This heat pump will have a peak electrical demand of only 0.6 kW compared to the 3 kW to 4 kW electrical demand of a direct electrical heater. This means the water heating peak demand of a household could be decreased by 83 %. This leads to a 23 % decrease in the total peak demand of a household.

1.1.6 Improved in-line water heating concept

Due to the fact that the heat pump has a low capacity, the heating of water takes longer than a conventional electrical heater. Because of the relatively short reheating periods required when the tank is filled with cold water, manufacturers usually install a heat pump which is much larger than is actually required. This decreases the effectiveness of the heat pump for both cost and energy-efficiency. Instead of installing an oversized heat pump, a few changes could to be made to the installation to provide for a sudden demand for extra hot water when the tank is cold.

A design approach is proposed (Greyvenstein & Rousseau, 1997:9) which permits practical daily runtime in excess of eighteen hours without inconvenience to the users. The new design approach involves changes to the water circulation system, the use of in-line supplemental electrical heaters, the use of a better control system and improvement of the heat pump design. Figure 1.4 shows the layout of the improved concept.

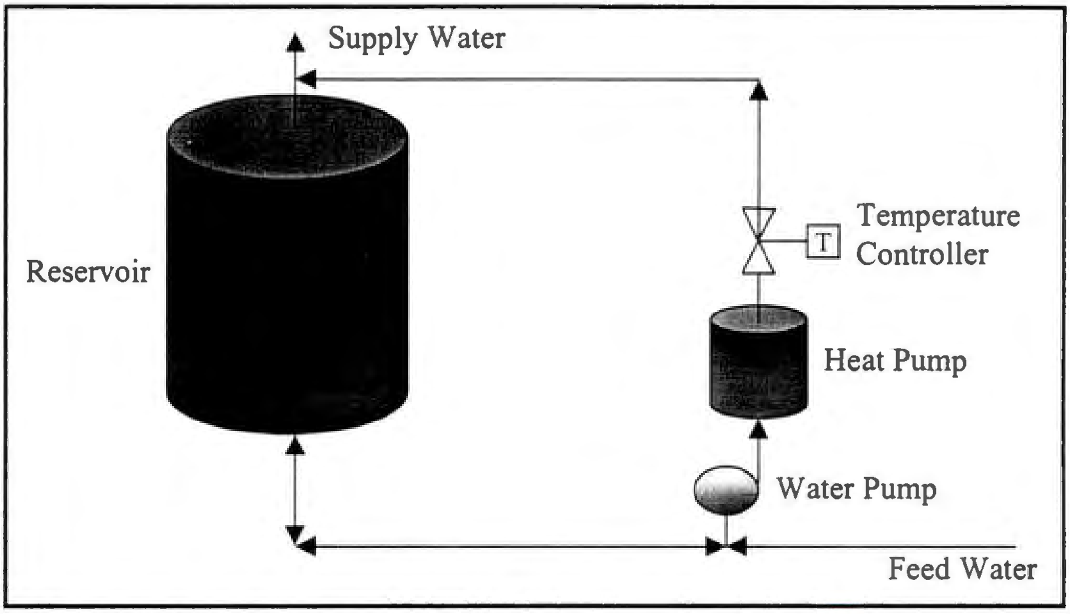

Figure 1.4: Improved in-line water heating concept.

The first improvement is the position of the pipe returning the heated water from the heat pump to the reservoir. The conventional way such as in hot water cylinders is that water is heated at the bottom of the reservoir, which then starts mixing upward with the cold water. With the new layout the water is fed to the top of the reservoir, directly into the supply water pipe.

The second improvement is the installation of a temperature controller in the water line from the heat pump. The temperature controller ensures that the water is always supplied to the top of the reservoir at the desired temperature, i.e. 60°C. With hot water being supplied to the top and cold water to the bottom, a temperature gradient exists throughout the reservoir.

An amount of water will always be available at the desired temperature, even if most of the reservoir were found to be cold. With a correctly sized heat pump and a good control strategy, the heating load may be spread evenly over a longer period of the day. In the next section the heat pump required for the domestic sector will be discussed. Reasons will be given for the selection of certain of the components.

1.1.7 Micro heat pump

Figure 1.5 shows the components of the micro heat pump which will be discussed below.

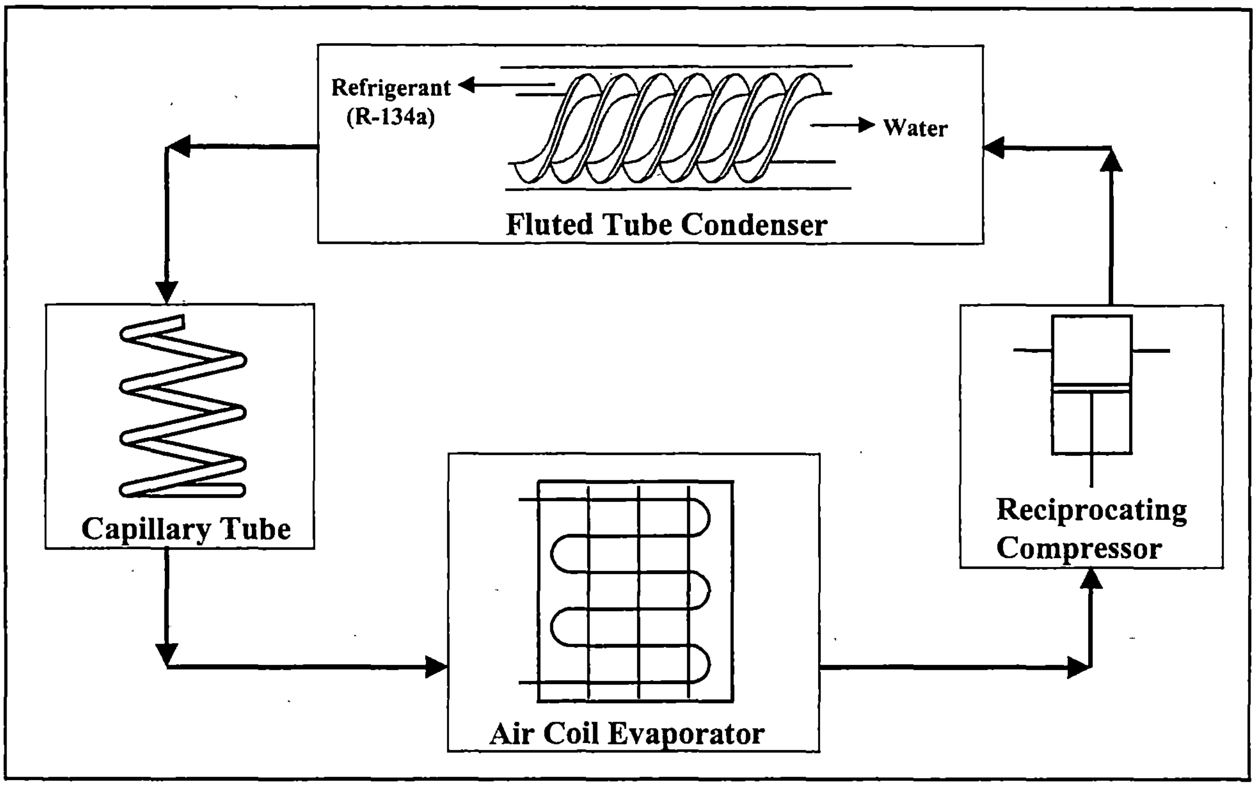

Figure 1.5: Components of a micro heat pump cycle

Only an overview of each component in the cycle will be given here. An in-depth study of each component will be done in Chapter 3 (Theoretical background).

Fluted tube condenser

A fluted tube condenser is an improvement on a conventional tube-in-tube condenser because it provides an enhanced heat transfer. The difference is that the inside tube of a fluted tube condenser is twisted (fluted), as can be seen in Figure 1.5. The outside tube is then shrunk over the inside tube, forming an annulus. The fluted tube increases the heat transfer due to increased friction and swirl in the flow path of the refrigerant and the water. With fluted tubes both the local heat transfer coefficient and the unit per surface area are increased. The heat transfer is enhanced by two mechanisms, namely:

- The drawing of liquid refrigerant into the corners of the channel by surface tension exposing the heat transfer area to hot gas.

- The creation of microcirculation of the liquid due to the twisted geometry. This leads to the removal of already cooled liquid away from the surface, replacing it with hot liquid or gas.

The condenser is operated in a counter-flow configuration with the water flowing inside the fluted tube and the refrigerant (R 134a) in the annulus. The reason for the refrigerant flowing inside the annulus is that this is the smallest area, thus enhancing the heat transfer of the refrigerant. The advantage of a counter-flow condenser is that the outlet water temperature can be lifted above the condensing temperature of the refrigerant by means of the superheated refrigerant. The only problem with fluted tubes is that the geometry is complicated. Only a few manufacturers in the world have the equipment and the knowledge to manufacture fluted tubes. The School of Mechanical and Materials Engineering at the Potchefstroom University has the capability to manufacture fluted tubes for small diameter tubes.

Air-cooled evaporator

An air-cooled evaporator is a very common type of heat exchanger with wide application in the heat pump and air-conditioning environment. The refrigerant flows inside the tubes with the air flowing over the finned outside area. The advantage of a finned evaporator is that the outside heat transfer area is enhanced, increasing the heat transfer between the air and the refrigerant.

Reciprocating compressor

A reciprocating compressor was selected mainly because of its low initial cost compared to other types of compressors, i.e. scroll and rotary compressors. The operation of a reciprocating compressor is also very basic with a piston compression cycle. With the small size compressor required, about a one third horsepower, reciprocating compressors work well. However there is not sufficient performance data available from the manufacturers for these low capacity compressors.

Capillary Tube:

Capillary tubes are widely used for their simplicity, reliability and low cost. The capillary tube provides the required pressure drop between the condenser and the evaporator and regulates the mass flow rate to meet the demand on the cycle. The disadvantage of a capillary tube is that it cannot cope with large variable-load conditions and it will operate at maximum efficiency at only one set of operating conditions. If properly selected and applied, a capillary tube will perform satisfactorily over a reasonable range of operating conditions.

Refrigerant:

The refrigerant to be used is R 134a due to its wide application possibilities. It is also environmentally friendly and allows higher condensing temperature, which is ideal for heating water.

1.2 Purpose of this study

In the previous section the heat pump components to be used were described. However these components need to be sized for optimum performance. This could be done experimentally by a trial and error method, or by means of endless theoretical calculations. Both methods will provide an answer, but not in a short period of time. Another method is required by means of which the components could be sized and the change in refrigerant and water properties could be determined.

The purpose of this study is the development of a micro heat pump simulation routine which can be used for the design of low cost energy-efficient micro heat pumps. This simulation must be able to simulate every component in the heat pump cycle as accurately and quickly as possible.

The models for each component will be developed from first principles rather than by implementing empirical routines.

In order to develop this micro heat pump simulation programme, the following objectives must first be reached:

- A literature survey has to done on heat pumps and its components to obtain information on what has been done up to now, so that work which has already been done can be implemented.
- Theoretical investigation of each component in the heat pump cycle has to be done. This involves an understanding of the governing equations involved in each component.
- Development of simulation models for each of the four components should be done.

- The integration of all the models into a heat pump simulation programme should be undertaken.
- The simulation programme should be verified against experimental data.

After completion of this study, there will be a complete simulation programme available for the design of micro heat pumps. The focus will be on the simulation of the four main components and the details of each of these routines.

1.3 Impact of the Study:

On completion a C++ computer programme will be available for the simulation of the four major components of the micro heat pump. The heat pump simulation routine will become a handy tool in designing micro heat pump cycles. These micro heat pumps can then be optimised for both cost and energy-effectiveness. This study forms part of the larger objective, which is the design of low cost heat pump installations for the heating of domestic hot water. These installations will satisfy both the consumer and the electricity suppliers. When implemented, the heat pump installations can have a significant influence on the annual energy savings of the country as well as on the peak demand experienced by ESKOM.

References

GREYVENSTEIN, G.P. 1992. The simulation of the cost effectiveness of heat pumps in specific buildings. *ENERCONOMY '92,* Pretoria, South Africa, 2.6/1-2.6/13, Jun. 8/9.

GREYVENSTEIN, G.P. & ROUSSEAU, P.G. 1997. Improving the cost effectiveness of heat pumps for hot water installations. *Proceedings of the 5th international energy agency conference on heat pumping technologies*, Toronto, Canada. September.

GREYVENSTEIN, G.P. & ROUSSEAU, P.G. 1998. Application of heat pumps in the South African commercial sector.

LANE, I.E. 1996. Demand-side management options for the domestic sector. *DMEA rep. ED9207.*

ROUSSEAU, P.G. 1996. Energiebesparing: Suid-Afrika se onbenutte potensiaal. *Inaugural Lecture*. Potchefstroom University for Christian Higher Education, South Africa. November.

CHAPTER 2

LITERATURE SURVEY

CHAPTER 2

LITERATURE SURVEY

2.1 Introduction

In this chapter a summary of the literature that has been surveyed, is given. It must be noted that the focus of this survey was on the four micro heat pump components discussed in Chapter 1 (par. 1.1.7). The literature is divided into six categories namely:

- Heat pump cycles ⇒ A survey of heat pump simulation routines that have been developed over the years.
- Condenser ⇒ Literature concerning tube-in-tube condensers is discussed here. Two subdivisions are:
  - Research done in the field of fluted tube heat exchangers.
  - Research on heat transfer coefficients and friction correlations.
- Evaporator ⇒ Due to the wide application of evaporators it was decided to focus only on literature concerned with air coil evaporators with the following subdivision:
  - Research on heat transfer coefficients and friction correlations.
- Compressor ⇒ Different types of compressor simulation models are discussed. The main focus falls on reciprocating compressors.
- Capillary ⇒ Literature about existing capillary tube models has been evaluated.
- Refrigerant inventory ⇒ Literature discussing methods of determining the amount of refrigerant in the cycle will be looked at.

The literature in each category has been arranged chronologically. The literature was also evaluated by means of the following guideline questions:

- What is the aim of the work?
- Why was the work done?
- How was the work done?
- What are the most important results that have been obtained?
- What conclusions can be drawn from the work?

It is not always possible to obtain answers to all the above questions, but these questions also point out the shortcomings of the literature reviewed.

2.2 *Heat pump cycle*

In 1983 a mathematical model to predict the transient behaviour of a laboratory-scale refrigerating system was developed by Yasuda **et al.**, (1983:408). The system consisted of a single-cylinder reciprocating compressor, a shell-and-tube condenser, a thermostatic expansion valve, and a dry evaporator. The basic equations for the components were derived from the physical laws of mass and energy conservation. With the aid of timewise integration of the equations, the model can be used in a computer simulation of steady state as well as transient behaviour of the system. Simulation results were compared to experimental data and a good agreement was obtained regarding absolute values and trends. However, more work still had to be done on the model because of incorrect simulation results when the boundary point (between the evaporative region and the superheat region) moves towards the evaporator outlet temperature, as well as incorrect measurements for superheat temperatures lower than 5 degrees Kelvin.

In the following year MacArthur (1984:982) described a detailed mathematical model for vapour compression heat pumps containing model equations of each component in the heat pump. The model was developed by using a fundamental approach. The equations used were based on conservation principles. Each of the models representing a component utilised either explicit or implicit formulations or any combination thereof. This means that certain subroutines use implicit formulations due to non-linearities, and others are explicit, therefore the overall component model must incorporate both types of formulations and solve via iteration. The executable programme solves for overall system response by interconnecting subsystem modules and integrating in an explicit manner. The model has not been tested against specific heat pump data because the main objective was to develop a preliminary model based on first law principles. Future work includes the validation of the model, the refinement of the preliminary model, and the inclusion of the time-dependent momentum equation and associated pressure drop calculations.

In 1987 a mathematical model was developed for the processing of air in an air-to-air heat pump unit (Protsenko, 1987:135). The model can be used for drying and heating of air. By means of the model it is possible to optimise the temperatures of the heat transport medium, as well as the dimensions and hydraulic characteristics of the heat exchanger surface. The heat flux density in the heat exchangers has been chosen as the independent parameter. This model is very limited due to the governing equations being empirical and not fundamental. This limitation means that the model cannot be applied over a wide range of conditions.

In 1988 a computer model for the simulation of vapour compression cycles containing thermostatically controlled expansion valves was developed (Greyvenstein, 1988:494). The model describes the performance of the system given its design, environmental conditions and component specifications. The system described contains a water-cooled condenser and a direct expansion air-cooling evaporator coil. The condenser and evaporator are modelled by means of the log mean temperature difference (LMTD) method. The compressor model consists of a data input file containing mass flow and input power values as supplied by the manufacturers. An interpolation routine is used to determine the mass flow and input power for a given working point. The accuracy of the computer model depends on the accuracy of the subsystems. This is a very powerful simulation routine, which has already been implemented into a computer programme called *HPSIM* (HPSIM V2.0).

Baskin (1991:31) presented a method of numerically selecting performance-enhanced heat pump components and modelling the performance of these components. This is done by using a steady-state heat pump simulation routine. A heat pump prototype with manually selected improved components was built to evaluate the numerically selected components. It was found that enhancing the surfaces of the heat exchangers reduced the space requirement of the heat pump system. Increased capacity was obtained by reducing the face area of the air coil by increasing the number of fins per inch, number of tube rows, and tube diameter. The electrical cost was significantly diminished by employing a high efficiency reciprocating compressor.

Stefanuk **et al.**, (1992:172) presented a steady-state simulation model of a water-to-water vapour compression heat pump under superheat control. The model is derived from the basic conservation laws of mass, energy, momentum and equations of state as well as fundamental correlations of heat transfer. The model incorporates a refrigerant charge inventory in addition to the normal thermodynamic energy balance of the system. The log-mean temperature difference (LMTD) method was used in the component models. The simulation algorithm was developed for input data which are readily available, i.e. external operating conditions, component geometry and characteristics. The simulation model consists of two algorithms, namely a global search algorithm and an iterative convergence algorithm. The model was evaluated against experimental measurements to determine its accuracy and limitations. Results indicate that the superheat of the refrigerant leaving the evaporator and the refrigerant charge can be used as control variables to maximise system performance.

2.2.1 Summary

In the literature it was found that there are many heat pump simulations, of which the above are only a few. The problem with most simulation routines is that the routines only apply to a specific heat pump configuration. The equations are also mostly empirical, therefore limiting its use. It is accordingly difficult to modify one of these simulation routines to apply to our micro heat pump. The one model that can be applied to a wide range of configurations is the model presented by Greyvenstein (1988:494). All the equations were derived from first order mass and energy conservation, and the models were solved by means of the LMTD method. However, it does not incorporate a capillary tube model

2.3 Condenser

Yasuda **et al**., (1983:410) modelled a shell-and-tube condenser by means of a lumped method. The following assumptions were made to simplify the model:

- The superheat and liquid refrigerant regions are concentrated into the saturated region.
- The condenser characteristics are described by one refrigerant-side heat transfer coefficient.
- The refrigerant is in equilibrium in the condenser.
- Constant degree of subcooling.
- No pressure drop is present in the condenser.

Basic equations for the refrigerant, tubing, cooling water and condenser wall were derived from the laws of mass and energy conservation. The heat transfer coefficients were obtained from experimentally determined values. The only information given for the simulation tested against the experimental values is the condensation pressure and the superheat temperature. A good agreement was obtained in both cases.

MacArthur (1984:983) modelled the condenser in two sections, namely the heat exchange and the pressure response. An assumption was made that the flow is uniform and one-dimensional along the length of the heat exchanger. The condenser is divided into a series of control volumes. The equations for the heat exchanger response are all implicit. The pressure response can be determined by means of the known masses, volumes, and property data of the refrigerant. The model uses an iterative search for the temperature and enthalpy field at each time step. The direction of the search uses the fact that there is no axial conduction. With the heat exchanger equations evaluated, the condenser pressure response is determined in an explicit way.

Greyvenstein (1988:499) described in his heat pump simulation model a double tube, counter-flow, water-cooled condenser with all the governing equations. The refrigerant flows inside the inner tube, while water flows through the annulus. The condenser model is solved by means of the LMTD method. No experimental data were available at that stage, therefore in order to test the model, it was changed to an air-cooled fin and tube type condenser. The maximum difference in condensing temperature minus entering air temperature between the experimental data and simulation results was 2.5 %.

Stefanuk **et al**., (1992:176) used the LMTD method of heat exchanger analysis to solve the tube-in-tube condenser model. The condenser is analysed as three heat exchangers in series, which correspond with the three phases of the refrigerant (superheat, two-phase, subcool). The refrigerant flows inside the tube with the water in the annulus in a counter-flow configuration. It is assumed that the refrigerant is subcooled at the outlet. A step-by-step explanation of the model is given with the necessary governing equations. The model accuracy was within 10% of the experimental values for condensation pressure, heat transfer and COP. The accuracy was considered to be satisfactory. The heat transfer predicted was generally too high. A reason given was the overestimated prediction of the heat transfer coefficients. The accuracy of the coefficients is about 20% due to the insufficient test facility.

Berg (1993:275) discussed the use of the effectiveness-Ntu method for the sizing of air-cooled heat exchangers. One of the advantages of this method is that the exhaust air temperature does not have to be estimated. Another important advantage is its convergence stability for iterative computerised calculations. It is also shown that for a given example the effectiveness-Ntu method converges, while the LMTD method involves the log of a negative number and the programme terminates. The effectiveness-Ntu method was found to be accurate within 5% for a number of case studies. The LMTD method's best accuracy was only 15%.

2.3.1 Fluted tube condenser

In the micro heat pump cycle to be modelled a fluted tube condenser is used. The following articles concentrate on the theory involved in this type of heat exchanger.

Richards and Grant (1987:2011) presented the results of an experimental study of pressure drop and heat transfer for turbulent flow inside twelve different doubly-fluted tubes. All the data was obtained using water flowing inside a horizontal tube with steam condensing on the external surface of the tube. The performance of the tubes is examined by determining the volume reduction which can be achieved using doubly-fluted tubes. Volume reductions of 20% were achieved for designs where the tube side resistance was limiting. Further work was needed to develop a general correlation and to understand the physical mechanisms governing heat transfer enhancement in doubly-fluted tubes.

Schlager **et al.**, (1988:149) studied condensation and evaporation of refrigerant oil mixtures inside a smooth tube and also a micro-fin tube. The refrigerant flows inside the tube with the water flowing inside the annulus. It was shown that the micro-fin tube increased the average heat transfer coefficient for both condensation and evaporation by as much as a factor of 2.5 for refrigerant oil mixtures as well as for pure refrigerants. Small quantities of oil were found to enhance evaporation heat transfer compared to pure refrigerant evaporation. The micro-fin tube's heat transfer enhancement factor for condensation showed little dependence on the oil concentration.

Choudhury and Karki (1991:45) studied the influence of eccentricity of the inner cylinder and the presence of buoyancy forces on the laminar axial flow and heat transfer in a horizontal cylinder annulus. Studies were done on fully developed flow, with combined forced and free convection. At a given Rayleigh number the effect of buoyancy on the heat transfer coefficient is stronger for large Prandtl numbers due to the thinner thermal boundary layers near the heated inner cylinder. At higher Rayleigh numbers there is an optimum value of eccentricity, which leads to the highest heat transfer rate. Local heat transfer coefficients on the inner cylinder become highly non-uniform at high Rayleigh numbers.

In the same year Christensen and Srinivasan (1991) compiled a report consisting of two parts. The first part comprised flow inside fluted tubes, and the second part flow in the fluted tube annuli. Fourteen fluted tubes were tested to cover a wide range of geometrical parameters of the flutes. The work of the authors concentrated on friction enhancements due to the fluted tube. The friction factors and Nusselt numbers were found to be functions of the flute depth, pitch and helix angle. The friction factors were then correlated as a function of Reynolds number and non-dimensional geometrical parameters.

Two years later, in 1993, Das (1993:972) presented experimental data on pressure drop across six helical coils made of rough transparent PVC pipes for flow of water in turbulent conditions. A correlation for predicting the friction factor was developed. A detailed statistical analysis showed that the correlation was of an acceptable accuracy of 95%.

In the same year Chiang (1993:205) obtained the heat transfer characteristics of four enhanced tubes with many axial or helical fine internal fins, using R-22 as the working fluid. Depending on the mode of operation, test sections could be heated or cooled by water in the annuli. With the exception of evaporating heat transfer at the lower mass flux range, the axial grooved tubes tested were found to yield more favourable heat transfer and pressure drop performance. The performance was better than for helical grooved tubes of comparable tube weight per linear length. The condensation heat transfer coefficient of the axial micro-fin tubes were 10% to 20% higher than for helical grooved tubes. The axial micro-fin tube yielded 15% lower pressure loss than the helical tube of the same diameter.

Eckels **et al.**, (1994:283) reported the average in-tube heat transfer coefficients and pressure drops during condensation of refrigerant R-134a/lubricant mixtures in a smooth tube and a micro-fin tube. The outer diameter of the tubes was equal to 9.52-mm. The study focussed on three main objectives:

- Determining the effect of lubricant concentration,
- Comparing the performance of the smooth tube and the micro-fin tube,
- Developing design equations.

Heat transfer coefficients during condensation decreased with the addition of ester lubricants. Pure R-134a heat transfer coefficients in the micro-fin tube were 100% to 200% higher than those in the smooth tube, with the higher values occurring at the lower mass fluxes. Pressure drops in the micro-fin tube were 20% to 50% higher than those in the smooth tube. Eckels **et al.**, further presented design equations which helped to predict the heat transfer coefficients and pressure drops of R-134a/lubricant mixtures in the smooth and micro-fin tubes.

Chang **et al.**, (1996:821) studied the condensation heat transfer characteristics of four different horizontal enhanced tubes with refrigerant R-134a. Two drainage models in the literature were compared to experimental data. It was found that a model by Rudy and Webb provided the best prediction of condensation heat transfer coefficients.

2.3.2 Heat transfer coefficients and pressure drop

An important component of the development of a fluted tube condenser model is the use of heat transfer coefficients and friction correlations. In this section the different implementations found in the literature will be discussed.

As early as 1972 Traviss (1972:157) applied the momentum and heat transfer analogy to an annular flow model. He made use of the Von Karman universal velocity distribution to describe the liquid film. Since the vapour core is very turbulent, radial temperature gradients were neglected, and the temperatures in the vapour core and at the liquid vapour interface were assumed to be equal to the saturation temperature. Axial heat conduction and subcooling of the liquid film were also neglected. An order of magnitude analysis and non-dimensional heat transfer equations resulted in a simple formulation for the local heat transfer coefficient. The analysis was compared to experimental data and the results were used to develop a general design equation for forced convection condensation.

Shah (1979:548) presented a dimensionless correlation for predicting heat transfer coefficients during film condensation inside pipes. For flow in the two-phase region a correlation is used in terms of the quality and is combined with the Dittus-Boelter equation. It has been verified by comparing it to a wide variety of experimental data. The agreement is not very good, but in all cases was close enough to be considered satisfactory for practical design purposes. However, more tests still needed to be done for flow in annuli, especially at lower Reynolds numbers.

In 1981 Shah (1981:1086-1105) did a review of all the available literature and information for estimation of heat transfer during film condensation in tubes and annuli. The emphasis fell on fluids used in air-conditioning and refrigeration. Tables are provided with the available experimental data giving the range of important parameters covered in various studies. Important topics covered are:

- Condensation of low velocity and high velocity vapours,
- Effects of superheat and non-condensable,
- Effect of oil,
- Effect of interfacial phase change resistance.

Information on further verification of the Shah model is also given. It was found that no efficiently verified predictive technique was available for high velocity superheated vapour.

In 1990 Eckels and Pate (1990:256-265) compared the heat transfer coefficients for evaporation and condensation of R-134a and R-12 for a range of conditions typically found in heat exchangers used for refrigeration and air-conditioning applications. The heat transfer coefficients are calculated by using existing correlations found in the literature for two-phase and single-phase flow. Single-phase heat transfer coefficients for R-134a are shown to be significantly higher than R-12. Depending on the liquid refrigerant temperature, the predicted increase is between 27% to 38%, and for vapour an increase between 37% to 45%. Two-phase heat transfer coefficients also show a significant increase.

Singh **et al.**, (1996:596) investigated quasi-local condensation heat transfer coefficients at low mass fluxes inside smooth horizontal copper tubes, with refrigerant R-134a. The investigation was both experimental and analytical. The operating conditions were selected in order that the two-phase flow in the test section corresponded to a stratified-wavy regime. The heat transfer coefficients were found to be dependent on both the heat flux and the mass flux levels. A new correlation was proposed by means of which the overall heat transfer coefficient was taken as the sum of the heat transfer due to film condensation in the top portion of the tube and the forced convection of the condensate in the bottom portion of the tube. The new correlation predicted the experimental data within 7.5%.

In 1997 Wang **et al**., (1997:803) reported the two-phase flow pattern and frictional pressure characteristics for R-134a inside a 6.5-mm smooth tube. A correlation for the two-phase multipliers was proposed that could correlate the present test data with reasonable accuracy.

2.3.3 Summary

After all the literature has been reviewed, it was decided to use the models and information contained in the following literature for the fluted tube condenser model:

- Fluted tube geometry ⇒ The non-dimensional correlations by Christensen and Srinivasan (1991).
- Friction factor ⇒ The correlation by Christensen and Srinivasan (1991) based on non-dimensional geometry and Reynolds number.
- Two-phase refrigerant pressure drop ⇒ The correlation by Christensen and Srinivasan (1991) based on their friction factor correlation.
- Single-phase refrigerant pressure drop ⇒ Based on the technique by Das (1993:972).
- Inside heat transfer coefficient ⇒ The correlation by Christensen and Srinivasan (1991) based on non-dimensional geometry and Reynolds number.
- Outside two-phase heat transfer coefficient ⇒ The technique implemented by Shah (1979:548).
- Outside single-phase heat transfer coefficient ⇒ Based on the model by Christensen and Srinivasan (1991) which incorporates their friction factor correlation.

All the above techniques will be described in Chapter 3 (Theoretical background) for implementation into the condenser model.

2.4 *Evaporator*

The focus of the literature surveyed was on air-cooled evaporators. In this section some of the most effective models will be discussed.

Yasuda **et al.**, (1983:411) modelled a dry coil evaporator. Evaporator outlet temperature is considered to be important regarding system instability. A lumped model was utilised for the two-phase refrigerant flow in the evaporative region. Assumptions made regarding the evaporator model are:

- A boundary exists between the two-phase region and the superheat region.
- In the two-phase region characteristic values such as heat transfer coefficient and evaporating temperature are constant.
- Two-phase flow is homogeneous and in equilibrium.
- Superheated vapour is incompressible.
- A pressure drop of refrigerant flow occurs at the end of the two-phase region and at the end of the superheat region.

Basic equations were derived from mass and energy conservation. To solve the evaporator model, the evaporator length was divided into a large number of sections. Heat transfer coefficient and pressure drop for the two-phase region was obtained from experimental results. The heat transfer coefficient and pressure drop for the superheat region was obtained from the literature.

A year later MacArthur (1984:985) stated that an effective evaporator model could predict both the vapour and liquid flows, the stored refrigerant mass, and the temperature and enthalpy profiles during transient and steady-state operation. MacArthur focussed separately on the single-phase and two-phase regions. The evaporator model was obtained by discretizing the governing equations in both the spatial and time co-ordinates.

Greyvenstein (1988:497) considered a fin and tube evaporator in a stream of air. The evaporator model is solved by using the LMTD method. Conditions in both the two-phase and superheat regions are solved for a wet coil with the apparatus dew point equal to the mean outside surface temperature. The difference between the external wet-bulb temperature and the evaporating temperature for a given type of fin were compared for the simulation and experimental data. The maximum difference between the simulation and the experimental data is 4.4 % with a mean difference of 2.5 %.

In 1989 Braun **et al**., (1989:170) developed a method for modelling the performance of cooling towers and cooling coils. Braun used the effectiveness-NTU method for solving the cooling coil. Effectiveness relationships were developed by using air saturation specific heat and are for counter-flow geometries. Braun **et al**., also presented the basic theory of a counter-flow cooling coil, leading to the development of an effectiveness model. A method for analysing the performance of cooling coils which have both wet and dry sections is also described. The resulting effectiveness model was compared with results of finite difference solutions to the basic heat and mass transfer equations and manufacturers data. The difference in both the air heat transfer and the temperature effectiveness between the methods are 5% at the most.

Green and Roberts (1996:258) described the use of a mathematical model of a heat pump to determine how the design of the outdoor air-coil affects the heating performance of an air-to-water heat pump. The mathematical model used for the evaporator is the effectiveness-NTU method. It is shown that the optimum performance for frost-free conditions is reached using an evaporator with the following specifications:

- Large face area.
- Minimum depth.
- Minimum fin spacing.
- Low airflow rates.
- As high an evaporating temperature as possible.
- And no superheat across the coil.

The reason for no superheat is that it reduces the coil area available for evaporation, lowering the evaporating temperature. The problem with no superheat is that liquid could be pumped into the compressor. Compressors are capable of coping with a certain amount of liquid, but liquid is harmful to the compressor.

Design procedures of air-cooled evaporators generally assume a pure refrigerant and thermodynamic equilibrium between the phases inside the tubes. The effects of the presence of lubricating oil in the working fluid have been studied in the laboratory but have not been widely used in procedures. The same applies to non-equilibrium between the liquid and vapour phases in the evaporator. Conde (1996) presented a simulation model containing the above-mentioned two aspects for simultaneous consideration in the design of evaporator coils. The effect of these two aspects is a reduction in the temperature difference between the working fluid and the air, leading to lower evaporation pressures. A computer programme implementing this model has been developed for the improvement of evaporator design.

2.4.1 Heat transfer coefficients

Eckels and Pate (1990:256-265) compared the heat transfer coefficients for evaporation and condensation of R-134a and R-12 for a range of conditions typically found in heat exchangers used for refrigeration and air-conditioning applications. The heat transfer coefficients are calculated by using existing correlations found in the literature for two-phase and single-phase flow. Single-phase heat transfer coefficients for R-134a were shown to be significantly higher than R-12. Depending on the liquid refrigerant temperature, the predicted increase was between 27% and 38%, and for vapour between 37% and 45%. Two-phase heat transfer coefficients also show a significant increase.

Jung and Radermacher (1991:48) did a study on evaporative heat transfer coefficients of new ozone-safe refrigerants. A heat transfer coefficient correlation with a mean deviation of 7.2%, based on experimental data, was used for the prediction. For the prediction, the evaporator coil was assumed to be a straight tube. The results indicate that the convective evaporation was the main heat transfer mechanism. It was also found that nucleate boiling was fully suppressed at qualities larger than 20% for all fluids studied. R-134a showed an increase in heat transfer coefficient compared to R-12, and a decrease compared to R-22.

2.4.2 Summary

After all the literature has been reviewed, it was decided to use the models and information contained in the following literature for the air-cooled evaporator model:

- General model ⇒ The model presented by Braun **et al.**, (1989:170) because of the model's complete coverage of the coil operation.
- Heat transfer coefficients ⇒ One of the methods covered by Eckels and Pate (1990:256-265) with special reference to the method used by Shah.

The above techniques will be described in Chapter 3 (Theoretical background) for implementation into the evaporator model.

2.5 *Compressor*

Dabiri and Rice (1981:771) described a compressor simulation routine in 1981. The compressor routine uses empirical performance data available from the manufacturers. It applied corrections for operation at evaporator superheat levels which differed from those used in generating the manufacturers' data. With the data available the refrigerant mass flow rate and input power were obtained. On average, the model over-predicted the COP with 9%. The power input was also underpredicted by 10%, and the mass flow rate was overpredicted in one case by 3.1% and underpredicted in another case by 13.8%.

In 1983 Yasuda **et al.**, (1983:409) developed a model for a single-cylinder open-type reciprocating compressor. An available mathematical model was utilised as a basis, but the model was simplified by utilising the following assumptions:

- The discharge and suction valve are only fully open or fully closed.
- A four-phase compressor cycle is assumed (suction, compression, discharge, and expansion).
- No pressure pulsation is present.

Equations for the cylinder pressure and mass in the cylinder were derived from physical laws of mass and energy conservation for the four phases. The authors claim a good agreement between the experimental and simulation mass flow, but very little information is supplied to support this.

A year later MacArthur (1984:987) developed a model for simulating a compressor governed by the following five parameters:

- Clearance factor.
- Piston displacement.
- Compression efficiency.
- Heat transfer coefficient.
- Thermal mass.

The model still had to be validated by experimental results.

Greyvenstein (1988:496) made use of data files containing the mass flow and power input for a compressor as supplied by the manufacturers. An interpolation routine was used to determine the mass flow and input power given the inlet and outlet pressures. The accuracy of the model therefore depended on the accuracy of the performance data. Two other factors could also influence the accuracy of the compressor model. Firstly, the compressor data usually applies to a value of degree of superheat of approximately 11°C. Secondly, because the refrigerant mass flow and compressor input power are functions of the inlet and outlet pressures, it is important that these values should be accurately specified. The accuracy of the inlet and outlet pressures is a function of the evaporator and condenser model. In the case of a hermetically sealed compressor it is fair to assume that all the input power is transferred to the refrigerant, either in the form of heat or work. The model does compensate for different superheat values.

Stefanuk **et al.**, (1992:178) described a model of a reciprocating compressor with predictions of mass flow rate, and thermodynamic and electrical power to the compression process transferred to the refrigerant. A trial and error method was used in this project to select the parameters of the compressor model. The deviation between model predictions of the mass flow rate and the manufacturer-supplied measurements was 3.9% and for the power input 1.5%.

2.5.1 Summary

The majority of compressor models developed over the years are dependent on performance data supplied by the manufacturers. The model by Yasuda **et al.**, (1983:409) is only one of a few examples in the literature where a definite model based on conservation laws was developed. The model to be used in this dissertation will also be derived from physical laws. The technique to be used will be described in Chapter 3 (Theoretical background) for implementation into the compressor model.

2.6 *Capillary tube*

The capillary tube is a constant area expansion device used in vapour compression cycles. Improvements in performance and calls for new refrigerants have necessitated a re-evaluation of the modelling of individual components of heat transfer cycles, including the expansion devices.

In 1980 Koizumi and Yokoyama (1980:19) observed the refrigerant flow in a glass-capillary tube visually and reconfirmed it to be homogenous. The pressure and temperature distributions along the capillary tube were measured and it was recognised that the starting point of vaporisation became delayed. It was found that a theoretically calculated pressure distribution, assuming adiabatic and homogeneous flow, agreed accurately with measured values if the delay of vaporisation were estimated correctly. Using the theoretical equation, a method was developed for calculating the length of the refrigerant vaporising flow region in the capillary tube. Insufficient evaluation results are given to validate the accuracy of the capillary model.

Schulz (1985:92) did a review of the published literature on capillary tube expansion devices used in refrigeration applications. He concentrated on:

- Fluid flow as it passes through the small-bore tube.
- Considerations in selecting optimal geometry.
- Design criteria for the overall system.
- A performance comparison with other expansion devices.

When capillary tubes were compared to other expansion devices, such as thermostatic expansion valves, the following assumption was made: Even though the efficiency may be slightly reduced, the capillary tube was suitable not only for refrigerators, but also for systems exposed to variable loads.

In 1987 Kim (1987:1362) developed an iterative procedure yielding the length of the tube and predicting the quality at the exit of the tube. A computer programme replaced the iterative process, with the thermodynamic and physical property tables as the subroutines and function statement of the programme. An analysis of the capillary tube as an expansion device was carried out to provide the length, quality, flow rate, and flow condition. The given properties for the analysis were the pressure and temperature at the exit of the condenser and the evaporator temperature with the nominal flow rate. The model used both fundamental and explicit equations. No test results are given to evaluate the model.

In the following year Schulz (1988:507) presented a model for predicting the critical pressure of a refrigerant flow through an adiabatic capillary tube. Experimental capillary tube exit pressures obtained in a vapour compression loop were used to determine the analytical coefficients. The developed model took into account the non-ideal behaviour of the two-phase flow leaving the capillary tube. Its design had the objective of studying the behaviour of a series of capillary tubes and working fluids by:

- Adjusting and measuring the refrigerant flow rate.
- Varying and determining the entrance conditions.
- Measuring the capillary tube exit pressure.

The model improved the prediction of the exit pressure by about 15%, leading to a mass flow rate prediction within 10%.

Gorasia **et al.**, (1991:132) dealt with computer-aided design of straight, helical, and combination capillaries. A new expression for the friction factor was proposed, and better property correlations were developed. The results obtained agreed well with experimental works. For any entry parameters to capillary tubes this work may prove to be a useful guideline in evaluating the tube length required. Adiabatic slug flow of Refrigerant-12 with no heat exchange was considered. The only deficiency of the model is that it uses explicit defined equations.

In the same year Kuehl and Goldschmidt (1991:139) presented a steady-state model of refrigerant flow through a capillary tube. The model is based on homogenous flow assumptions for the two-phase flow region. It was found that a metastable (superheated liquid) region had to be accounted for in order to reach good agreement with a rather extensive data set. More work was needed to generalise the length of the metastable region from the data used for the analysis. The predictions are within 10% of the actual values.

Bittle and Pate (1996:52) designed a theoretical model for predicting adiabatic capillary tube performance. The comparison of the model predictions to the range of experimental data provided a comprehensive assessment of the model's accuracy. For a subcooled inlet condition and a mass flux less than 0.42 kg/s.cm^2, the model's predictions were within approximately 5% of the measured values. However, at mass fluxes in excess of 0.42 k/s.cm^2, the model began to underpredict the measured values by up to 6%. A general capillary tube friction factor equation was presented and incorporated within the flow model. The correlation expressed friction factor as a function of Reynolds number only. The flow model used two-phase viscosity to calculate the local Reynolds number and determine the local friction factor. For a subcooled inlet condition, the non-thermodynamic equilibrium liquid region existing within the adiabatic capillary tube flow was modelled, using the Chen [1990:551) metastable liquid flow model.

Bittle **et al.**, (1998:27-43) developed a new model for predicting refrigerant mass flow rate in an adiabatic capillary tube. The new model used generalised dimensionless correlations for both subcooled and quality inlet conditions. The Buckingham-Pi Theorem was used to create these dimensionless parameters. The parameters were based on tube geometry, fluid properties and inlet conditions. The outlet pressure was not important for the calculations because of the assumption of choked flow inside the capillary tube. The correlations were based on experimental data obtained with refrigerants R-134a, R-22, and R-410A over a wide range of operating conditions. The vast majority of measured flow data was predicted to within 10% by means of the correlation. The dimensionless parameters were based on fundamental correlations, with the coefficients being explicit. The above model could easily be implemented, with if necessary the only change being made to the coefficients.

2.6.1 Summary

A shortcoming of most of the capillary tube models is that explicit equations are used. This limits the range over which the models can be applied. The model which covered the widest range of capillary performance aspects and general features is the model by Bittle and Pate (1996:52). The dimensionless correlation method used by Bittle **et al.**, (1998:27) is also a very versatile method. It is also less complicated than their first model, but not as thorough. Both of these capillary tube models will be used in this dissertation to obtain the best model for the application of this study. The governing equations and basic theory will be described in Chapter 3 (Theoretical background) for implementation into the capillary tube models.

2.7 *Refrigerant inventory*

In most cases the refrigerant inventory for vapour compression systems is determined by using an inefficient trial and error procedure. A computer model that has the capability to predict the amount of refrigerant in air-cooled condensers is described by Orth (1995:1367). For the accurate prediction of refrigerant inventory, two important steps are required. Firstly to model the heat transfer of the coil in order to separate the three regions of the coil (superheat, two-phase, and subcooled), and secondly to predict the ratio of area occupied by gas to liquid (void fraction) throughout the condensing region. The model is used to illustrate the effects of different operating conditions and void fraction correlation on the refrigerant inventory in condensers. The results obtained showed that the accuracy is dependent on the void fraction correlation and the amount of subcooling, or the predicted length of subcooling in the condenser. Further work includes the experimental validation of the inventory model.

2.8 *Conclusion*

During the literature survey it was found that very little research has been done on micro heat pumps over the years. This identified a gap in the research of heat pump cycles, where this study can make a significant contribution in the research field. The theory behind air-cooled evaporators is more widely known and implemented and existing methods can therefore be used to solve this model. The fluted tube condenser model to be developed will have to be a combination of existing tube-in-tube models and research done on the heat transfer in fluted tube heat exchangers. As can be seen from the literature survey, limited information is available on compressor simulation models. As stated, most of the models used data files containing manufacturers' data. A need for a model that could predict the behaviour of a compressor given its geometry and input pressure and temperature therefore exists. It was found that a lot of research has been done on capillary tubes as a substitute for expansion valves. The problem which most researchers experienced, was that their models underpredicted or overpredicted the length of the capillary. Another problem was that most models used explicit equations. A combination of existing theories could perhaps yield a model for predicting the length of a capillary more accurately. Taking all of the above into account, the theoretical background for each component in the heat pump cycle could be developed.

References

BASKIN, E. 1991. Optimization of water-to-air heat pump through manual and numerical component selections. *Advances in Heat Exchanger Design, Radiation, and Combustion, ASME*, 182:31-36.

BERG, J.L. 1993. Estimating the size of air cooled heat exchangers with the Ntu method. *Heat Transfer – Atlanta, AIChE Symposium Series*, 89(295):274-283.

BITTLE, R.R., PATE, M.B. 1996. A theoretical model for predicting adiabatic capillary tube performance with alternative refrigerants. *ASHRAE Transactions*, 102(2):52-64.

BITTLE, R.R., WOLF, D.A., PATE, M.B. 1998. A generalized performance prediction method for adiabatic capillary tubes. *International Journal of Heating, Ventilating, Air-Conditioning and Refrigerating Research*, 4(1):27-43; Jan.

BRAUN, J.E., KLEIN, S.A., MITCHELL, J.W. 1989. Effectiveness models for cooling towers and cooling coils. *ASHRAE Transactions*, 95(2):164-174.

CHIANG, R. 1993. Heat transfer and pressure drop during evaporation and condensation of refrigerant-22 in 7.5 mm and 10 mm diameter axial and helical grooved tubes. *Heat Transfer – Atlanta, AIChE Symposium Series*, 89(295):205-210.

CHANG, Y-J., HSU, C.T., WANG, C-C. 1996. Single-tube performance of condensation of R-134a on horizontal enhanced tubes. *ASHRAE Transactions*, 102(1):821-829.

CHEN, Z.H., LI, R.Y., CHEN, A.Y. 1990. A correlation for metastable flow of R-12 through capillary tubes. *ASHRAE Transactions*, 90(1):550:554.

CHOUDHURY, D., KARKI, K.C. 1991. Laminar mixed convection in a horizontal eccentric annulus. *ASME, Mixed Convection Heat Transfer*, 163:45-52.

CHRISTENSEN, R.H., SRINIVASAN, V. 1991. Spirally-fluted tubes and enhanced tubes in confined crossflow. Part I: Flow inside fluted tubes. Final Report. The Ohio State University.

CHRISTENSEN, R.H., SRINIVASAN, V. 1991. Spirally-fluted tubes and enhanced tubes in confined crossflow. Part II: Fluted-tube annuli. Final Report. The Ohio State University.

CONDE. M.R. 1996. An advanced simulation model for direct expansion evaporator coils. *5th IEA Heat Pump Conference*, Toronto.

DABIRI, A.E., RICE, C.K. 1981. A compressor simulation model with corrections for the level of suction gas superheat. *ASHRAE Transactions*, 87(2):771-782.

DAS, S.K. 1993. Water flow through helical coils in turbulent condition. *The Canadian Journal of Chemical Engineering*, 71:971-973, Dec.

ECKELS, S.J., PATE, M.B. 1990. A comparison of R-134a and R-12 in-tube heat transfer coefficients based on existing correlations. *ASHRAE Transactions*, 96(1):256-265.

ECKELS, S.J., DOERR, T.M., PATE, M.B. 1994. In-tube heat transfer and pressure drop of R-134a and ester lubricant mixtures in a smooth tube and a micro-fin tube: part II – condensation. *ASHRAE Transactions*, 100(2):283-294.

GORASIA, J.N., DUBEY, N., JAIN, K.K. 1991. Computer-aided design of capillaries of different configurations. *ASHRAE Transactions*, 97(1):132-138.

GREEN, R.H., ROBERTS, L. 1996. The effect of air-coil design on the performance of heat pumps and air conditioners. *ASHRAE Transactions*, 102(1):257-265.

GREYVENSTEIN, G.P. 1988. A computer simulation model for the design and optimization of heat pumps and refrigeration systems. *Suid-Afrikaanse Tydskrif vir Wetenskap*, 84:494-502, Jun.

JUNG, D.S., RADERMACHER, R. 1991. Prediction of heat transfer coefficients of various refrigerants during evaporation. *ASHRAE Transactions*, 97(2):48-53.

KIM, R.H. 1987. Computer-aided design of a capillary tube for the expansion valve of the refrigeration machine. *ASHRAE Transactions*, 93(2):1362-1370.

KOIZUMI, H., YOKOYAMA, K. 1980. Characteristics of refrigerant flow in a capillary tube. *ASHRAE Transactions*, 86(2):19-27.

KUEHL, S.J., GOLDSCHMIDT, V.W. 1991. Modeling of steady flows of R-22 through capillary tubes. *ASHRAE Transactions*, 97(1):139-148.

MACARTHUR, J.W. 1984. Analytical representation of the transient energy interactions in vapor compression heat pumps. *ASHRAE Transactions*, 90(1B):982-996.

ORTH, L.A., ZIETLOW, D.C., PEDERSEN, C.O. 1995. Predicting refrigerant inventory of R-134a in air-cooled condensers. *ASHRAE Transactions*, 101(1):1367-1375.

PROTENSKO, V.P., SAFONOV, V.K. 1987. A method for optimizing an air-to-air heat pump unit. *Power Engineering*, 25(4):135-141.

RICHARDS, D.E., GRANT, M.M. 1987. Turbulent flow and heat transfer inside doubly-fluted tubes. *ASHRAE Transactions*, 93(2):2011-2026.

SCHLAGER, L.M., PATE, M.B., BERGLES, A.E. 1988. Evaporation and condensation of refrigerant-oil mixtures in a smooth tube and a micro-fin tube. *ASHRAE Transactions*, 94(1):149-166.

SCHULZ, U.W. 1985. State of the art: the capillary tube for, and in, vapor compression systems. *ASHRAE Transactions*, 91(1A):92-105.

SCHULZ, U.W. 1988. A correlation of experimental exit pressures for refrigeration flow through a capillary tube expansion device. *ASHRAE Transactions*, 94(1):507-519.

SHAH, M.M. 1979. A general correlation for heat transfer during film condensation inside pipes. *International Journal of Heat and Mass Transfer*, 22:547-556.

SHAH, M.M. 1981. Heat transfer during film condensation in tubes and annuli: a review of the literature. *ASHRAE Transactions*, 87(1):1086-1105.

SINGH, A., OHADI, M.M., DESSIATOUN, S.V. 1996. Empirical modeling of stratified-wavy flow condensation heat transfer in smooth horizontal tubes. *ASHRAE Transactions*, 102(2):597-603.

STEFANUK, N.B.M., APLEVICH, J.D., RENKSIZBULUT, M. 1992. Modeling and simulation of a superheat-controlled water-to-water heat pump. *ASHRAE Transactions*, 98(2):172-184.

TRAVISS, D.P., ROHSENOW, W.M., BARON, A.B. 1972. Forced convection condensation inside tubes: a heat transfer equation for condenser design. *ASHRAE Transactions*, 79(1):157-165.

WANG, C-C., CHIANG, C-S., LIN, S-P. 1997. Two-phase flow pattern for R-134a inside a 6.5-mm (0.25-in.) smooth tube. *ASHRAE Transactions*, 103(1):803-812.

YASUDA, H., TOUBER, S., MACHIELSEN, C.H.M. 1983. Simulation model of a vapor compression refrigeration system. *ASHRAE Transactions*, 89(2A):408-425.

CHAPTER 3

THEORETICAL BACKGROUND

CHAPTER 3

THEORETICAL BACKGROUND

3.1 Introduction

Before the micro heat pump simulation model could be developed, it was necessary to gain a full understanding of the theory governing the heat pump cycle. This chapter considers the relevant theory and governing equations that influence the development of the micro heat pump simulation.

The theory will be divided into sections for each of the main components, namely:

- Fluted tube condenser model.
- Air-cooled evaporator model.
- Reciprocating compressor model.
- Capillary tube model.
- Heat pump cycle simulation.

3.2 Fluted tube condenser

The theory governing the fluted tube condenser is divided into the following subsections:

- General theory.
- Effectiveness-Ntu method.
- Fluted tube geometry.
- Heat transfer coefficients.
- Pressure drop through condenser.

3.2.1 General theory

The refrigerant-to-water heat exchanger for condensing the refrigerant forms an important component of the micro heat pump cycle. One reason for this is that the effectiveness of heat exchange in the condenser influences the overall effectiveness of the heat pump cycle. It is desirable to keep the temperature difference, ΔT, between the refrigerant and the water in the condenser as small as possible. This leads to a lowering in the ΔT over which heat must be transferred and thus to an increase in the coefficient of performance (COP). The type of water heat exchanger used in the micro heat pump cycle is a fluted tube heat exchanger, with water in the centre in counter-flow with the refrigerant in the twisted annulus. Figures 3.1 and 3.3 illustrate the heat exchanger geometry.

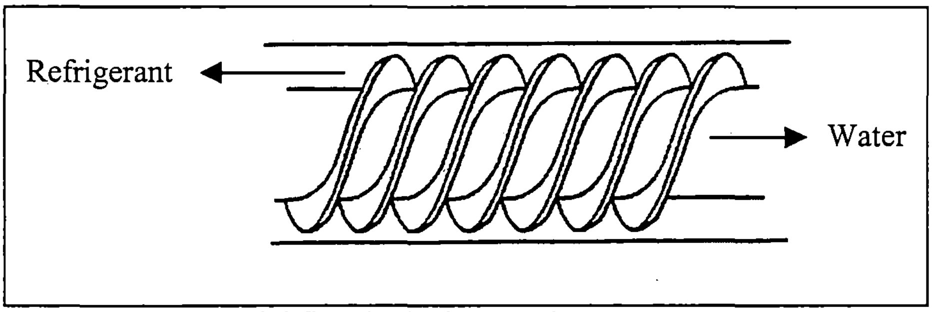

Figure 3.1: Co-axial fluted tube heat exchanger

Fluted tube condensers are able to produce high heat transfer coefficients on both sides of the transfer surface by enhancing the flow conditions for both sides. The water heat transfer coefficient is improved by micro-circulation of the water without a significant increase in the pressure drop. Heat transfer in the annulus is improved by the following two phenomena. In the first instance the condensate is drawn towards the corners of the channels by surface tension, clearing the remaining surface in contact with the hot gas. Secondly, the liquid phase experiences some micro-circulation, particularly towards the outlet side, leading to the replacement of cold liquid next to the surface with hotter liquid. This leads to only a relatively small increase in the pressure drop.

In the condenser a counter-flow arrangement is used to obtain the maximum heat transfer where it is possible to achieve outlet water temperatures above the condensing temperature and approaching the superheat temperature of the refrigerant gas. This is illustrated in Figure 3.2 where the inlet cold water is at T_{w1} and the hot outlet water is at T_{w4}. It is clear that T_{w4} is higher than the refrigerant condensing temperature, which is between T_{r2} and T_{r3}.

The reason for the refrigerant being subcooled (T_{r4}), is that this leads to a lower enthalpy and quality at the entrance to the evaporator. This means that more heat transfer can take place in the evaporator.

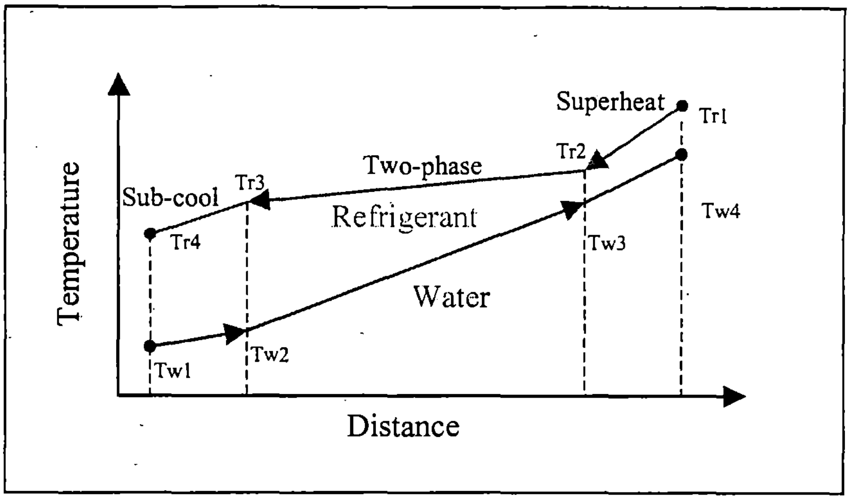

Figure 3.2: Temperature change in condenser

The refrigerant charge inventory for the condenser in our application is based on the theory that the fraction of liquid inside the condenser is constant for a specific heat pump over a wide range of conditions. This is done instead of determining the void fractions as described by Orth (1995:1367). Measurement of the degree of subcooling for a range of test data yields the average liquid fraction that can be used during simulation of the condenser.

Fluted tube heat exchangers pose a problem when it comes to modelling because of the following:

- The complexity of two-phase heat exchange on the refrigerant side.
- There are also two zones of single-phase heat transfer namely the superheated and subcooled zones.
- The geometry of the fluted tube is complex and very little work has been done on two-phase and single-phase heat transfer relations for these geometries.

All the above problems will be solved in the following sections.

3.2.2 Effectiveness-Ntu method

In the literature (Incropera & De Witt, 1990:658-666) there are two main methods for solving the heat transfer in a heat exchanger, namely:

- Effectiveness-Ntu method.
- Log mean temperature difference (LMTD) method.

The LMTD approach to heat-exchanger analysis is useful when the inlet and outlet temperatures are known or are easy to determined.

The LMTD is then easily calculated and the heat flow surface area or overall heat-transfer coefficient may be determined. When the inlet or exit temperatures are to be evaluated for a given heat exchanger, the analysis frequently involves an iterative procedure because of the logarithmic function in the LMTD. The problem this entails is that for certain estimated values or iteration values the logarithmic function is calculated for a negative value.

In these cases the analysis is performed more easily by utilising a method based on effectiveness of the heat exchanger in transferring a given amount of heat. The effectiveness-Ntu method also offers many advantages for analysis of problems in which a comparison between various types of heat exchangers must be made for purpose of selecting the type best suited to accomplish a particular heat-transfer objective.

With the outlet conditions in the condenser unknown, it was decided to use the effectiveness-Ntu method rather than the LMTD method. Both methods will give correct solutions, but it was felt that the effectiveness-Ntu method might be more appropriate for our implementation. The effectiveness-Ntu method will be discussed in detail in the following part of this section, as found in the literature (Incropera & De Witt, 1990:658).

The equation for the number of transfer units (Ntu) relative to the outside surface area is given by

$$Ntu = \frac{U.A_o}{(\dot{m}.c_p)_{min}}. \tag{3.2.1}$$

The overall heat transfer coefficient (U) is given by

$$U = \frac{1}{A_o\left(\frac{1}{A_i.h_i} + \frac{\ln\left(\frac{d_o}{d_i}\right)}{2\pi kL} + \frac{1}{A_o.h_o}\right)}. \tag{3.2.2}$$

$(\dot{m}.c_p)_{min}$ is the smallest of either the refrigerant $(\dot{m}.c_p)_{refrigerant}$ and the water $(\dot{m}.c_p)_{water}$, where $\dot{m}$ is the mass flow rate and c_p the specific heat.

The maximum value $(\dot{m}.c_p)_{max}$ of either the refrigerant or the water can also be determined. These two values can be written as a ratio equation

$$(\dot{m}.c_p)_{ratio} = \frac{(\dot{m}.c_p)_{min}}{(\dot{m}.c_p)_{max}}. \tag{3.2.3}$$

The effectiveness equation for counter-flow is given in the literature (Incropera & De Witt, 1990:661) as

$$\varepsilon = \frac{1-\exp\left(-Ntu\left(1-\left(\dot{m}\,Cp\right)_{ratio}\right)\right)}{1-\left(\dot{m}\,Cp\right)_{ratio}.\exp\left(-Ntu\left(1-\left(\dot{m}\,Cp\right)_{ratio}\right)\right)}. \tag{3.2.4}$$

During condensation in the two-phase region the refrigerant temperature stays essentially constant, thus acting as if it had infinite specific heat. There exist a temperature drop through the two-phase region due to a pressure drop, but the temperature stays essentially constant. For the two-phase region $(\dot{m}.c_p)_{ratio} \rightarrow 0$ and all the heat exchanger effectiveness relations approach a simple equation given by

$$\varepsilon = 1 - e^{-NTU}. \tag{3.2.5}$$

The effectiveness is also given by:

$$\varepsilon = \frac{q}{q_{max}} \tag{3.2.6}$$

with the maximum possible heat transfer determined by

$$q_{max} = (\dot{m}.c_p)_{min}.\Delta T_{max}. \tag{3.2.7}$$

The heat transfer (q) can be determined from the waterside or the refrigerant side and is given by:

$$q = (\dot{m}.c_p)_w.\Delta T_w \tag{3.2.8}$$

and

$$q = \dot{m}_r.\Delta h_r. \tag{3.2.9}$$

The above equations can easily be implemented into a fluted tube condenser model. The integrated simulation model will be described in the next chapter. To find a solution for the above equations, the factors having an influence on the heat transfer and area have to be discussed.

3.2.3 Fluted tube geometry

As stated earlier, the geometry of a fluted tube is quite complicated. Most of the work in this section is based on work conducted by Prof. G.P. Greyvenstein of the PU for CHE. Figure 3.3 shows a cross-sectional view of a fluted tube heat exchanger which will be used in the rest of this section together with Figure 3.1.

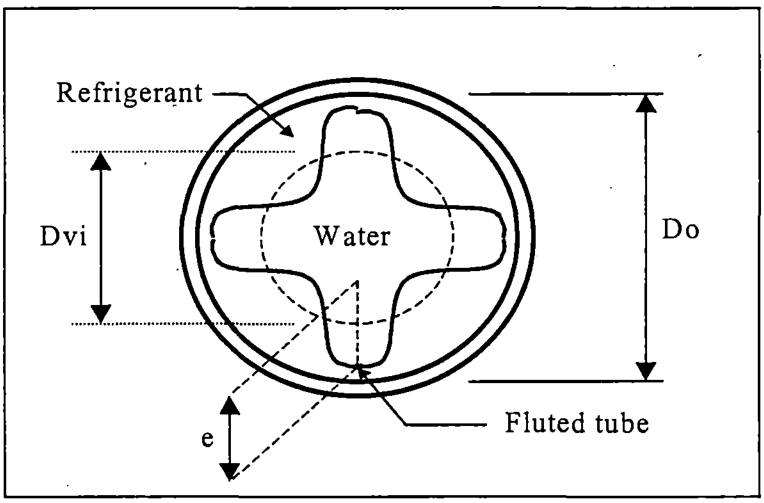

Figure 3.3: Fluted tube geometry

Due to the shape of the fluted tube is it difficult to determine the inside diameter. The diameter is rather given in terms of the volume inside the tube.

Volume based inside diameter:

$$D_{vi} = \sqrt{\frac{4.Vol}{\pi.L}} \qquad (3.2.10)$$

where Vol = volume inside tube.

The same problem exists with regard to the outside diameter of the fluted tube. If the volume based inside diameter were known, the outside diameter can be determined by:

Volume based outside diameter:

$$D_{vo} = D_{vi} + 2.t \qquad (3.2.11)$$

where

t = tube wall thickness.

With the volume based inside diameter known, the flow area can be determined.

Flow area tube side:

$$A_i = \frac{\pi D_{vi}^2}{4}. \tag{3.2.12}$$

With the inside diameter of the outside tube known, the annulus flow area can be determined.

Flow area annulus side:

$$A_o = \frac{\pi\left(D_o^2 - D_{vo}^2\right)}{4} \tag{3.2.13}$$

where

D_o = inner diameter of the outside tube.

The Reynolds number of the inner fluid flow can be determined from the volume based inside diameter and the velocity of the fluid.

Reynolds number tube side:

$$Rey = \frac{\rho.V.D_{vi}}{\mu} \tag{3.2.14}$$

where

V = velocity based on A_i.

The Reynolds number inside the annulus is determined by means of the hydraulic diameter.

Reynolds number annulus side:

$$Rey = \frac{\rho.V.D_h}{\mu} \tag{3.2.15}$$

where

V = velocity based on A_o

D_h = hydraulic diameter given by

$$D_h = D_o - D_{vo}.$$

To determine the inside heat transfer coefficient, Christensen and Srinivasan (1991:61) give an equation, which uses non-dimensional parameters. The parameters are as follows:

The first non-dimensional parameter is the non-dimensional flute depth, which is a function of the measured depth of any flute.

Non-dimensional flute depth:

$$e^* = \frac{e}{D_{vi}} \tag{3.2.16}$$

where

e = flute depth.

The second non-dimensional parameter is a function of the flute pitch.

Non-dimensional flute pitch:

$$p^* = \frac{p}{D_{vi}} \tag{3.2.17}$$

where

p = flute pitch, defined as the axial distance between any two adjacent flutes.

The third non-dimensional parameter is the non-dimensional helix angle.

Helix angle:

This is the effective angle of the flow in the flute with respect to the centre axis of the tube as shown in Figure 3.4. Therefore for every distance πD that the flow has moved perpendicular to the axis, it also moves a distance N.p along the axis.

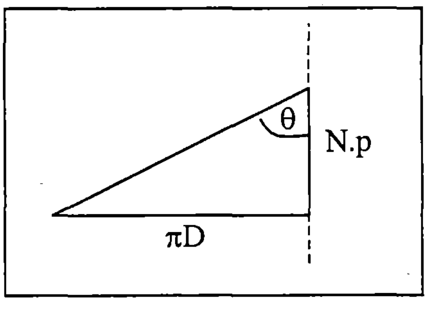

Figure 3.4: Helix angle

Thus the helix angle is given by:

$$\theta = \arctan\left(\frac{\pi D_{vo}}{N.p}\right) \quad (3.2.18)$$

where

N = number of flute starts at any cross section.

Non-dimensional helix angle:

$$\theta^* = \frac{\theta}{90} \quad (3.2.19)$$

Fluted tube annulus radius ratio:

The diameters in the annulus can also be written as a ratio.

$$r^* = \frac{D_{vo}}{D_o} \quad (3.2.20)$$

Equation 3.2.10 to equation 3.2.20 are used when the geometry of the fluted tube is determined, given that the flute depth and pitch are known. In the next sections the geometry will be used to determine the pressure drop and the heat transfer coefficients.

3.2.4 Refrigerant pressure drop

The refrigerant pressure drop can be divided into a two-phase pressure drop and a single phase pressure drop.

Two-phase refrigerant pressure drop:

The two-phase pressure drop is determined by a technique used by Christensen and Srinivasan (1991:82)

$$\Delta p = 0.09.Rey_v^{-0.2}.x^{1.8}\left[1 + 2.85\left(\mu_x^{-0.1}\left(\frac{1-x}{x}\right)^{0.9}\rho_x^{0.5}\right)^{0.523}\right]^2.\frac{G^2}{\rho D_{ho}} \quad (3.2.21)$$

The friction factor is determined with the technique described by Das (1993:972).

$$fsc = 0.079.Rey_v^{-0.25} + 0.075\left(\frac{D_{ho}}{d_{coil}}\right)^{0.5} \quad (3.2.22)$$

$$ff = fsc + 17.5782.Rey_v^{-0.3137}\left(\frac{D_{ho}}{d_{coil}}\right)^{0.3621}\left(\frac{e}{D_{ho}}\right)^{0.6885} \quad (3.2.23)$$

where $d_{coil} = \dfrac{D_{hi}}{\sin\left(\theta^{*}.\dfrac{\pi}{2}\right)}$. (3.2.24)

To determine the influence of the friction on the pressure drop, the following equations is used.

$$ff = ff*4 \qquad (3.2.25)$$

$$y = \ln\left(\frac{5.74}{Rey_v^{\,0.9}}\right) \qquad (3.2.26)$$

$$ratio = \frac{ff}{\left(\dfrac{0.25}{y^2}\right)} \qquad (3.2.27)$$

The pressure drop is multiplied by the ratio.

$$\Delta p = \Delta p * ratio \qquad (3.2.28)$$

The above pressure drop includes pressure due to the increased friction with the fluted tube.

Single-phase refrigerant pressure drop:

The friction factor is determined with the technique described by Das (1993:972).

$$fsc = 0.079.Rey_v^{-0.25} + 0.075\left(\frac{D_{ho}}{d_{coil}}\right)^{0.5} \qquad (3.2.29)$$

$$ff = fsc + 17.5782.Rey_v^{-0.3137}\left(\frac{D_{ho}}{d_{coil}}\right)^{0.3621}\left(\frac{e}{D_{ho}}\right)^{0.6885} \qquad (3.2.30)$$

$$ff = ff*4 \qquad (3.2.31)$$

The pressure drop is then determined by the following equation.

$$\Delta p = \frac{ff.L.\rho.V^2}{2.D_{ho}} \qquad (3.2.32)$$

where

V = velocity

The above equations can be implemented into a fluted tube model to determine the pressure drop in the refrigerant for both the two-phase and the single-phase regions.

3.2.5 Heat transfer coefficients

The heat transfer coefficients can be divided into the outside and inside heat transfer coefficient. The outside heat transfer coefficient on the refrigerant side can further be divided into a two-phase heat transfer coefficient and a single-phase heat transfer coefficient.

Inside heat transfer coefficient:

The inside heat transfer coefficient is determined by the technique of Christensen and Srinivasan (1991:61).

The inside Reynolds number is a function of the inside hydraulic diameter. For fluted tubes the inside hydraulic diameter is equal to the volume-based inside diameter.

$$Rey = \frac{\rho.V.D_{hi}}{\mu} \tag{3.2.33}$$

If Rey is lower than 5000:

$$Nu = 0.014.Rey^{0.842}\left(e^{*}\right)^{-0.067}\left(p^{*}\right)^{-0.293}\left(\theta^{*}\right)^{-0.705}Pr^{0.4} \tag{3.2.34}$$

else

$$Nu = 0.064.Rey^{0.773}\left(e^{*}\right)^{-0.242}\left(p^{*}\right)^{-0.108}\left(\theta^{*}\right)^{0.599}Pr^{0.4} \tag{3.2.35}$$

where the non-dimensional parameters are determined as discussed in paragraph 3.2.3.

The Prandtl number is determined by

$$Pr = \frac{c_p.\mu}{k} \tag{3.2.36}$$

With the above equations the inside heat transfer coefficient can be determined:

$$h_i = \frac{Nu.k}{D_{hi}} \tag{3.2.37}$$

Outside Two-Phase Heat Transfer Coefficient:

To determine the two-phase heat transfer coefficient, a technique used by Shah (1979:547) is implemented. The liquid heat transfer is determined by the Dittus-Boelter equation.

$$ho_{liq} = 0.023.Rey_{liq}^{\ 0.8}.Pr^{0.4}.\frac{k_{liq}}{D_{ho}} \tag{3.2.38}$$

The correlation of Shah (1979:548) was then implemented to obtain the two-phase heat transfer.

$$ho_{tpc} = ho_{liq}\left[(1-x)^{0.8} + \frac{3.8.x^{0.76}(1-x)^{0.04}}{pr^{0.38}}\right] \tag{3.2.39}$$

where

x = quality

$$pr = \frac{\text{actual pressure}}{\text{critical pressure}}$$

Outside single-phase heat transfer coefficient:

In the single phase the Dittus-Boelter equation is used to obtain the heat transfer coefficient.

Superheat:

$$ho = 0.023.Rey^{0.8}.Pr^{0.3}.\frac{k}{Dh_o} \tag{3.2.40}$$

Because of a fluted tube geometry, the Dittus-Boelter equation had to be modified to incorporate the increased friction as determined by equation 3.2.27.

$$\text{friction ratio} = 0.25(\text{ratio} - 1) + 1 \tag{3.2.41}$$

The heat transfer coefficient is multiplied by the ratio determined from the friction factor.

$$ho = ho * \text{ratio} * \text{enhancement factor.} \tag{3.2.42}$$

The enhancement factor is a constant value supplied by the manufacturers, and for fluted tubes is in the order of 1.15.

Subcool:

$$ho = 0.023.Rey^{0.8}.Pr^{0.3}.\frac{k}{Dh_o} \tag{3.2.43}$$

The enhancement factor is a constant value supplied by the manufacturers, and for fluted tubes is in the order of 1.15.

$$ho = ho * \text{enhancement factor} \tag{3.2.44}$$

3.2.6 Summary

With the above theory a simulation model could be developed for the simulation of fluted tube heat exchangers. The model will incorporate both single-phase and two-phase properties of the refrigerant. The heat transfer coefficients and pressure drop can be implemented as shown above. In the next chapter a detailed discussion follows on how the theory and its equations were implemented into the condenser model.

3.3 Air-cooled evaporator

As stated in Chapter 2, the evaporator design will be based on the technique described by Braun **et al.**, (1989:170-173) which used the effectiveness-Ntu method. The model is fundamental because it used first law governing equations. Their model took into account the effect of a dry coil or a wet coil, and a combination of both. Their model was initially developed for water flowing in the tubes. However, it will be adapted here for the heat transfer of R-134a inside the evaporator by making use of the correlation of Shah (Eckels & Pate, 1994:264) for the inside heat transfer coefficient.

The use of multi-pass cross-flow geometry complicates the analysis of cooling coils. However, as the number of passes increases beyond about four, the performance of a cross-flow heat exchanger approaches that of counter-flow. For our application the evaporator will be regarded as a cross-flow heat exchanger because it will be divided into smaller cross-flow sections, as will be discussed in Chapter 4.

The equation for the number of transfer units (Ntu) relative to the outside surface area is given by

$$Ntu = \frac{U.A_o}{(\dot{m}.c_p)_{min}}. \tag{3.3.1}$$

The overall heat transfer coefficient is determined at the outside surface of the air coil. It is given by:

$$U = \frac{1}{A_o\left(\frac{1}{A_i.h_i} + \frac{\ln\left(\frac{d_o}{d_i}\right)}{2\pi kL} + \frac{1}{A_o.h_o.\eta_o}\right)}. \tag{3.3.2}$$

Where

η_o = overall fin efficiency.

$(\dot{m}.c_p)_{min}$ is the smallest of either the refrigerant $(\dot{m}.c_p)_{refrigerant}$ and the air $(\dot{m}.c_p)_{air}$, where $\dot{m}$ is the mass flow rate and c_p the specific heat.

The maximum value $(\dot{m}.c_p)_{max}$ of either the refrigerant or the air can also be determined. These two values can be written as a ratio equation

$$(\dot{m}.c_p)_{ratio} = \frac{(\dot{m}.c_p)_{min}}{(\dot{m}.c_p)_{max}}. \tag{3.3.3}$$

If $(\dot{m}.c_p)_{refrigerant}$ is equal to $(\dot{m}.c_p)_{min}$ the effectiveness equation for cross-flow is given by

$$\varepsilon = 1 - \exp\left(\frac{-1 + \exp(-Ntu(\dot{m}.c_p)_{ratio})}{(\dot{m}.c_p)_{ratio}}\right). \tag{3.3.4}$$

If $(\dot{m}.c_p)_{air}$ is equal to $(\dot{m}.c_p)_{min}$ the effectiveness equation for cross-flow is given by

$$\varepsilon = \frac{1 - \exp((-1 + \exp(-Ntu))(\dot{m}.c_p)_{ratio})}{(\dot{m}.c_p)_{ratio}}. \tag{3.3.5}$$

During evaporation in the two-phase region the refrigerant temperature stays essentially constant thus acting as if it had infinite specific heat. Through the two-phase region there exist a temperature drop due to a pressure drop, but the temperature stays essentially constant.

The effectiveness is also given by:

$$\varepsilon = \frac{q}{q_{max}} \tag{3.3.6}$$

with the maximum possible heat transfer determined by

$$q_{max} = (\dot{m}.c_p)_{min}.\Delta T_{max}. \tag{3.3.7}$$

The heat transfer (q) can be determined from the refrigerant side by:

$$q = \dot{m}_r.\Delta h_r\,. \tag{3.3.8}$$

The air side can be divided into a dry coil heat transfer and a wet coil heat transfer, which will be discussed below.

3.3.1 Dry coil heat transfer

If the coil surface temperature at the outlet were found to be greater than the dew point of the incoming air, the coil is completely dry throughout. Standard heat exchanger effectiveness relationships then apply. The dry coil heat transfer rate is

$$\dot{Q}_{dry} = \dot{m}_a c_{pa} \Delta T\,. \tag{3.3.9}$$

The exit air humidity ratio is equal to the inlet value, while the exit air and refrigerant temperatures are determined from energy balances on the flow stream.

3.3.2 Wet coil heat transfer

If the coil surface temperature at the inlet were found to be less than the dew point of the incoming air, the coil is completely wet and dehumidification occurs throughout. For a completely wet coil the heat transfer rate is equal to:

$$\dot{Q}_{wet} = \dot{m}\Delta h \tag{3.3.10}$$

3.3.3 Overall heat transfer coefficient

The overall heat transfer coefficient is determined at the outside surface of the air coil. It is given by:

$$U = \frac{1}{A_o\left(\frac{1}{A_i.h_i} + \frac{\ln\left(\frac{d_o}{d_i}\right)}{2\pi kL} + \frac{1}{A_o.h_o.\eta_o}\right)}\,. \tag{3.3.11}$$

Where

η_o = overall fin efficiency,

Inside single phase heat transfer coefficient:

The inside single phase heat transfer coefficient is determined by the Dittus-Boelter equation.

$$h_i = 0.023.Rey^{0.8}.Pr^{0.4}\left(\frac{k_l}{di}\right) \tag{3.3.12}$$

Inside two-phase heat transfer coefficient:

The inside two-phase heat transfer coefficient is determined by the correlation of Shah (Eckels & Pate,1990:264), with the correlation being:

$$\Psi = \frac{h_{TP}}{h_l}. \tag{3.3.13}$$

where h_l is the traditional Dittus-Boelter correlation. The parameter Ψ can be found from equations which are functions of the boiling number, Bo, and the convection number, Co. Ψ can be determined from the largest value of Ψ_{nb}, Ψ_{cb}, or Ψ_{bs}, as follows:

For $N > 1.0$

$$\Psi_{nb} = 230.Bo^{0.5} \quad \text{for } Bo > 0.3x10^{-4} \tag{3.3.14}$$

$$\Psi_{nb} = 1 + 46.Bo^{0.5} \quad \text{for } Bo < 0.3x10^{-4} \tag{3.3.15}$$

or

$$\Psi_{cb} = \frac{1.8}{N^{0.8}} \tag{3.3.16}$$

For $0.1 < N \leq 1.0$

$$\Psi_{bs} = F.Bo^{0.5}.\exp(2.74\ N^{-0.1}) \tag{3.3.17}$$

For $N \leq 0.1$

$$\Psi_{bs} = F.Bo^{0.5}.\exp(2.74\ N^{-0.15}) \tag{3.3.18}$$

F can be determined from the following:

for $Bo \geq 11x10^{-4}$ then $F = 14.7$

for $Bo < 11x10^{-4}$ then $F = 15.43$.

N can be determined as follows:

For horizontal tubes is N = Co. .

The boiling number (Bo) is given by:

$$Bo = \frac{q}{G.h_{fg}}. \tag{3.3.19}$$

The convection number is given by (Shah, 1979:548):

$$Co = \left(\frac{1}{x} - 1\right)^{0.8} \left(\frac{\rho_g}{\rho_l}\right)^{0.5} \tag{3.3.20}$$

Outside heat transfer coefficient:

When the air coil has fins, their efficiency has an influence on the heat transfer on the outside surface. The theory is explained in Incropera and DeWitt (1990).

$$m_f = \sqrt{\frac{2.h_o}{k.t}} \tag{3.3.21}$$

where

t = fin thickness

Fin efficiency is given by

$$\eta_f = \frac{\tanh(m_f.L_f)}{m_f.L_f}. \tag{3.3.22}$$

The fin efficiency only characterise the performance of a single fin, where the overall surface efficiency characterise an array of fins and the base surface to which the fins are attached. The overall surface efficiency is given by:

$$\eta_o = 1 - \left(\frac{A_f}{A_{tot}}\right)(1 - \eta_f). \tag{3.3.23}$$

The outside heat transfer coefficient is determined from data obtained from Greyvenstein for different types of fin configurations.

For a dry coil:

$$h_o = (Cofd1.Fpi + Cofd2).Va^{Md} \tag{3.3.24}$$

where Cofd1, Cofd2 and Md are coefficients obtained from a fin table.

For a wet coil:

$$h_o = (Cofw1.Fpi + Cofw2).Va^{Mw} \tag{3.3.25}$$

where Cofw1, Cofw2 and Mw are coefficients obtained from a fin table.

3.3.4 Summary

The air-cooled evaporator simulation model will be explained in the next chapter. The model can be implemented with the use of the effectiveness-Ntu method and the heat transfer correlations of Shah. The only part of the model which is dependent on explicit coefficients is the outside heat transfer coefficient, which is dependent on the data available from Greyvenstein.

3.4 Reciprocating compressor

Most compressor simulations until now have worked according to the principle of a data file containing the mass flow rates and power inputs for a certain compressor as supplied by the manufacturers. One example of the above-mentioned method is the simulation of Greyvenstein (1988). An interpolation routine is used to determine the mass flow and input power given the inlet and outlet pressures. The accuracy of the model therefore depends on the accuracy of the performance data supplied by the manufacturers. Two other factors could also influence the accuracy of the compressor model. Firstly, the compressor data usually applies to a value of degree of superheat of approximately 11°C. The second reason is that the refrigerant mass flow and compressor input powers are functions of the inlet and outlet pressures. It is important that these values should be accurately specified. The accuracy of the inlet and outlet pressures is a function of the evaporator and condenser model. In the case of a hermetically sealed compressor it is fair to assume that all the input power is transferred to the refrigerant, either in the form of heat or work.

Due to the fact that insufficient performance data is available for the low capacity reciprocating compressors to be used, it was decided to create a compressor model that can simulate the compressor conditions more accurately.

The following assumptions are made to simplify the model:

- The discharge and suction valve are two-position elements, thus fully open or fully closed, and the dynamic behaviour of the valve plates is not considered.
- A four-phase compressor cycle is assumed, consisting of the phases of suction, compression, discharge, and expansion, in this order only. The model will not account for valve flutter or hammering.
- No pressure pulsation is present in the plenum chamber or suction and discharge lines.

The compressor model will be explained in Figure 3.5, which shows the inside volumes of the compressor.

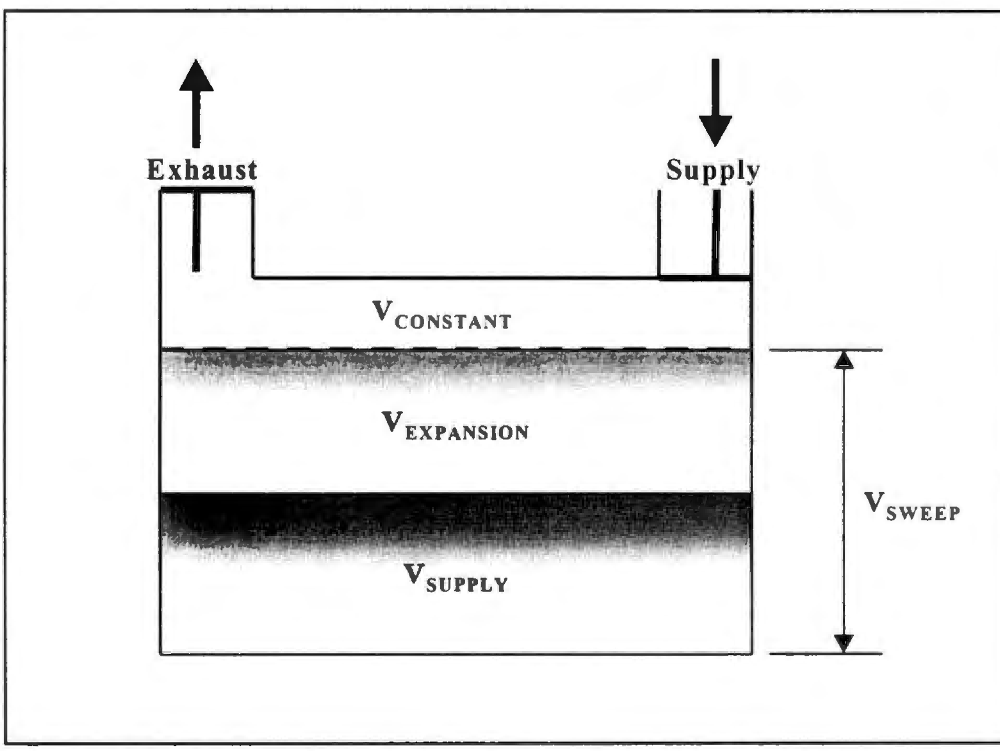

Figure 3.5: Reciprocating compressor

The volume of the compressor can be divided into two parts, namely:

- The constant or dead volume (Vc) of the compressor, that is the highest point the piston can reach at the top of its stroke.
- The sweep volume (Vsw) is the swept of the piston which can be divided into the following two regions.
    - The expansion volume (Ve).
    - The actual supply volume (Vsu) of refrigerant which enters the compressor.

The only new refrigerant which is supplied to the compressor is V_{SU}, which can be calculated from

$$V_{SU} = V_{SW} - V_E. \tag{3.4.1}$$

An assumption is made that the process is polytropic, or adiabatic and reversible, which means that work stays constant throughout the process, given by

$$W = PV^{\gamma} = \text{constant}. \tag{3.4.2}$$

The outlet (ex) must be equal to the inlet (su) for the above equation to comply, thus

$$P_{ex}V_C^{\gamma} = P_{su}(V_E + V_C)^{\gamma}. \tag{3.4.3}$$

Rearranging the equation yields

$$\frac{V_E + V_C}{V_C} = \left(\frac{P_{ex}}{P_{su}}\right)^{\frac{1}{\gamma}}. \tag{3.4.4}$$

Or in terms of V_E

$$V_E = V_C\left[\left(\frac{P_{ex}}{P_{su}}\right)^{\frac{1}{\gamma}} - 1\right]. \tag{3.4.5}$$

Because of a constant mass flow the specific volume at the inlet and outlet must also hold.

$$P_{ex}v_{ex}^{\gamma} = P_{su}v_{su}^{\gamma}. \tag{3.4.6}$$

Rearranging equation 3.4.6, yields

$$\frac{P_{ex}}{P_{su}} = \left(\frac{v_{su}}{v_{ex}}\right)^{\gamma}. \tag{3.4.7}$$

Substitute equation 3.4.7 into equation 3.4.5 to obtain an equation of V_E in terms of specific volume:

$$V_E = V_C\left[\frac{v_{su}}{v_{ex}} - 1\right]. \tag{3.4.8}$$

Substituting equation 3.4.8 into equation 3.4.1 yields:

$$V_{SU} = V_{SW} - V_C\left(\frac{v_{su}}{v_{ex}} - 1\right). \tag{3.4.9}$$

Equation 3.4.9 can also be written in terms of volume flow $\left(\frac{m^3}{s}\right)$:

$$\dot{V}_{SU} = N\left[V_{SW} - V_C\left(\frac{v_{su}}{v_{ex}} - 1\right)\right] \quad \left[\frac{m^3}{s}\right]. \tag{3.4.10}$$

With $\dot{V}_{SU}$ and the density of the supply gas known, the mass flow rate can be calculated from:

$$\dot{m}_r = \frac{\dot{V}_{su}}{\rho_{SU}} \tag{3.4.11}$$

For a given compressor the frequency N is known and v_{SU} and v_{EX} can be calculated at the inlet and outlet conditions of the compressor. With the aid of an iteration process the sweep volume (V_{SW}) and the dead volume (Vc) can be calculated for a given compressor.

With the compressor model not only the mass flow rate can be determined, but also the work on the refrigerant given by:

$$\dot{W}_{cp} = \dot{m}\Delta h. \tag{3.4.12}$$

The exit enthalpy can be determined for the isentropic efficiency of the compressor given by:

$$\eta_s = \frac{h_{out,s} - h_{in}}{h_{out} - h_{in}}. \tag{3.4.13}$$

3.4.1 Summary

When the compressor model is used in the simulation programme, the inlet conditions will be known from the evaporator outlet. With Vc and V_{SW} known for the specified compressor, the mass flow rate and the outlet conditions of the compressor can be determined.

3.5 Capillary tube

Capillary tubes have found universal acceptance as expansion devices in refrigerating and air-conditioning units due to their simplicity, reliability and low cost. Capillary tubes have no moving parts, unlike thermostatic expansion valves. With the availability of more versatile compressors, better refrigerants, and leak-proof systems, the use of capillary tubes has become more popular. Capillary tubes provide the required pressure drop between the condenser and the evaporator and regulate the mass flow rate to meet the demands on the system. The negative side to the use of a capillary tube is that it cannot cope with large variable-load conditions and operates at maximum efficiency only at one set of operating conditions. At all other conditions, their efficiency is somewhat less than maximum. However, it should be kept in mind that capillary tubes are to some extent self-compensating devices. If properly designed and applied, will give satisfactory performance over a reasonable range of operating conditions. The simplicity of the capillary tube gives it the advantage of reduced cost.

Every refrigerating unit requires a pressure-reducing device to meter the flow of refrigerant to the low side in accordance with the demands placed on the system. The capillary operates on the principle that liquid passes through it much more readily than gas. It consists of a small diameter line, which connects the outlet of the condenser to the inlet of the evaporator. If properly sized for the application, the capillary compensates automatically for load and system variations and gives acceptable performance over a wide range of operating conditions.

Due to the nature of the type of heat pump which is going to be designed, it is not appropriate to use an expansion valve. The reason for this is that an expansion valve is too expensive compared to the cost of the total system which must be kept to a minimum. As discussed in Chapter 2, there are two capillary tube models that can be implemented. The first model to be used is based on the theoretical model of Bittle and Pate (1996:52), while the second model is based on the dimensionless correlation of Bittle **et al.**, (1998:27). Their work is very comprehensive and makes use of first order governing equations.

3.5.1 Theoretical model of Bittle and Pate (1996)

The equations that govern capillary tube flow are:

- Continuity equation.
- Conservation of momentum equation.
- Conservation of energy (first law of thermodynamics) equation.

In modelling the flow through the capillary tube the above-mentioned equations as well as the second law of thermodynamics have to be satisfied in the single phase subcooled liquid region and also in the two-phase liquid/vapour region. The following assumptions are made in the development of the model:

- Adiabatic flow with no external work applied.
- Thermodynamic equilibrium through the two-phase region.

- Homogenous two-phase flow.
- Metastable liquid region modelled using the Chen under-pressure model.

Governing equations:

The fundamental equations governing the capillary tube flow are derived for an asymmetric control volume of length ΔL as shown in Figure 3.6.

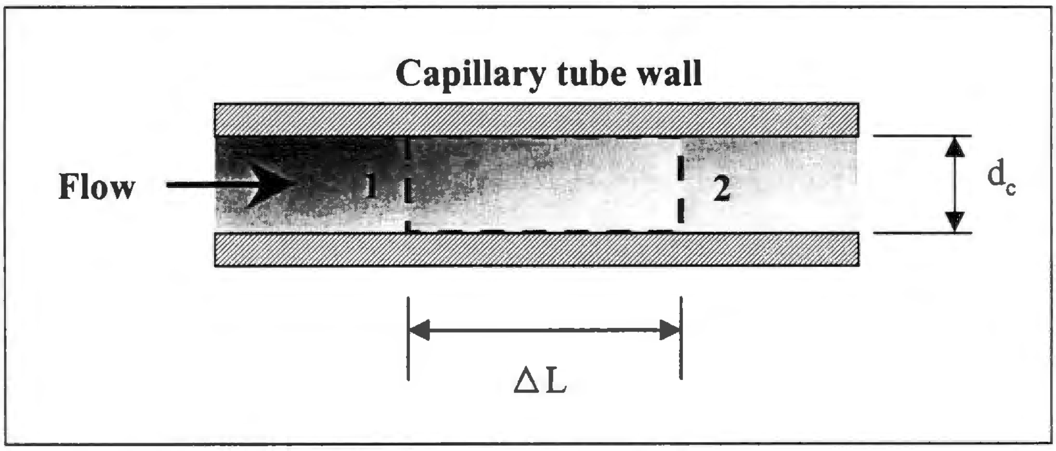

Figure 3.6: Control volume inside capillary tube

Continuity equation:

The integral form of the continuity equation for the control volume is

$$\frac{\partial}{\partial t}\int_{cv} \rho . d\overline{V} + \int_{cs} \rho . \vec{V} . d\vec{A} = 0. \tag{3.5.1}$$

The mass flow rate normal to any cross-section can be written as

$$\dot{m} = \rho \overline{V} A,$$

where $\overline{V}$ is the average velocity across the plane.

For steady flow, equation 3.5.1 can be integrated over the inlet and exit planes shown in Figure 3.6 using the average velocity. The continuity equation then becomes

$$\frac{\overline{V_1} A_1}{\nu_1} = \frac{\overline{V_2} A_2}{\nu_2} \tag{3.5.2}$$

For a capillary tube, the cross-sectional area is assumed to be constant throughout the length of the tube, i.e. $A_1 = A_2$.

In the case of a subcooled liquid region the adiabatic assumption yields a constant liquid temperature which is equal to the inlet temperature. Specific volume is assumed constant, and equation 3.5.2 reduced to

$$\overline{V_1} = \overline{V_2} \tag{3.5.3}$$

Therefore, the average velocity in a capillary tube is constant through the subcooled liquid region.

Momentum equation:

The integral form of the momentum equation in the flow direction is

$$\Sigma F = \frac{\partial}{\partial t}\int_{cv} u\rho d\overline{V} + \int_{cs} u\rho \vec{V}.d\vec{A}. \tag{3.5.4}$$

The steady-state form of the above equation expressed as a pressure drop across the control volume is given by

$$(P_1 - P_2) = \frac{f\Delta L.\overline{V}^2}{2.\nu.d_c} + G(\overline{V}_2 - \overline{V}_1). \tag{3.5.5}$$

Where G is mass flux and f is the internal friction factor given by

$$f = \frac{(dP/dL)_{fric}.d_c}{\frac{1}{2}\rho\overline{V}^2}. \tag{3.5.6}$$

Equation 3.5.5 shows that the total pressure drop is equal to the sum of the pressure drop due to friction and the pressure drop due to flow acceleration.

Through the subcooled liquid region $\overline{V_1} = \overline{V_2}$ and the total pressure drop is only due to friction. Therefore the total pressure drop through the liquid region of length ΔL_{liq} is

$$(P_1 - P_2) = \Delta P_{liq} = \frac{f\Delta L.\overline{V}^2}{2.\nu.d_c} \tag{3.5.7}$$

Through the two-phase region the acceleration component has an influence, because the specific volume is increased as the quality increases. For the two-phase region equation 3.5.5 becomes

$$(P_1 - P_2) = \frac{f_m\Delta L.\overline{V_m}^2}{2.\nu_m.d_c} + G(\overline{V}_2 - \overline{V}_1). \tag{3.5.8}$$

Where $\overline{V_m}$, f_m and ν_m are the average values across the control volume given by

$$\overline{V_m} = \frac{\overline{V_1} + \overline{V_2}}{2}, \tag{3.5.9}$$

$$f_m = \frac{f_1 + f_2}{2}, \tag{3.5.10}$$

$$\nu_m = \frac{\nu_1 + \nu_2}{2}. \tag{3.5.11}$$

Energy equation:

The integral form of the energy equation is

$$\dot{Q} - \dot{W} = \frac{\partial}{\partial t}\int_{cv} e\rho d\overline{V} + \iint_{cs}\left(h + \frac{V^2}{2} + gz\right)\rho\vec{V}.d\vec{A}, \tag{3.5.12}$$

where $\dot{Q}$ is the net heat transfer rate to the control volume and $\dot{W}$ all the work done by the control volume on the surroundings. For adiabatic capillary tube flow, there is no heat transfer or external work. Further assuming steady flow and no elevation change, the energy equation applied to the control volume becomes

$$\left(h_1 + \frac{\overline{V_1}^2}{2}\right) = \left(h_2 + \frac{\overline{V_2}^2}{2}\right). \tag{3.5.13}$$

In the subcooled liquid region $\overline{V_1} = \overline{V_2}$, so that equation 3.5.13 is reduced to

$$h_1 = h_2 \tag{3.5.14}$$

Since the change in enthalpy for a subcooled liquid can be considered to be a function of temperature only, there is no change in refrigerant temperature through the subcooled liquid region.

In the two-phase region the enthalpies and specific volumes are calculated using

$$h = h_f + x(h_g - h_f), \tag{3.5.15}$$

$$\nu = \nu_f + x(\nu_g - \nu_f), \tag{3.5.16}$$

where x is the refrigerant quality in the capillary tube.

Empirical and other model components:

To solve the set of governing equations, several modelling details have to be considered. The following section describes the empirical relations and modelling components incorporated within the overall flow solution.

Friction factor:

The equation for friction factor was developed from a general fit of capillary tube flow data from Kuehl and Goldschmidt (1991:141) with their results for water and secondly nitrogen flow data. Over the entire range of capillary tube flow evaluated, the friction factor was assumed to be a function of only the Reynolds number.

$$f = 0.23.\mathrm{Re}_d^{-0.216} \tag{3.5.17}$$

Entrance correction:

The entrance to the capillary tube can be characterised as a sudden contraction from a 6.35-mm cross-sectional diameter to the capillary tube diameter. Collier and Thome (1994) reported a correlation to calculate the pressure drop associated with a sudden contraction.

$$\Delta P_{entrance} = \frac{G^2}{2\rho_f}\left[\left(\frac{1}{C_c}-1\right)^2+\left(1-\frac{1}{\sigma_A^2}\right)\right]\left[1+\left(\frac{v_g}{v_f}\right)x\right] \tag{3.5.19}$$

where σ_A is the ratio of flow areas before and after the contraction and C_c is given by

$$C_c = 0.54\left(\frac{1}{\sigma_A}\right)^3 - 0.242\left(\frac{1}{\sigma_A}\right)^2 + 0.111\left(\frac{1}{\sigma_A}\right) + 0.585. \tag{3.5.20}$$

For a subcooled inlet condition the quality x in equation 3.5.19 is zero.

Metastable region:

For the case of subcooled inlet conditions, the thermodynamic equilibrium flash-point occurs where the refrigerant pressure is equal to the saturation pressure. Downstream of the flash-point the pressure continues to decrease due to friction and vapour acceleration, which results in a decrease in temperature. An assumption is made that the liquid and vapour are in equilibrium. The flash-point does not actually occur at the location where the pressure is equal to the saturation pressure but is delayed. This results in a liquid region existing at pressure below saturation pressure where thermodynamic equilibrium should not allow a liquid to exist. This region is referred to as a metastable liquid region, or a superheat liquid region.

The effect of the metastable liquid region is that the actual capillary tube flow rate will be greater than the flow rate existing under ideal thermodynamic conditions. Before the flash-point, the liquid experiences a constant pressure drop due to friction alone. After the flash-point in the two-phase region the pressure drop increases rapidly due to both the two-phase friction and vapour acceleration. The pressure drop through the subcooled and two-phase regions is proportional to its contribution to the overall flow resistance within the capillary tube. Since the metastable liquid region increases the liquid length, the length of the two-phase region decreases and the overall resistance to flow is reduced. The existence of the metastable liquid region results in a higher flow rate than under ideal thermodynamic equilibrium conditions.

Chen **et al**., (1990:551) developed a model for metastable flow and predicted under-pressure associated with the delay of vaporisation.

$$\frac{(P_{sat} - P_v)(kT_s)^{0.5}}{\sigma^{1.5}} = 0.679\left(\frac{v_g}{v_g - v_f}\right)\mathrm{Re}^{0.914}\left(\frac{\Delta T_{sc}}{T_{crit}}\right)^{-0.208}\left(\frac{d_c}{D'}\right)^{-3.18} \tag{3.5.21}$$

D' is the reference length given by

$$D' = \left(\frac{kT_s}{\sigma}\right)^{0.5} \mathrm{x}\, 10^4 \tag{3.5.22}$$

Under-pressure (P_{sat} - P_v) is the difference between the saturation pressure corresponding to the liquid temperature and the actual pressure associated with the onset of vaporisation. The correction is applied to the liquid phase only. Once the flash-point location has been established, thermodynamic equilibrium conditions are assumed to exist throughout the two-phase region.

From the above equations for the capillary tube a simulation model can be developed which will be able to predict the outlet conditions accurately when the inlet conditions and the length of the capillary is known.

3.5.2 Dimensionless correlation of Bittle **et al.**, (1998)

It must be noted that for all test data used to develop the performance prediction correlations the exit conditions were choked. Variables that affect the capillary tube flow rate from a practical viewpoint are as follows:

- Capillary tube diameter.
- Tube length.
- Inlet pressure.
- Inlet subcool level or inlet quality.

The exit pressure is not included in the list since choked flow conditions exist in capillary tube flow for typical steady-state applications. For the rest of this discussion the focus will fall on subcooled inlet conditions only, due to the application in the micro heat pump.

Fluid properties which can also be included in the variable list are:

- Specific volume of both the liquid and vapour phases.
- Viscosity of both the liquid and vapour phases.

From the effect of vapour bubble formation and growth on flow, the following variables can be included:

- Heat of vaporisation.
- Liquid surface tension.

Liquid specific heat is included as a variable to make the inlet subcool level non-dimensional. The relationship between mass flow rate and the above-mentioned variables is:

$$\dot{m} = f(d_c, L_c, P_{in}, \Delta T_{sc}, \mu_f, \mu_g, v_f, v_g, c_{pf}, \sigma, h_{fg}) \tag{3.5.23}$$

With the twelve variables shown above, and defining the four repeating variables as d_c, v_f, ΔT_{sc}, and μ_f, the result is eight dimensionless Π-groups. The Π-groups are as follows:

$$\Pi_1 = \frac{L_c}{d_c} \qquad \text{(Geometry)} \tag{3.5.24}$$

$$\Pi_2 = \frac{d_c^2 . h_{fg}}{\nu_f^2 . \mu_f^2} \qquad \text{(Vaporisation)} \qquad (3.5.25)$$

$$\Pi_3 = \frac{d_c . \sigma}{\nu_f . \mu_f^2} \qquad \text{(Bubble growth)} \qquad (3.5.26)$$

$$\Pi_4 = \frac{d_c^2 . P_{in}}{\nu_f . \mu_f^2} \qquad \text{(Inlet pressure)} \qquad (3.5.27)$$

$$\Pi_5 = \frac{d_c^2 . c_{pf} . \Delta T_{sc}}{\nu_f^2 . \mu_f^2} \qquad \text{(Subcool inlet condition)} \qquad (3.5.28)$$

$$\Pi_6 = \frac{\nu_g}{\nu_f} \qquad \text{(Density)} \qquad (3.5.29)$$

$$\Pi_7 = \frac{\mu_f - \mu_g}{\mu_g} \qquad \text{(Viscosity)} \qquad (3.5.30)$$

$$\Pi_8 = \frac{m}{d_c . \mu_f} \qquad \text{(Flow rate)} \qquad (3.5.31)$$

An assumption made by Bittle **et al.**, (1998) was that the dimensionless mass flow rate parameter, Π_8, has a power law dependency on the remaining Π parameters. The power law form was selected because of its successful application in many thermal science problems. Thus

$$\Pi_8 = B\Pi_1^{m1}\Pi_2^{m2}\Pi_3^{m3}\Pi_4^{m4}\Pi_5^{m5}\Pi_6^{m6}\Pi_7^{m7} \qquad (3.5.32)$$

Taking the $\log_{10}$ of both sides of the equation gives:

$$\log_{10}(\Pi_8) = \log_{10}(B) + (m_1)\log_{10}(\Pi_1) + (m_2)\log_{10}(\Pi_2) + \ldots + (m_7)\log_{10}(\Pi_7) \qquad (3.5.33)$$

Define $X_n = \log_{10}(\Pi_n)$ and $b = \log_{10}B$, equation 3.5.33 becomes:

$$X_8 = b + (m_1)X_1 + (m_2)X_2 + \ldots + (m_7)X_7 \qquad (3.5.34)$$

The values $m_1, m_2, \ldots, m_7$ are constant coefficients to $X_1, X_2, \ldots, X_7$, and b is the intercept constant.

The independent parameters Π_1 through Π_7 are evaluated one at a time to determine those which has the largest effect on Π_8 in order of importance. Π_8 was first assumed to be a single function of each independent parameter:

$$\Pi_8 = B\Pi_n^{mn}, \qquad \text{with } n = 1, 2, 3, 4, 5, 6, 7 \qquad (3.5.35)$$

Transforming Π_8 gives:

$$X_8 = b + (m_n)X_n \tag{3.5.36}$$

Values for B and m_n for each of the seven Π parameters can be determined by applying a least squares linear regression to the respective transformed data sets. The most important parameter was the one yielding the smallest sum of squares error between the predicted and the actual Π_8 value. The parameter was found to be Π_4, the inlet pressure parameter.

Π_8 was now assumed to be a function of two parameters:

$$\Pi_8 = B\Pi_4^{m4}\Pi_n^{mn} \tag{3.5.37}$$

The transformation of equation 3.5.37 yields

$$X_8 = b + (m_4)X_4 + (m_n)X_n \tag{3.5.38}$$

A set of values for B, m_4, and m_n are determined for the remaining six Π parameters. The second most important parameter was found to be Π_1, the geometry parameter. The process is repeated for the remaining parameters. The final subcooled inlet correlation obtained is:

$$\Pi_8 = 1.893\Pi_4^{1.369}\Pi_1^{-0.484}\Pi_5^{0.019}\Pi_2^{-0.824}\Pi_6^{0.773}\Pi_7^{0.265} \tag{3.5.39}$$

It must be mentioned that all property values were evaluated at the capillary tube inlet temperature. Due to the fact that the correlation was derived with the use of a range of operating conditions obtained from experiments, the implementation of the model should be done with caution. It is possible that the conditions of application fall outside the range covered by Bittle **et al.**, (1998).

3.5.3 Summary

The theoretical model has been thoroughly covered by Bittle and Pate (1996), including all the governing equations. The only element missing from their model is an expansion from the capillary to the evaporator inlet. The governing equations can be combined into a simulation routine, as will be discussed in Chapter 4.

The dimensionless correlation forms a useful application because of the Π-groups being based on fundamental aspects. There exist the possibility that different coefficients (B, m1, m2, ..., m7) have to be derived for our heat pump application due to operating conditions.

3.6 Heat pump cycle solution

When all the components are combined into a simulation routine a method for solving the cycle is needed. The method used and its general equations will be discussed below.

3.6.1 Solving non-linear equations simultaneously (Newton-Raphson method)

There exist n non-linear functions $F_1, \dots, F_n = 0$ with n variables $x_1, \dots, x_n$. Solutions have to be found for $x_1, \dots, x_n$. Thus

$$\begin{aligned} &F_1(x_1; x_2; \dots; x_n) = 0, \\ &F_2(x_1; x_2; \dots; x_n) = 0, \\ &\dots \\ &F_n(x_1; x_2; \dots; x_n) = 0. \end{aligned} \tag{3.6.1}$$

The Taylor series expansion of F_j are as follows: (first order)

$$\begin{aligned} F_j(x_1 + \Delta x_1; x_2 + \Delta x_2; \dots; x_n + \Delta x_n) = F_j(x_1; x_2; \dots; x_n) &+ \Delta x_1 \frac{\partial}{\partial x_1} F_j(x_1; x_2; \dots; x_n) \\ &+ \Delta x_2 \frac{\partial}{\partial x_2} F_j(x_1; x_2; \dots; x_n) \\ &+ \dots \\ &+ \Delta x_n \frac{\partial}{\partial x_n} F_j(x_1; x_2; \dots; x_n). \end{aligned} \tag{3.6.2}$$

By writing the Taylor series expansion in terms of $F_1, \dots, F_n$ and setting it equal to zero, gives:

$$\begin{aligned} &\frac{\partial F_1}{\partial x_1}\Delta x_1 + \frac{\partial F_1}{\partial x_2}\Delta x_2 + \dots + \frac{\partial F_1}{\partial x_n}\Delta x_n = -F_1 \\ &\frac{\partial F_2}{\partial x_1}\Delta x_1 + \frac{\partial F_2}{\partial x_2}\Delta x_2 + \dots + \frac{\partial F_2}{\partial x_n}\Delta x_n = -F_2 \\ &\dots \\ &\frac{\partial F_n}{\partial x_1}\Delta x_1 + \frac{\partial F_n}{\partial x_2}\Delta x_2 + \dots + \frac{\partial F_n}{\partial x_n}\Delta x_n = -F_n \end{aligned} \tag{3.6.3}$$

The above equations are a set of n linear equations with n unknown parameters $x_1, \ldots, x_n$. The above set of equations can be solved with the use of Gauss elimination to determine Δx_1; Δx_2; ...; Δx_n.

New values for $x_1, x_2, \ldots, x_n$ can be obtained by:

$$x_1 = x_1 + \Delta x_1$$

$$x_2 = x_2 + \Delta x_2$$

$$\ldots$$

$$x_n = x_n + \Delta x_n \qquad (3.6.4)$$

These new values give better solutions for $F_1, F_2, \ldots, F_n = 0$. This process is iterated until $F_1, F_2, \ldots, F_n \approx 0$.

A test is built in to check for convergence and is given by $\frac{\Delta n_i}{x_i} <<$ (very small value).

For one equation and one variable it works as follows:

$$F(x) = 0$$

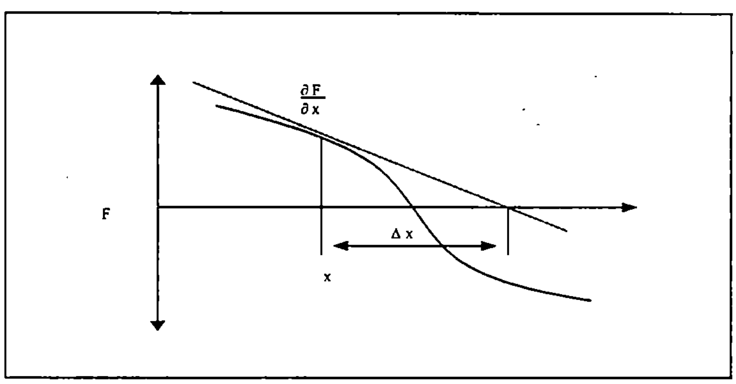

Figure 3.7: Gradient for function F(x)

$$F(x + \Delta x) = F(x) + \Delta x \frac{\partial F}{\partial x}(x) = 0 \qquad (3.6.5)$$

Thus

$$\Delta x = \frac{-F(x)}{\frac{\partial F(x)}{\partial x}}. \qquad (3.6.6)$$

A new value for the variable x is now given by

$$x_{new} = x_{old} + \Delta x$$

It must be noted that due to the gradient being used at x and the gradient being non-linear, the next answer, x_{new}, is only a more accurate approximation and not the correct value. The process must be iterated until the correct answer is reached.

3.6.2 Secant method

The partial derivatives in the Newton-Raphson are determined numerically. The secant method is used when the explicit form of the partial derivatives is not available and has to be determined. The partial derivatives are then determined as follows:

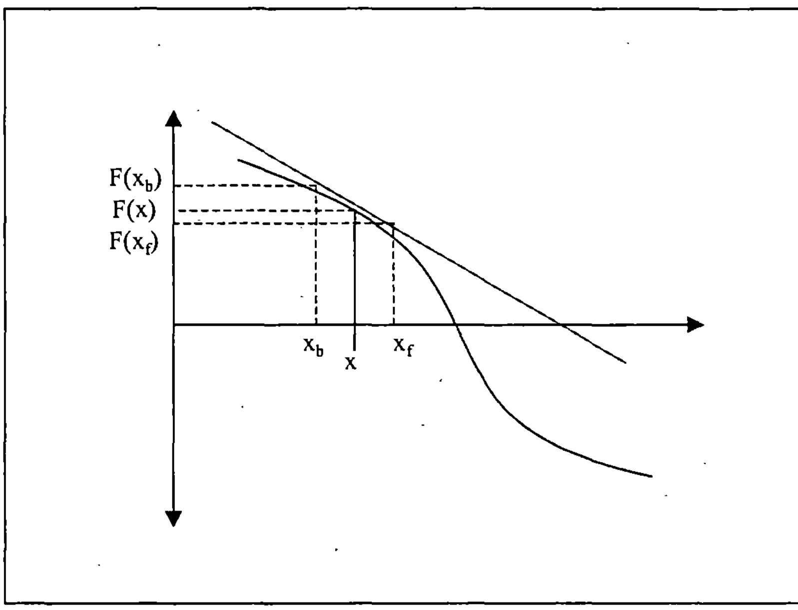

Figure 3.8: Partial derivative for secant method

Two steps are taken for the variable x, namely a forward step (x_f) and a backward step (x_b).

$$x_f = 1.001x$$

$$x_b = 0.999x$$

The partial derivative is determined by:

$$\frac{\partial F_j}{\partial x} = \frac{F_j(x_1; x_2; ...; x_{fi}; ...; x_n) - F_j(x_1; x_2; ...; x_{bi}; ... x_n)}{x_{fi} - x_{bi}}. \tag{3.6.7}$$

The second order partial derivative is determined as follows:

$$x_{ff} = 1.001x_f \qquad x_{fb} = 0.999x_f$$

$$x_{bf} = 1.001x_b \qquad x_{bb} = 0.999x_b$$

$$\frac{\partial^2 F_j}{\partial x_i^{\,2}} = \frac{\partial}{\partial x_i}\left(\frac{\partial F_j}{\partial x_i}\right)$$

$$= \left[\frac{\dfrac{F_j(x_1; x_2; \ldots; x_{ffi}; \ldots; x_n) - F_j(x_1; x_2; \ldots; x_{fbi}; \ldots; x_n)}{x_{ff} - x_{fb}} - \dfrac{F_j(x_1; x_2; \ldots; x_{bfi}; \ldots; x_n) - F_j(x_1; x_2; \ldots; x_{bbi}; \ldots; x_n)}{x_{bf} - x_{bb}}}{x_f - x_b}\right] \tag{3.6.8}$$

With the above equations the cycle can be solved with the functions F being the four components of the heat pump. The variables x are parameters, such as the mass flow rate, inlet conditions of a component, etc.

3.7 Conclusion

In this chapter a study was made of the theory which governs the different heat pump components. The capillary tube and the air-cooled evaporator models are based on methods found in the literature. The compressor model was developed from fundamental equations, and the condenser model was developed by implementing techniques of different researchers. All the equations can be implemented into simulation models for each component. In the next chapter the implementation of these equations and the changes made to them for the heat pump simulation model will be described.

References

BITTLE, R.R., PATE, M.B. 1996. A theoretical model for predicting adiabatic capillary tube performance with alternative refrigerants. *ASHRAE Transactions*, 102(2):52-64;

BITTLE, R.R., WOLF, D.A., PATE, M.B. 1998. A generalized performance prediction method for adiabatic capillary tubes. *International Journal of Heating, Ventilating, Air-Conditioning and Refrigerating Research*, 4(1):27-43; Jan.

BRAUN, J.E., KLEIN, S.A., MITCHELL, J.W. 1989. Effectiveness models for cooling towers and cooling coils. *ASHRAE Transactions*, 95(2):164-174.

CHEN, Z.H., LI, R.Y., CHEN, A.Y. 1990. A correlation for metastable flow of R-12 through capillary tubes. *ASHRAE Transactions*, 90(1):550:554.

CHRISTENSEN, R.H., SRINIVASAN, V. 1991. Spirally-fluted tubes and enhanced tubes in confined crossflow. Part I: Flow inside fluted tubes. Final Report. The Ohio State University.

CHRISTENSEN, R.H., SRINIVASAN, V. 1991. Spirally-fluted tubes and enhanced tubes in confined crossflow. Part II: Fluted-tube annuli. Final Report. The Ohio State University.

COLLIER, J.G., THOME, J.R. 1994. Convection boiling and condensation. New York: Oxford University Press.

DAS, S.K. 1993. Water flow through helical coils in turbulent condition. *The Canadian Journal of Chemical Engineering*, 71:971-973, Dec.

ECKELS, S.J., PATE, M.B. 1990. A comparison of R-134a and R-12 in-tube heat transfer coefficients based on existing correlations. *ASHRAE Transactions*, 96(1):256-265.

GREYVENSTEIN, G.P. 1988. A computer simulation model for the design and optimization of heat pumps and refrigeration systems. *Suid-Afrikaanse Tydskrif vir Wetenskap*, 84:494-502, Jun.

HPSIM V2.0 USER MANUAL. ENERFLOW Technologies CC, P.O. Box 20758, Noordbrug, 2522, Potchefstroom, South Africa.

INCROPERA, F.P., DE WITT, D.P. 1990. Fundamentals of heat and mass transfer. 3rd ed. Canada: John Wiley & Sons.

KUEHL, S.J., GOLDSCHMIDT, V.W. 1991. Modeling of steady flows of R-22 through capillary tubes. *ASHRAE Transactions*, 97(1):139-148.

SHAH, M.M. 1979. A general correlation for heat transfer during film condensation inside pipes. *International Journal of Heat and Mass Transfer*, 22:547-556.

CHAPTER 4

MODEL IMPLEMENTATION

CHAPTER 4

MODEL IMPLEMENTATION

4.1 Introduction

The previous chapter focussed on the relevant theoretical background needed for the development of the heat pump cycle. In this chapter the focus falls on the implementation of the theory into a simulation routine. There are two parts to the implementation phase, namely:

- Development of simulation routines for each of the components.
- The simulation of the heat pump cycle, in other words the integration of the component simulation routines into a cycle simulation.

The basic heat pump cycle with its main components is shown in Figure 4.1. The numbers (1 to 11) will be used in this chapter where the different components are evaluated. The numbers indicate different stages of the refrigerant in the cycle, as can be seen in Figure 4.2, where a typical pressure enthalpy diagram is shown. The working points given in Figure 4.1 are for the refrigerant side (R-134a) of the cycle.

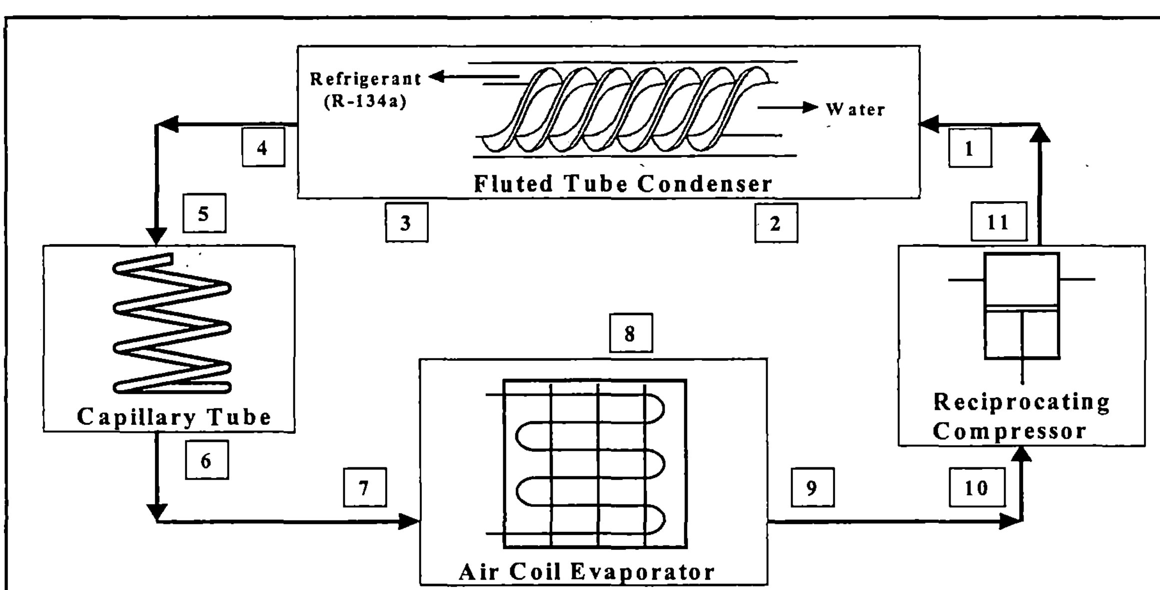

Figure 4.1: Micro heat pump cycle

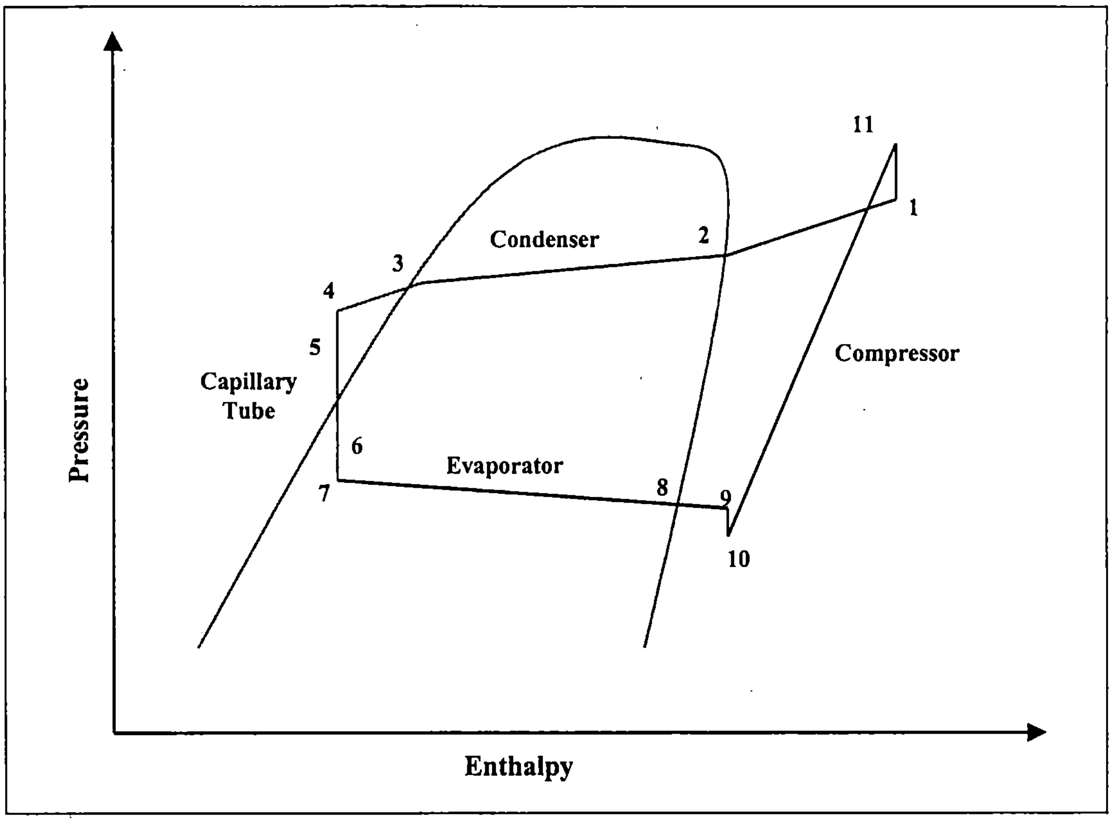

Figure 4.2: Pressure enthalpy relation for the heat pump cycle

The working points in the above figures are used to simplify the development of the simulation routines. The working points given are for the refrigerant side (R-134a) of the cycle, and are defined as:

- Condenser:
  - Working point 1 ⇒ Inlet conditions in superheat region.
  - Working point 2 ⇒ Superheat/Two-phase interface.
  - Working point 3 ⇒ Two-phase/Subcool interface.
  - Working point 4 ⇒ Outlet conditions in subcooled region.
- Capillary tube:
  - Working point 5 ⇒ Subcooled inlet conditions.
  - Working point 6 ⇒ Two-phase outlet conditions.
- Evaporator:
  - Working point 7 ⇒ Two-phase inlet conditions.
  - Working point 8 ⇒ Two-phase/Superheat interface.
  - Working point 9 ⇒ Superheat outlet conditions.

- Compressor:
  - Working point 10 ⇒ Superheat inlet conditions.
  - Working point 11 ⇒ Superheat outlet conditions.

In the following paragraphs the development of the simulation routines for each component will be looked at first. The components will be explained in the same order as in the previous chapter (condenser, evaporator, compressor and capillary). In the second part of this chapter the simulation of the heat pump cycle will be explained, including a detailed discussion of the method used for solving the cycle.

4.2 Component models

4.2.1 Fluted tube condenser

The type of condenser to be used is a fluted tube heat exchanger operated in the counter-flow mode. The simulation model was developed in such a way that it can actually be used for any type of tube-in-tube heat exchanger, with the only modifications being made to the pressure drop through the heat exchanger and different heat transfer coefficients. The simulation routine will be explained with the aid of Figure 4.3, the pressure enthalpy diagram of the condenser, and Figure 4.4, a flow diagram of the simulation routine.

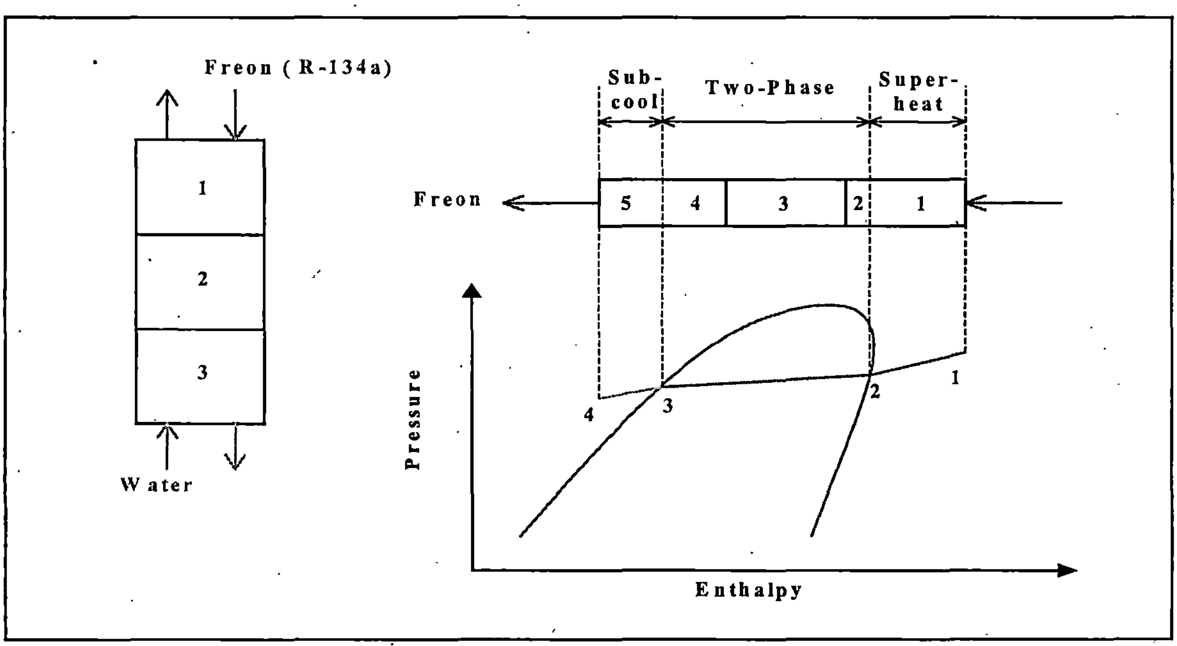

Figure 4.3: Pressure enthalpy diagram for the fluted tube condenser

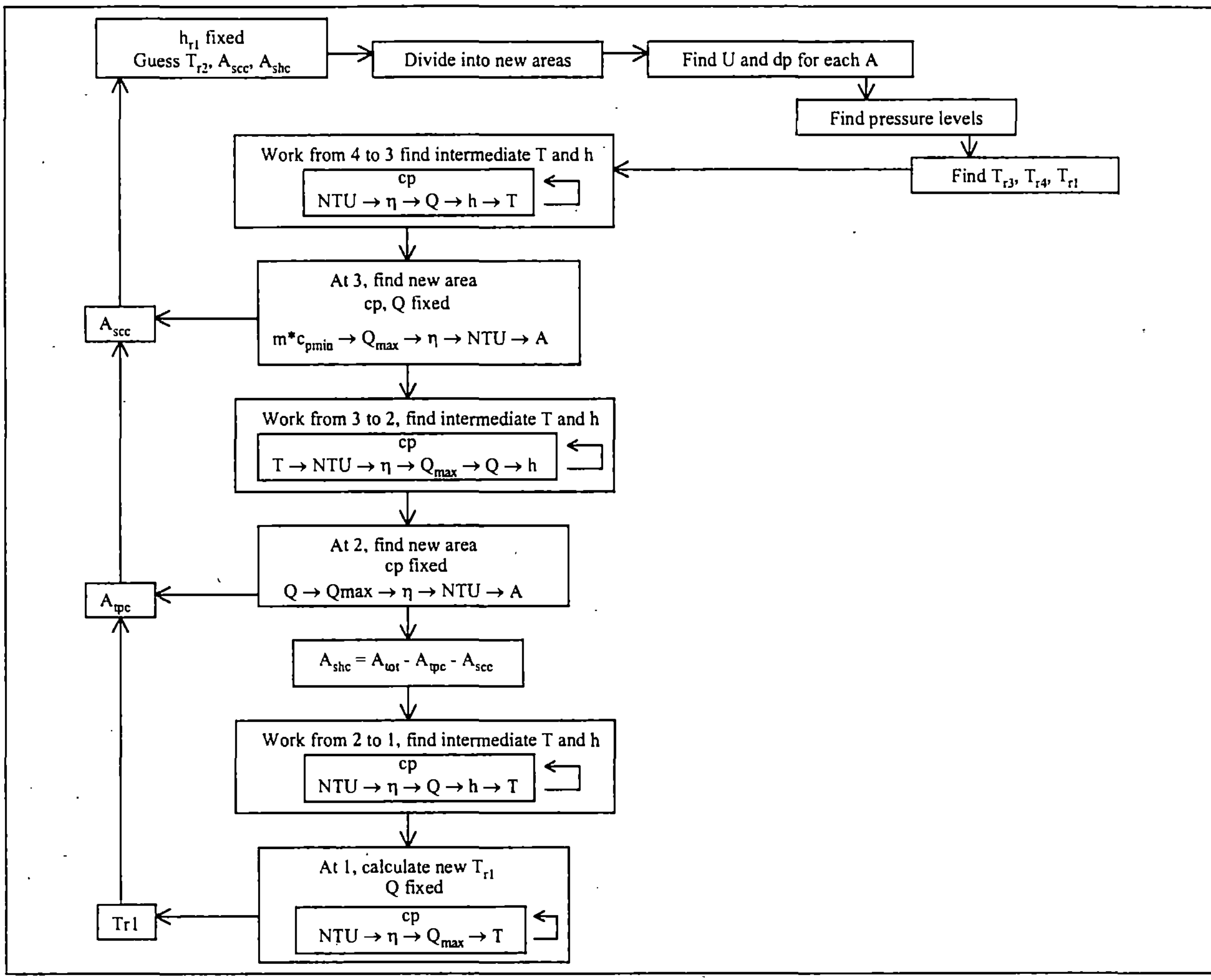

Figure 4.4: Flow diagram for the condenser simulation routine

The main purpose of the model is to obtain the pressure level in the condenser where the heat transfer (Q) is in equilibrium. The simulation routine was developed in such a way that it can be operated in a simulation mode or a design mode. In design mode the degree of subcooling is specified and the routine is then solved for this constraint. In simulation mode the fraction of the condenser which is subcooled is specified. The routine is then solved for these two constraints.

For both modes the following parameters are specified and given as inputs:

- Tube dimensions:
  - Length.
  - Volumetric inside and outside diameters of the fluted tube.
  - Inside diameter of the outside tube, which is shrunk over the fluted tube.

- Fluted tube geometry:
  - Flute depth and pitch.
  - Helix angle.
- Flow properties:
  - Type of refrigerant, i.e. R-134a.
  - Mass flow rate of the refrigerant and the water.
  - Inlet enthalpy of the refrigerant.
  - Inlet temperature and pressure of the water.

As output of the simulation routine the following main parameters are required:

- Inlet temperature and pressure of the refrigerant.
- Outlet pressure and enthalpy of the refrigerant.
- Outlet temperature and pressure of the water.

In the part to follow, only the design mode will be described with some mention of the simulation mode. The first step in the design routine is to specify into how many sections the condenser length has to be divided. The reason is that the accuracy of calculations increases with a decrease in section lengths. The condenser on the left-hand side of Figure 4.3 was divided into three sections (n = 3). The simulation starts by assigning estimated values for:

- The temperature of the refrigerant at working point 2 (T_{r2}).
- The subcooled area.
- The superheat area.

The above-mentioned n sections are now divided into m new areas, where m = n + 2. This is done in order to find the two-phase/superheat interface, and the two-phase/subcooled interface as can be seen in Figure 4.3 above the pressure enthalpy diagram.

Estimated values for pressures and enthalpies can now be determined at each interface between new areas with the aid of the estimated temperature T_{r2} and the subcooled and superheat areas. For each new area (m) the pressure drop (dp) across the section and the overall heat transfer coefficient (U) are determined as discussed in Chapter 3. The pressure at each interface between the new areas can now be determined together with the temperatures at point 1, 3, and 4. The temperature at working point 4 is equal to the temperature at working point 3 minus the fixed degree of subcooling. Up to this point all the values determined are based on the estimated values. This applies only to the first iteration of the simulation routine.

The condenser is operated in a counter-flow configuration, therefore the inlet of the water is at the outlet of the refrigerant. With the inlet water temperature specified, the simulation starts in the subcooled region of the refrigerant side, solving from working point 4 back to working point 1. In the following paragraphs the simulation routine for each region in the condenser will be discussed in detail.

Subcooled region

The simulation starts at working point 4 and works backward through the subcooled region till the two-phase/subcooled interface (working point 3) is reached. The interface temperatures and enthalpies are determined over each increment (m) while going through the routine. This is done in the following manner:

An estimated value is assigned to the specific heat (c_p) of the refrigerant. The number of transfer units (NTU) is then determined in the same way as stated in Chapter 3 (equation 3.2.1). The effectiveness of the counter-flow arrangement is then determined by means of equation 3.2.4. With the effectiveness known, the heat transfer (Q) can be determined for the specific section of the condenser by means of equation 3.2.7. The enthalpy at the entrance of the section can now be determined with the outlet enthalpy and the heat transfer known. The enthalpy is given by

$$h_{in} = h_{out} + \frac{Q}{m_r} \quad \text{, where } m_r \text{ is the mass flow of the refrigerant.} \tag{4.1}$$

With the enthalpy known, the temperature at the inlet can be determined. A new specific heat value is now determined as follows:

$$c_{pr} = \frac{h_{in} - h_{out}}{T_{in} - T_{out}} \tag{4.2}$$

This cycle is iterated until the correct specific heat value is reached. This procedure is repeated for every area in the subcooled region until the last area before working point 3 is reached.

At working point 3, the size of the last subcooled area has to be determined because of the known values at working point 3 after sizing from working point 2. The specific heat and the heat transfer are fixed because the enthalpies and temperatures across the last section are known. The maximum heat transfer over the section is determined by means of equation 3.2.7. With both the maximum heat transfer and the actual heat transfer known, the effectiveness can be calculated. The maximum number of transfer units is calculated by taking the area for this last section as the total condenser area minus the subcooled area calculated up to now. With the maximum number of transfer units known, the actual number of transfer units can be calculated. From this the area of the last section in the subcooled region is determined.

If the routine were to be operated in a simulation mode, the whole subcooled process is repeated by iterating the subcooled temperature until the specified subcooled area has been reached.

Over each increment the change in the water temperature is also calculated until the water temperature at working point 3 is known. The simulation now proceeds to the two-phase section, as will be explained below.

Two-phase region

In the two-phase region the simulation starts at working point 3 and work backwards through the two-phase region until the two-phase/superheat interface at working point 2 has been reached. As in the subcooled region, the interface temperatures and enthalpies are determined over each increment (m) while going through the routine. The two-phase region is solved in the following manner:

The conditions at working point 3 are known from the estimated value at working point 2. Like the subcooled region, an estimated value is assigned to the specific heat of the refrigerant. With the pressure known at each interface, the temperature can be determined. The number of transfer units can be calculated over each area because of the already determined heat transfer coefficients. With the number of transfer units determined, the counter-flow effectiveness over the increment can be calculated. Because the water temperature is known at the outlet and the refrigerant temperature is also known at the inlet due to the incremental pressure drop, the maximum heat transfer for the section can be calculated.

With both the effectiveness and the maximum heat transfer determined, the heat transfer for the section can be calculated. The enthalpy at the inlet to the section can now be determined by using equation 4.1.

A new specific heat value is now determined by using equation 4.2. This cycle is iterated until the specific heat of the refrigerant converges. This procedure is repeated for every area in the two-phase region until the last area before working point 2 is reached.

At working point 2 the size of the last two-phase area has to be determined. The specific heat is fixed because the enthalpies and temperatures across the last section are known. The heat transfer for this section can be determined with the known enthalpies. With the water temperature at the outlet and also the refrigerant temperature at the inlet known, the maximum heat transfer can be determined. The effectiveness of the section can now be calculated. The maximum number of transfer units is calculated by taking the area as the total condenser area minus both the subcooled area and the two-phase area calculated up to now. With the maximum number of transfer units known, the actual number of transfer units can be calculated. With all the above determined, the area of the last section is calculated.

With all the areas known, the two-phase area can easily be calculated. With both the subcooled area and the two-phase area known, the superheat area is equal to the total area minus these two areas. Over each increment, the change in the water temperature is also calculated until the water temperature at working point 2 is known. The simulation proceeds now to the superheat section of the condenser, which will be explained below.

Superheat region

This part of the simulation starts at the two-phase/superheat interface (working point 2) and works backward through the superheat region until working point 1 is reached. The interface temperatures and enthalpies are determined over each increment (m) while going through the routine. This is done in the following manner:

An estimated value is assigned to the specific heat of the refrigerant. The number of transfer units for the section is then determined. The effectiveness of the counter-flow arrangement can be determined with the number of transfer units. With the effectiveness known, the heat transfer for the specific section of the condenser can be calculated by means of equation 3.2.6. The enthalpy at the inlet of the section is a function of the outlet enthalpy and the heat transfer. With the enthalpy and the pressure known, the temperature at the inlet of the section can be determined.

A new specific heat value is now calculated. This cycle is iterated until the correct specific heat value has been reached. This procedure is repeated for every area in the superheat region until the area at working point 1 has been reached.

At working point 1 the new refrigerant inlet temperature, T_{r1}, is determined in the following way. The heat transfer is fixed because of the known enthalpies, keeping in mind that the enthalpy at working point 1 is given as a fixed input to the simulation programme. An estimated value is assigned to the specific heat (c_p). With the heat transfer known, the number of transfer units and the effectiveness for the last section can be calculated. The maximum heat transfer for the last section can then be determined. With the water temperature at the outlet of the section and the maximum heat transfer known, the new refrigerant temperature at the inlet to the condenser can be written as a function of both. This process is then iterated for the specific heat until the correct value has been reached.

From the new temperature at working point 1 a new value is assigned to working point 2. With this value and the newly determined areas, the simulation can be repeated from the beginning. It must be noted that the working line connecting the working points in Figure 4.3 can only shift up or down until the correct values have been reached, because of the fixed enthalpy at working point 1.

This routine is iterated until the temperature at working point 7 as well as the areas in the three phases converges. This gives the change of the refrigerant through the condenser as well as the water temperature rise through the condenser. In the next chapter the verification of the model will be discussed. In Appendix B sample calculations are performed containing formulae and numerical values to demonstrate the procedure used in the fluted tube condenser.

4.2.2 Air-cooled evaporator

As stated in Chapter 1, the type of evaporator to be used is an air coil unit. The simulation model was developed in such a way that it can be used for parallel flow refrigerant configuration and an inline tube configuration. It can further be used for any type of fin configuration, with the only modifications being made to the air side pressure drop through the heat exchanger and the outside surface heat transfer coefficients. The simulation routine will be explained by means of Figure 4.5 (the pressure-enthalpy diagram of the evaporator) and Figure 4.6 (a flow diagram of the simulation routine).

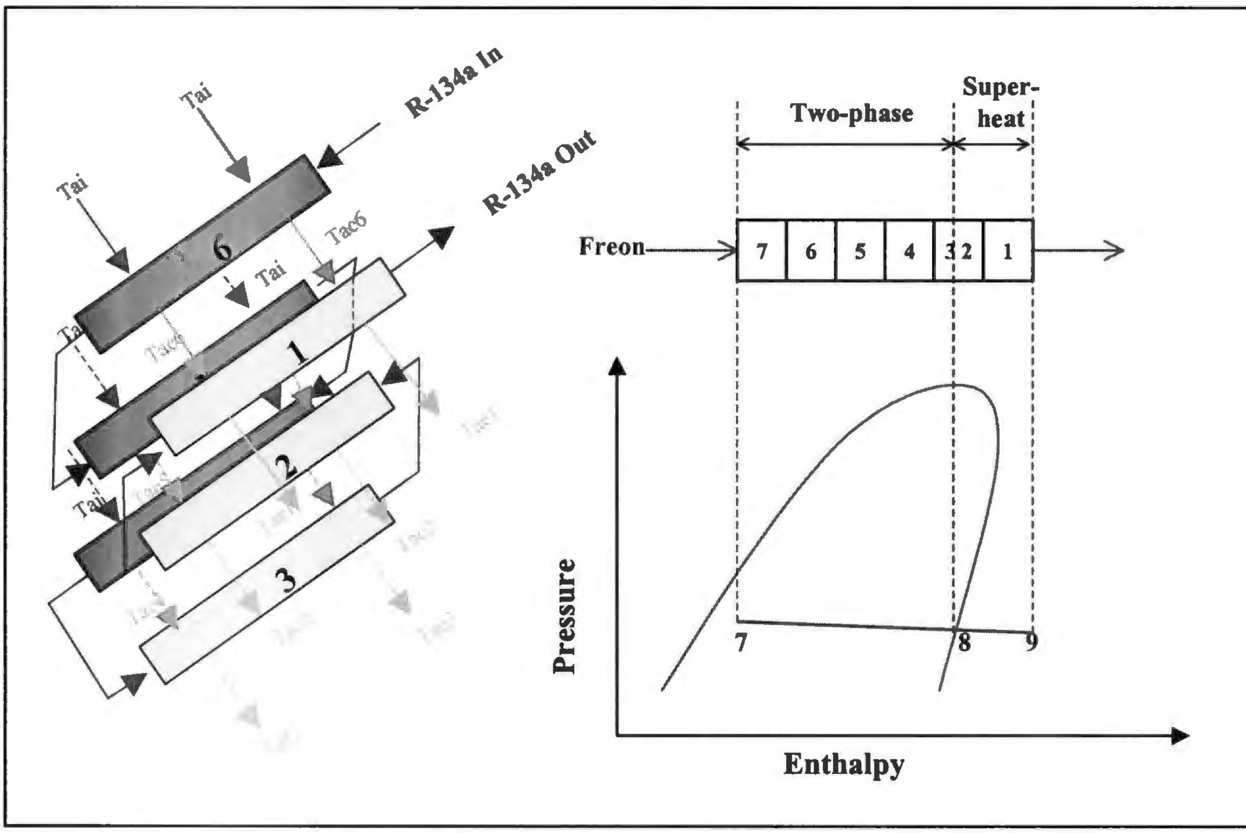

Figure 4.5: Pressure enthalpy diagram for the air-cooled evaporator

The main purpose of the model is to obtain the pressure level in the evaporator where the heat transfer (Q) is in equilibrium. The evaporator can be divided into any number of sections with each section responding as a small cross-flow heat exchanger on its own. For the discussion of the model, the evaporator was divided into the total number of tubes in the coil. It must be noted that each tube can also be divided into smaller sections for a more detailed simulation.

For the evaporator routine the following parameters are specified and given as inputs:

- Tube geometry:
  - Number of rows high.
  - Number of rows deep.
  - Total outside area including the fins.

- Flow properties:
  - Type of refrigerant (R-134a).
  - Degree of superheat.
  - Mass flow rates of the refrigerant and the air.
  - Inlet enthalpy of the refrigerant at working point 7.
  - Inlet temperature and pressure of the air.

As output of the simulation routine the following main parameters are required:

- Inlet temperature and quality of the refrigerant.
- Outlet pressure and enthalpy of the refrigerant.
- Outlet temperature and pressure of the air.

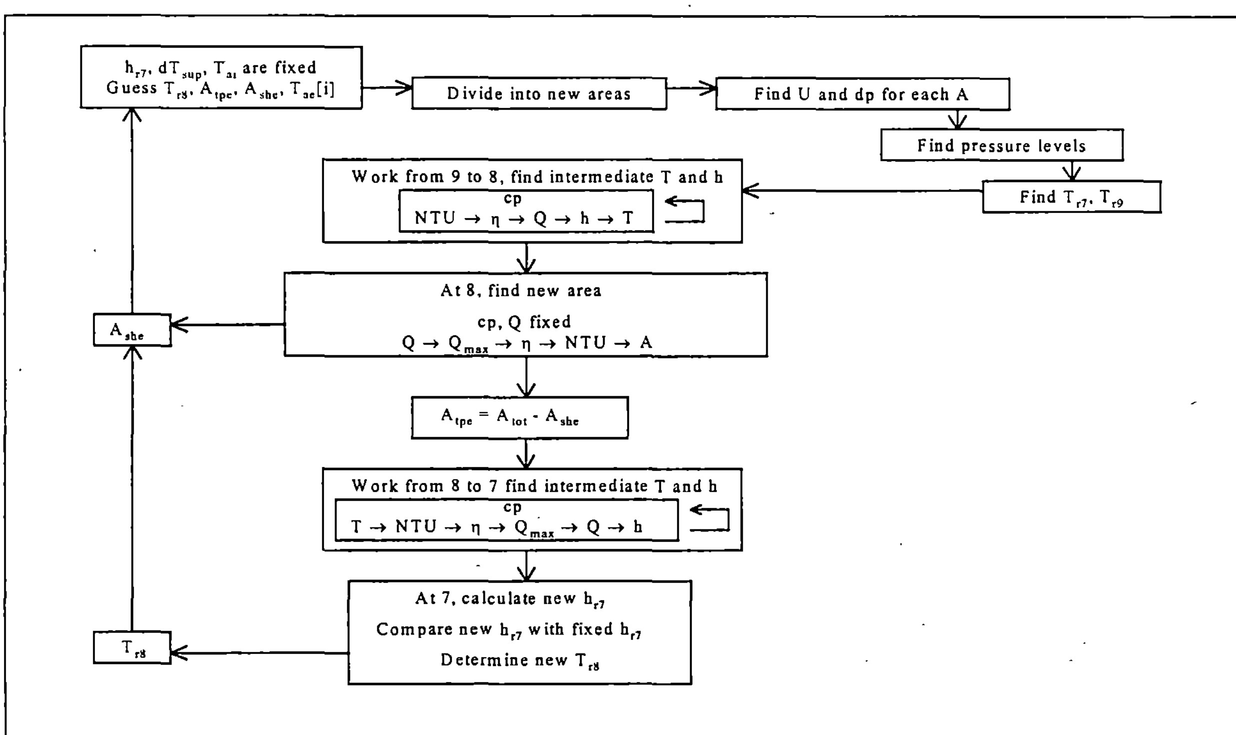

Figure 4.6: Flow diagram for the evaporator simulation routine

The first step in the simulation is to determine into how many equal sections the evaporator has to be divided. The total outside area is divided into n sections, where

$$n = r \, . \, k \, ,$$

with r the number of tubes high, and k the number of rows deep.
The example evaporator on the left-hand side of in Figure 4.5 is three tubes high and two rows deep.

The following parameters are assigned estimated values:

- The temperature of the refrigerant at working point 8 (T_{r8}).
- The two-phase area.
- The superheat area.
- The air temperature for each tube exluding the first row.

The above-mentioned n sections are now divided into m new areas, where m = n + 1, as can be seen above the pressure enthalpy diagram of Figure 4.5. This is done in order to find the two-phase/superheat interface. For each new area the fraction of air mass flow over it is determined.

Estimated pressures and enthalpies can now be determined at each interface between new areas with the aid of the estimated temperature at T_{r8} and the superheat and two-phase areas. For each new area (m) the pressure drop (dp) across the section and the overall heat transfer coefficient (U) are determined as discussed in Chapter 3. The pressure at each interface between the new areas can now be determined together with the temperatures at working points 7 and 9. Up to this point, all the values determined are based on the estimated values. This applies only to the first iteration of the simulation routine.

The evaporator is operated in a parallel flow configuration, therefore the inlet of the refrigerant is at the same side as the inlet of fresh air, as in Figure 4.5. With the degree of superheat specified as input, the simulation starts in the superheat region of the refrigerant at working point 9 and work backwards through the evaporator until working point 7 has been reached.

It was mentioned earlier that the model was developed for a parallel flow, inline configuration. Therefore indices must be applied to each of the m sections in the evaporator.

The purpose of indices is to keep a record of which tube follows after another, and where each tube is situated in the tube bank. This will be explained by means of the schematic evaporator on the left-hand side of Figure 4.5.

Indices

It can be seen from Figure 4.5 that the example evaporator is three tubes high and two rows deep. The path of the refrigerant is easy to determine, because it flows from tube 6 to tube 1 in declining numerical order. The refrigerant flows from the first row to the second row between tube 4 and tube 3. The reason why the order of tubes declines is because the simulation starts at working point 9, the outlet of the refrigerant, and works its way back towards working point 7 at the inlet.

To keep track of the airflow is not as straightforward as for the refrigerant. In Figure 4.5 the first row is subjected to the fresh air (T_{ai}) which moves through the evaporator. The outlet air of the first row is the inlet air of the second row. This is valid for any number of rows, with the outlet of the previous row serving as the new inlet. However, the outlet temperature of each tube in a row is not the same because of heat transfer between the refrigerant and the air, with the refrigerant temperature and enthalpy changing as it flows through the tubes. Track must therefore be kept of the tubes in a row and also in which row the tubes are located. This was done as follows.

The first problem was that the n sections is divided into m = n+1 sections to incorporate the superheat/two-phase interface. In the example evaporator of Figure 4.5 tube 2 includes the superheat/two-phase interface. Row 2 now sees the outlet air of m sections as follows:

- Tube 1 the outlet air of tube 7.
- Tube 2 the outlet air of tube 6.
- Tube 3 the outlet air of tube 6.
- Tube 4 the outlet air of tube 5.

For the superheat region the indexing is done as follows:

In the second row, tube 1 uses the outlet air of tube 7, row 1, and also the outlet refrigerant of tube 2. Thus, the inlet air of tube 1 equals the outlet air of

$$T_{ai1} = T_{ae}[index+1], \qquad (4.3)$$

where index = 2 x (specified tubes in a row (r)),

The tubes in a row equal 3, thus the inlet air of tube 1 equals the outlet air of tube 7.

Tube 2 uses the outlet air of tube 6 and the outlet refrigerant of tube 3. The inlet air for tube 2 is equal to

$$T_{ai2} = T_{ae}[index+2] \qquad (4.4)$$

where index = 2 x (specified tubes in a row (r)) – 2.

Thus

$$T_{ai2} = T_{ae}[6].$$

A pattern develops while moving through the second row, which can be written as follows:

$$T_{aij} = T_{ae}(j + i) \qquad \text{where j is the current tube number and} \qquad (4.5)$$

i equals …, 6, 4, 2, …

Thus i = 2x (specified tubes in a row (r)) for the first tube of the second row, and i = i - 2 for each of the tubes following in the row.

For the two-phase region the indexing is done as follows:

As stated, the evaporator was divided into n equal areas, and then into m areas. Accordingly, there are two areas of which the summation is equal to one of the n areas. When the simulation routine moves from the superheat region to the two-phase region, the following is done.

If no areas were discarded in the superheat region, as will be explained later, the following correction is made to the indexing:

$$i = i - 1.$$

For the example in Figure 4.5 it works as follows. Tube 2 of the m areas was the last superheat area, but tube 2 and tube 3 are both using the outlet air of tube 6. Consequently, to get the indexing correct, the properties of i had to be changed. This gives $T_{ai3} = T_{ae}[3 + 3] = T_{ae}[6]$.

From here on the indexing of i is again i = i – 2, for the rest of the row. For a new row in the two-phase area the same process as in the superheat area is repeated.

When areas were discarded in the superheat area, the following change to the indexing had to be made so that the inlet temperature of a tube in the two-phase region is equal to the correct outlet temperature of the tube in front.

$$i = i - 2 \times (j\_sh - j) + 1 \tag{4.6}$$

where j_sh is the start of the first two-phase area, and j is the number of the first area to be discarded in the superheat region. After the correction to the indexing has been made, the process can continue in the same way as described in the superheat region.

With the above explanation of the indices in mind, the simulation routine can now be discussed. In the following paragraphs the simulation routine for each region in the evaporator will be discussed in detail by means of Figure 4.6.

Superheat region

The simulation routine starts in the superheat region due to the fact that the degree of superheat is a fixed input parameter helping to size the areas. This part of the simulation starts at the outlet of the evaporator (working point 9) and works backward through the superheat region until the two-phase/superheat interface (working point 8) is reached. The interface temperatures and enthalpies are determined over each increment (m) while going through the routine. This is done in the following manner:

At working point 9 the temperature and enthalpy of the refrigerant is known from the estimated value of T_{r8}. An estimated value is assigned to the specific heat (c_p) of the refrigerant. The number of transfer units is then determined for the section. The effectiveness of the cross-flow arrangement can be determined from the number of transfer units. With the effectiveness known the heat transfer can be determined for the specific section of the evaporator by means of the following equation:

$$Q = \frac{\eta . m . c_{pmin}}{\left(\frac{1 - (\eta . m . c_{pmin})}{m_r . c_{pr}}\right)} \left(T_{ae}(j+i) - T_r\right) \tag{4.7}$$

The enthalpy at the outlet of the section can now be determined with the inlet enthalpy and the determined heat transfer known. With the enthalpy and the pressure in the superheat region known, the refrigerant outlet temperature can be determined. A new specific heat value is now determined. This cycle is iterated until the correct specific heat value has been reached. The outlet air temperature of each section can now also be calculated by

$$T_{ae}[j] = T_{ae}[j+i] - \frac{Q}{m_{a}.C_{pa}}. \quad (4.8)$$

This procedure is repeated for every area in the superheat region until working point 8 has been reached.

At working point 8, the size of the last superheat area has to be determined because of the estimated values at this working point. The specific heat and the heat transfer are fixed because the enthalpies and temperatures across the last section are known. An estimated value is assigned to the area of the last section. The fraction of the total air mass flow rate over this area is determined. For this estimated area the number of transfer units are determined. The effectiveness of this section is then determined from the number of transfer units, after which the heat transfer for this estimated section is determined. This process is iterated for the area until the correct heat transfer has been obtained.

Two-phase region

The new two-phase region is equal to the total area minus the newly determined superheat area. The simulation starts at working point 8 (the two-phase/superheat interface) and work backwards through the two-phase region until working point 7 is reached. The interface temperatures and enthalpies are determined over each increment (m) while going through the routine. This is done in the following manner:

An estimated value is assigned to the specific heat (c_p) of the refrigerant. The specific heat of the air is a function of the air inlet temperature. The refrigerant inlet temperature of an increment is determined with the estimated pressure at the inlet. The number of transfer units (NTU) is then determined. The effectiveness of the cross-flow arrangement is then determined using the number of transfer units.

The maximum heat transfer for the section can also be determined as follows:

$$Q_{max} = m.c_{pmin}\left(T_{ae}(j+i) - T_r\right). \tag{4.9}$$

T_{ae} is the outlet air of the previous row or for the first row the fresh air inlet. T_r is the outlet refrigerant temperature.

With the effectiveness as well as the maximum heat transfer known, the heat transfer (Q) for the specific section of the evaporator can be determined. The enthalpy at the inlet of the section can now be determined with the outlet enthalpy and the determined heat transfer known. The enthalpy is given by

$$h_{in} = h_{out} - \frac{Q}{m_r} \quad \text{, where } m_r \text{ is the mass flow of the refrigerant.} \tag{4.10}$$

A new specific heat value is now determined. This cycle is iterated until the correct specific heat value has been reached. The air temperature change over the section is also determined. This procedure is repeated for every area in the two-phase region until working point 7 has been reached.

As stated earlier, the enthalpy at working point 7 was given as a fixed input value. At this working point there now exist a newly determined enthalpy value. The new value is compared with the fixed value. If the new enthalpy were found to be less than the fixed input value the temperature of working point 8 is moved up. It could also be moved down. This routine is iterated until the correct enthalpy at working point 7 as well as the convergence of the two-phase and superheat areas has been reached. After convergence, the refrigerant temperature change through each row in the evaporator as well as the air temperature change over each row are known.

In the next chapter the evaluation of the model will be discussed when compared to experimental data for the micro heat pump. In Appendix B sample calculations are performed containing formulae and numerical values to demonstrate the procedure used in the air-cooled condenser.

4.2.3 Reciprocating compressor

As stated in Chapter 1, a reciprocating compressor should be used. The reason for the use of a simulation routine instead of an interpolation routine is that there is not sufficient performance data available from the manufacturers for the small size of compressor to be used. The simulation routine will be explained by means of Figure 4.7, the pressure enthalpy diagram of the compressor, and Figure 4.8, a flow diagram of the simulation routine.

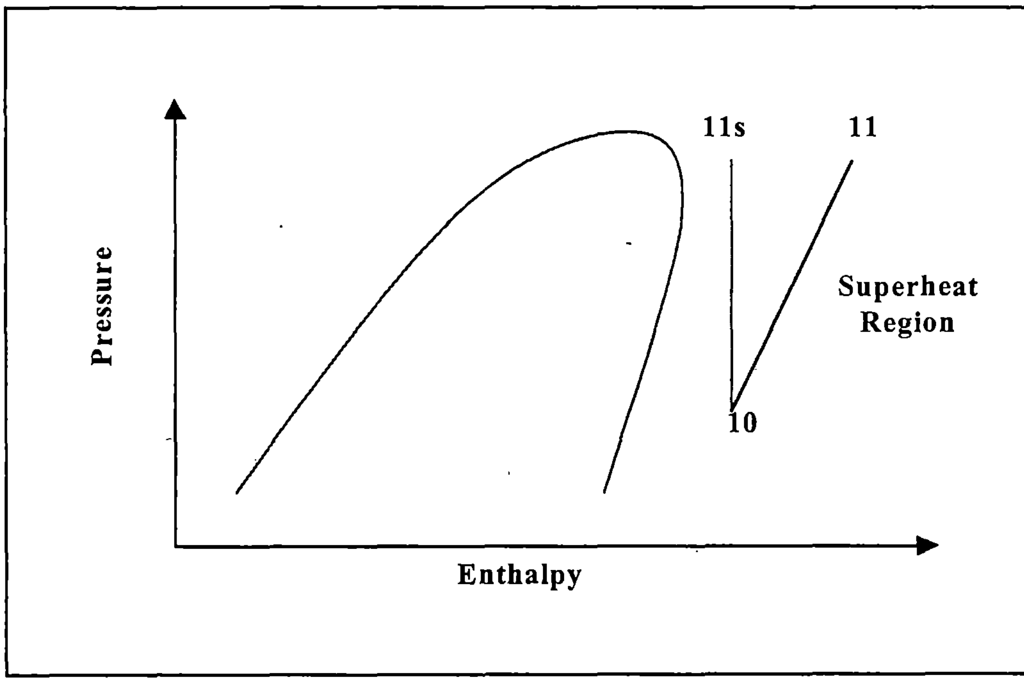

Figure 4.7: Pressure enthalpy diagram for the compressor

For the compressor simulation routine the following parameters are specified and given as inputs:

- Inlet pressure and temperature at working point 10.
- Outlet pressure at working point 11.
- Type of refrigerant.

As output of the simulation routine, the following main parameters are required:

- Mass flow of the refrigerant.
- Outlet temperature and enthalpy of the refrigerant.
- The work done by the compressor on the refrigerant.

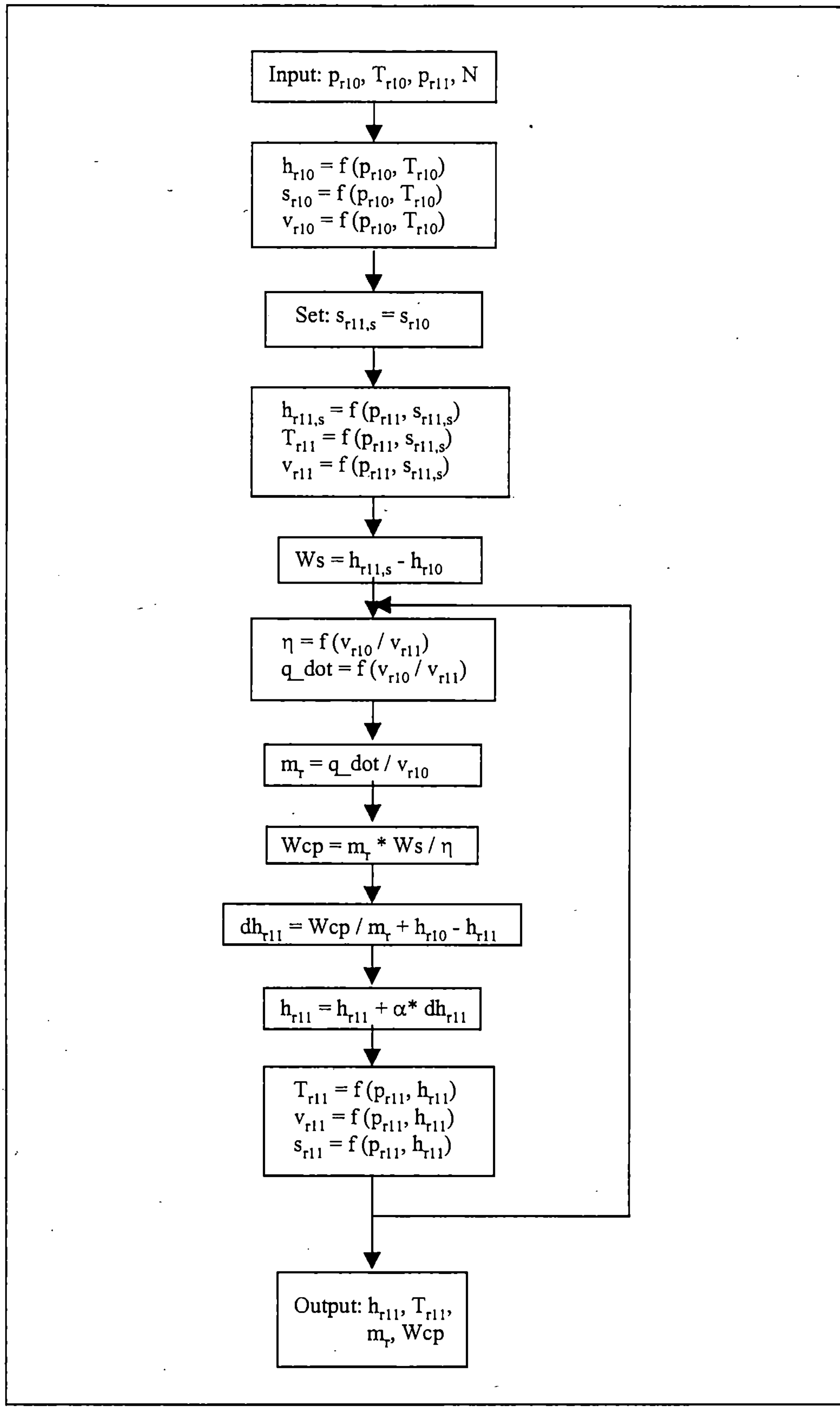

Figure 4.8: Flow diagram for the compressor simulation routine

The inlet conditions at working point 10 must be kept in the superheat region in order to avoid liquid being pumped through the compressor. With the temperature and pressure known at working point 10, the enthalpy, entropy and specific volume can be determined.

The simulation routine is started by assuming the compressor process to be isentropic. This means the entropy at working point 11 is equal to the entropy at working point 10. In Figure 4.7 this process is defined by the line connecting working points 10 and 11s. With the outlet pressure as well as the estimated entropy known the enthalpy, temperature and specific volume at working point 11s can easily be determined. With the inlet and outlet enthalpy known, the isentropic work (Ws) can easily be determined. The simulation routine now enters the section in which the correct outlet conditions will be determined.

For a specific compressor the isentropic efficiency and the volume flow have to be determined. The efficiency and the volume flow need to be functions of the inlet specific volume (v_{r10}) and the outlet specific volume (v_{r11}). The pressure ratio can be written as:

$$\text{pressure ratio} = \frac{v_{r11}}{v_{r10}} \tag{4.11}$$

The development of these two equations needed for the simulation was done by Pieter Coetzer, a final year student of the School of Mechanical and Materials Engineering, as part of his final year project. The best fit for the efficiency is a polynomial equation, and for the volume flow a linear equation. Figure 4.9 is an example of the above equations developed for one of the test compressors.

The definition of isentropic efficiency is given by

$$\eta = \frac{h_{r11s} - h_{r10}}{h_{r11} - h_{r10}}. \tag{4.12}$$

The refrigerant mass flow can now be determined with both the volume flow and the inlet specific volume known. The compressor work on the refrigerant is determined by

$$Wcp = m_r\left(\frac{Ws}{\eta}\right). \tag{4.13}$$

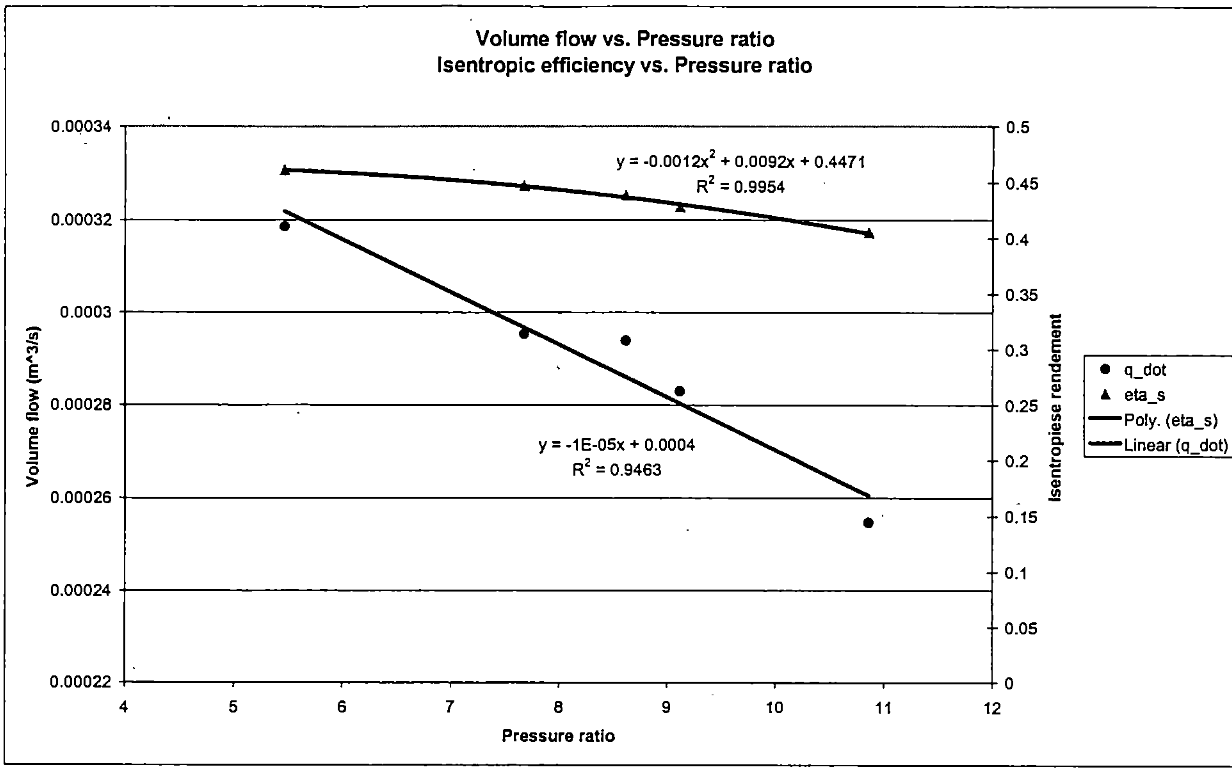

Figure 4.9: EMBRACO: FG 95 HAKW – 10.62 cm³

The change in outlet enthalpy (dh_{r11}) can now be determined by means of the following equation:

$$dh_{r11} = \frac{Wcp}{m_r} + h_{r10} - h_{r11}, \tag{4.14}$$

with h_{r11} equal to h_{r11s} for the first iteration.

$$h_{r11} = h_{r11} + dh_{r11}. \tag{4.15}$$

The new outlet conditions can now be determined at the new h_{r11}. This simulation is repeated until the correct outlet enthalpy has been reached.

When the correct outlet conditions have been reached, the mass flow can be used in the condenser and evaporator models and the compressor work on the refrigerant for heat transfer calculations for the cycle. The power input of the compressor can be determined by:

$$P_m = \frac{Wcp}{\eta_m} \tag{4.16}$$

where the mechanical efficiency (η_m) of the compressor depends on the phase angle ($\varnothing$) of the electricity supply and heat losses.

The verification of the model will be discussed in the next chapter. In Appendix B sample calculations are performed containing formulae and numerical values to demonstrate the procedure used in the compressor simulation.

4.2.4 Capillary tube

As stated in Chapter 3, two different capillary tube-modelling techniques have to be implemented. The first is the theoretical model by Bittle and Pate (1996), and the second the dimensionless correlation by Bittle **et al.**, (1998). Both models will be discussed in detail.

Theoretical Model of Bittle and Pate (1996)

The simulation routine will be explained by means of Figure 4.10, the pressure enthalpy diagram of the capillary tube, and Figure 4.11, a flow diagram of the routine. The general solution scheme of the model involves the variation of the mass flow rate variable until the calculated capillary length agrees with the specified length and all constraints on the final flow solution have been satisfied.

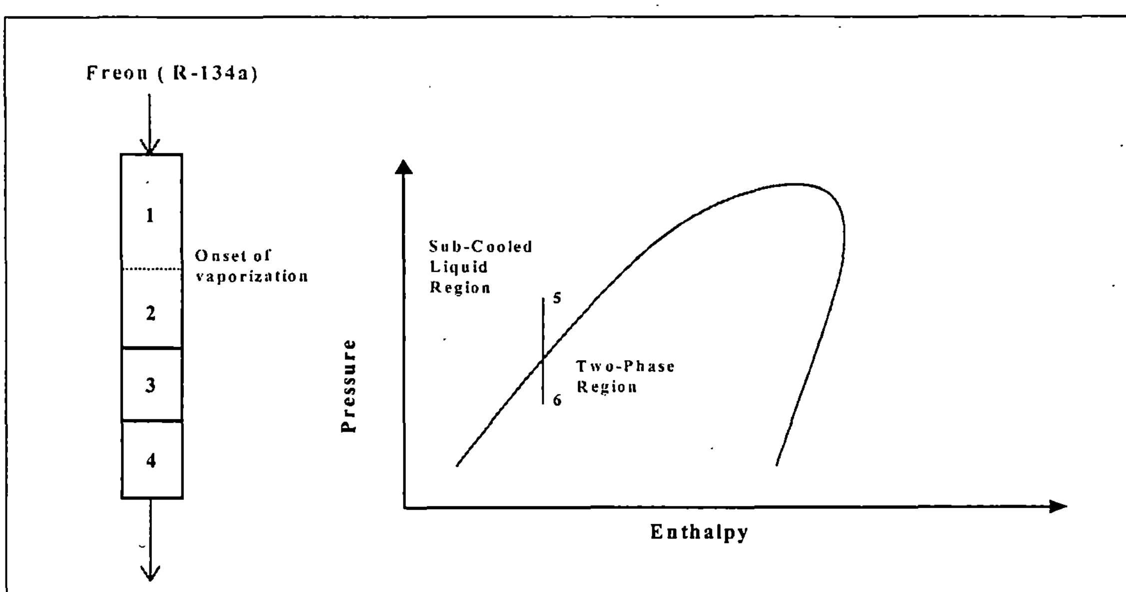

Figure 4.10: Pressure enthalpy diagram for the capillary tube

The only difference between our simulation model and the model by Bittle and Pate (1996) is that their model made use of an incremental temperature drop through the capillary tube, and the model for this dissertation used an incremental pressure drop through the capillary.

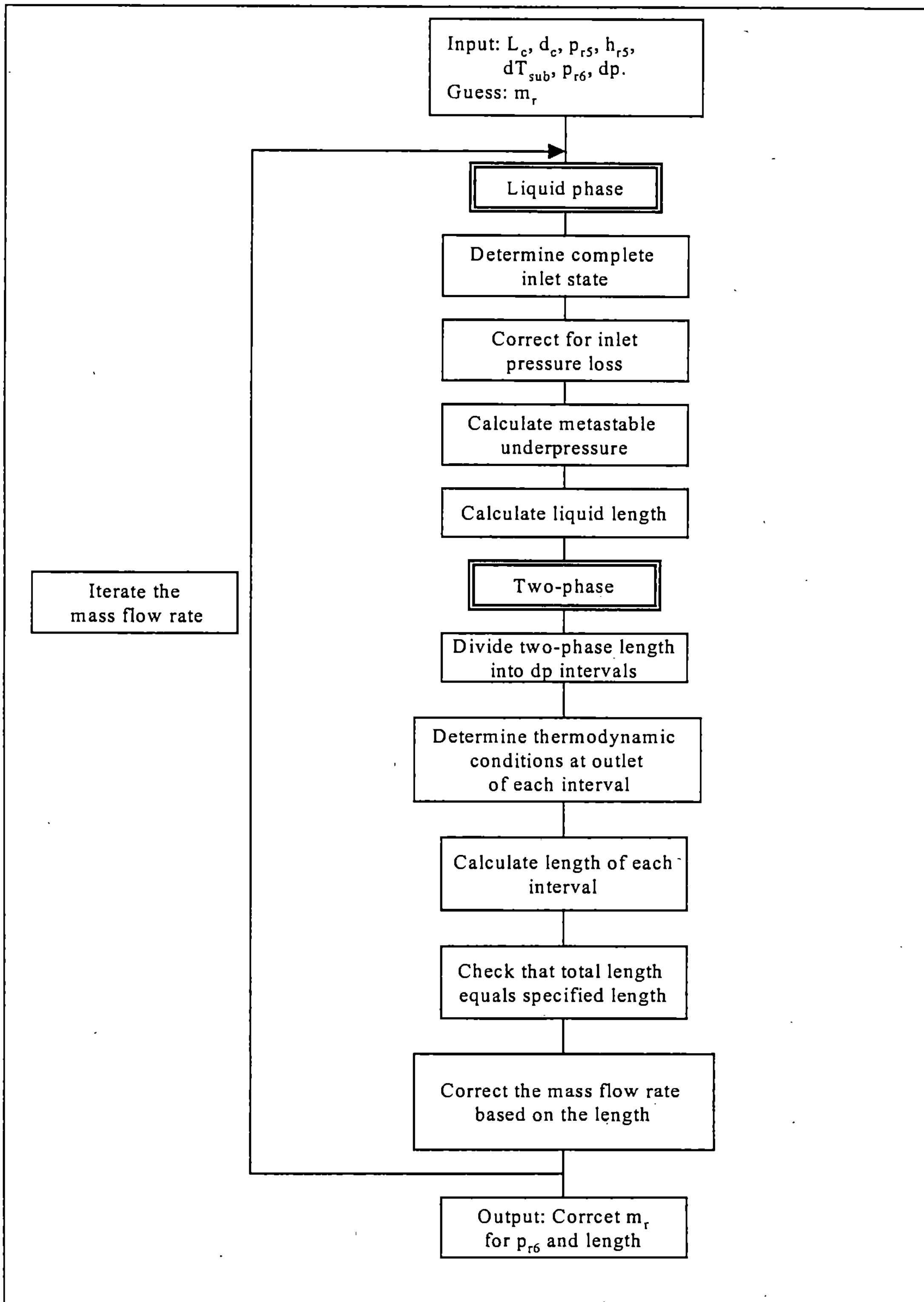

Figure 4.11: Flow diagram for the capillary tube simulation routine

The following parameters are specified as inputs:

- Inlet pressure and temperature at working point 5.
- Outlet pressure at working point 6.
- The capillary tube geometry (length and diameter).
- An initial assumed value for the mass flow rate.
- An incremental pressure drop through the two-phase region.
- Type of refrigerant.

As output of the routine the following main parameters are obtained:

- Mass flow of the refrigerant.
- Outlet quality and enthalpy of the refrigerant.

The simulation routine starts at the inlet of the capillary tube, which is in the subcooled liquid region. The complete inlet state of the capillary is determined including the following:

- Density of the refrigerant.
- Enthalpy at working point 5.
- Viscosity of the refrigerant.
- Velocity at the inlet.
- The mass flux based on the estimated value for the mass flow rate.
- The Reynolds number.
- Friction factor.

A correction factor is calculated for the sudden contraction from the delivery tube to the capillary tube. Equations 3.5.19 and 3.5.20 are used to obtain the pressure drop due to the sudden contraction. A correction must be applied to the liquid region for the metastable region as discussed in Chapter 3. The correction uses equations 3.5.21 and 3.5.22. It must be kept in mind that the liquid phase is a constant enthalpy process in order to obtain the end of the liquid region.

The liquid length is calculated directly by means of equation 3.5.7, which is rewritten in terms of the known parameters:

$$\Delta L_{liq} = \frac{2\nu \Delta p_{liq} d_c}{f \bar{V}^2}. \qquad (4.17)$$

Δp_{liq} is the difference between the liquid pressure just inside the capillary tube after accounting for the inlet contraction loss, and the pressure corresponding to the onset of vaporization. Δp_{liq} includes the under-pressure level calculated using the Chen model. ΔL_{liq} sets the flash-point location to be used in the two-phase flow region.

Throughout the two-phase region the model assumes the existence of thermodynamic equilibrium. The two-phase region is divided into incremental pressure drops from the flash-point to the known outlet pressure. The solution scheme works downstream from the flash-point over the incremental pressure drops. For each increment the entering flow conditions are known from the calculations of the previous as well as the outlet pressure due to the specified pressure drops. In order to evaluate the model by Bittle and Pate (1996), two different approaches were used in the two-phase region, namely:

- Implementing both the continuity equation and the energy equation. This is done because as the quality of the refrigerant increases, the influence of the velocity increases.
- For the second approach constant enthalpy through the two-phase region is assumed. This is an assumption that is widely used when capillary tubes are simulated.

For the first approach the complete set of flow conditions at the exit of an increment can be determined by combining the continuity equation (equation 3.5.2) and the energy equation (equation 3.5.13).

$$h_2 + \frac{\nu_2^2}{2} G^2 = h_1 + \frac{\bar{V}_1^2}{2}. \tag{4.18}$$

Substituting for h_2 and v_2 using equations 3.5.15 and 3.5.16 leads to:

$$h_{f2} + (h_{g2} - h_{f2})x_2 + \frac{1}{2}\left[\nu_{f2} + (\nu_{g2} - \nu_{f2})x_2\right]^2 G^2 = h_1 + \frac{\bar{V}_1^2}{2}. \tag{4.19}$$

Grouping terms yields a quadratic equation in terms of quality, x_2:

$$\left[\frac{1}{2}G^2(\nu_{g2} - \nu_{f2})^2\right]x_2^2 + \left[G^2\nu_{f2}(\nu_{g2} - \nu_{f2}) + (h_{g2} - h_{f2})\right]x_2 + \left[G^2\left(\frac{\nu_{f2}^2}{2}\right) + h_{f2} - h_1 - \frac{\bar{V}_1^2}{2}\right] = 0 \tag{4.20}$$

Equation 4.20 is a quadratic equation in terms of the outlet quality of a section. By iterating the exit quality, a solution can be found which satisfies the equation. When the quality is known, the thermodynamic properties, velocity and friction at the exit of the increment can be determined.

With the outlet properties known, the incremental length corresponding to the incremental pressure drop can be determined, using the two-phase momentum equation (equation 3.5.8) as follows:

$$\Delta L = \frac{2 \nu_m d_c \left[(p_1 - p_2) - G\left(\bar{V}_2 - \bar{V}_1 \right) \right]}{f_m \bar{V}_m^2}, \tag{4.21}$$

where V_m, f_m and ν_m are average values across the incremental length and determined as stated in Chapter 3.

The length of each pressure drop increment can be determined in sequence. The total length calculated is compared to the actual length of the capillary tube. The mass flow rate is iterated until the correct length has been obtained.

For the second approach constant enthalpy is assumed. Instead of equations 4.18 to 4.20, the next equation is used:

$$h_{f2} + (h_{g2} - h_{f2})x_2 = h_1 . \tag{4.27}$$

The outlet quality for each incremental pressure drop can now be solved easily. With the outlet quality known, the thermodynamic properties, velocity and friction at the outlet of the increment can be determined. The incremental length over the pressure drop can now be determined by means of equation 4.21. This is repeated for every pressure increment. The calculated total length is compared to the actual length of the capillary tube. The mass flow rate is iterated until the correct length has been obtained.

The results from both approaches will be discussed in the next chapter. A comparison between the models and the model by Bittle and Pàte (1996) will be discussed.

Dimensionless correlation of Bittle et al. (1998)

The implementation of the dimensionless correlation is very straightforward because the parameters only depend on the inlet conditions of the capillary tube.

The simulation routine works exactly as shown in Figure 4.12. The inputs to the simulation routine are as follows:

- Length and diameter of the capillary tube,
- Pressure and temperature at the inlet to the capillary tube,
- The degree of subcool.

The exit pressure has no influence on the performance of the capillary tube, since choked flow conditions exist in capillary tube flow for typical steady-state applications. The following properties are all calculated at the inlet of the capillary tube with the use of the inlet temperature:

- Enthalpy of the refrigerant,
- Specific volume of the fluid and the gas,
- Viscosity of the fluid and the gas,
- Specific heat of the fluid.

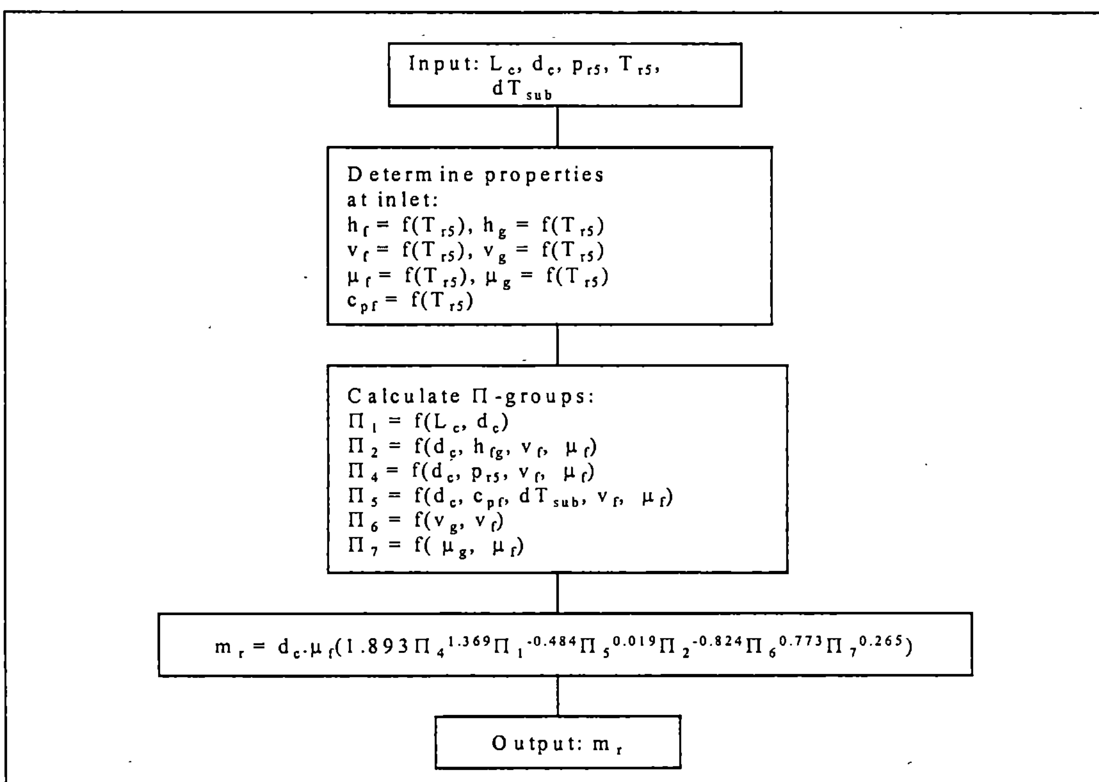

Figure 4.12: Flow diagram for the dimensionless correlation

The dimensionless parameters (Π_1, Π_2, …, Π_7) can easily be calculated from equation 3.5.28 to 3.5.34. The dimensionless parameter Π_8 is a function of the mass flow rate, diameter and the viscosity of the fluid as in equation 3.5.35. Π_8 correlation for subcooled inlet conditions is given by equation 3.5.43. The mass flow rate through the capillary tube can therefore be established easily by combining equation 3.5.35 and 3.5.43 giving:

$$m_r = d_c.\mu_f.(1.893\Pi_4^{1.369}\Pi_1^{-0.484}\Pi_5^{0.019}\Pi_2^{-0.824}\Pi_6^{0.773}\Pi_7^{0.265}) \tag{4.28}$$

An important assumption made during the implementation of the model is that constant enthalpy exist throughout the capillary tube. The above model is a straightforward method to obtain the mass flow rate through a capillary tube and can easily be implemented into the heat pump cycle simulation. In Appendix B sample calculations are performed containing formulae and numerical values to demonstrate the procedure used in the capillary simulation.

4.3 Integrated heat pump cycle simulation

In this section of the chapter a brief overview follows on how the component models were integrated into a cycle simulation routine. The cycle simulation will be explained by means of Figure 4.2, the pressure enthalpy diagram of the heat pump cycle.

An assumption is made that the outlet conditions of one component equal the inlet conditions of the next. This means the effect of tubing between components are not taken into consideration during the simulation.

The micro heat pump cycle simulation uses four component models to solve for the following seven variables:

- Pressure at working point 1.
- Enthalpy at working point 1.
- Pressure at working point 10.
- Enthalpy at working point 10.
- Mass flow rate of compressor.
- Mass flow rate of capillary.
- Degree of superheat in evaporator.

The cycle is solved with a secant method as described in Chapter 3 by minimizing the following seven functions:

- F_1 monitors the convergence of the pressure p_{r1}.
- F_2 monitors the convergence of the enthalpy h_{r1}.
- F_3 monitor the convergence of the mass flow rate.
- F_4 monitors the convergence of the pressure p_{r10}.
- F_5 monitors the convergence of the enthalpy h_{r10}.
- F_6 checks that the mass flow rate through the compressor and the capillary tube converges to the same value.
- F_7 monitor the convergence of the degree of superheat (dT_{sup}) in the evaporator.

In brief, the compressor and capillary tube models use the refrigerant conditions to determine the mass flow rate, and the condenser and evaporator models use the mass flow rate and determine refrigerant conditions. The cycle simulation is iterated until the mass flow rate and refrigerant conditions converge. In the next chapter cycle simulation results are supplied and compared to experimental results.

4.4 Conclusion

In this chapter all four component models were described as implemented in the micro heat pump simulation routine. Two capillary models were implemented, which will both be evaluated in the next chapter. A brief overview of the cycle simulation of the components was also outlined. A model is never complete if it has not been tested against experimental data. In the next chapter the models will be compared to experimental data to obtain the validity of each component model. In Appendix B sample calculations are performed containing formulae and numerical values to demonstrate the procedure used in each of the simulation models.

CHAPTER 5

VERIFICATION OF THE MODEL

CHAPTER 5

VERIFICATION OF THE MODEL

5.1 Introduction

The previous chapter focussed on the implementation of the four components as well as the total heat pump cycle into a simulation routine. In this chapter the focus falls on the verification of the model by comparing it with the experimental results. The chapter will be divided into the following sections:

- Experimental setup ⇒ Here brief overview is given of how the experiments were conducted, including the geometry of the different components used in the heat pump.
- Experimental results ⇒ A number of important results obtained from the experiments will be listed.
- Verification of simulation ⇒ The simulation results of each component model will be compared with the experimental results in the following categories:
    - Fluted tube condenser.
    - Air-cooled evaporator.
    - Reciprocating compressor.
    - Capillary tube.
    - Integrated heat pump cycle.

The results and comparisons will be provided in graphical form only. Tables with complete comparative results for all of the working points are provided in the appendices. The results are also discussed and evaluated.

5.2 *Experimental setup*

5.2.1 Heat pump geometry

Before the results of the simulations and experiments can be compared, the physical characteristics of the micro heat pump is required. Each component in the existing R-134a micro heat pump and its geometry will be discussed here.

Fluted tube condenser

The total length of the condenser is 3.8 meters. The fluted tube was manufactured from 12.7-mm (0.5-in.) outside diameter soft drawn copper tubing. The outside tube was made of 15.875–mm ($\frac{5}{8}$-in.) outside diameter soft drawn copper tubing. The outside tube is shrunk over the fluted tube so that an annulus is formed. The refrigerant (R-134a) flows inside the annulus with the water inside the fluted tube. The condenser is operated in a counter-flow configuration.

Air-cooled evaporator

The evaporator specifications are as follows:

Outside tube diameter	9.375-mm (3/8 in.)
Tube wall thickness	0.35-mm
Length of each tube	200.0-mm
Total height of evaporator	203.0-mm
Rows high	8
Rows deep	4
Number of circuits	1
Fins per inch	12
Fin type	Sine wave
Fin material	Aluminum

Table 5.1: Air-cooled evaporator specifications

Reciprocating compressor

The compressor used is an Embraco FG 95HAKW 220-240V 50Hz. It operates on refrigerant R-134a. Its commercial designation is $\frac{1}{3}$ h.p., with a high back pressure heating capacity of 1055 Watt.

Capillary tube

The capillary tube used is from Watsco Components, Inc. Its specification is a number 117, with a 1.778-mm (0.070-in.) inside diameter. The length of the capillary is 1.5 meter.

5.2.2 Measuring instrumentation

In order to obtain accurate flow measurements for both the refrigerant and the water, the following apparatus were used.

Refrigerant

- Pressure measurements ⇒ Pressure transducers.
- Temperature measurements ⇒ Thermocouples.

Both the pressure data and temperature data were logged on a computer via ADAM modules.

Water

- Temperature measurements ⇒ Thermocouples.
- Mass flow rate ⇒ Rotameter.

Measurements on the waterside were recorded manually..

The positions of the pressure transducers and the thermocouples are shown on Figure 5.1 and are as follows:

- P1, T1 ⇒ Inlet pressure and temperature of the condenser.
- T2 ⇒ Condensing temperature.
- P2, T3 ⇒ Exit pressure and temperature of the condenser.

- P3, T4 ⇒ Inlet pressure and temperature of the evaporator.
- T5 ⇒ Refrigerant temperature on the second column of the evaporator.
- T6 ⇒ Refrigerant temperature on the third column of the evaporator.
- P4, T7 ⇒ Exit pressure and temperature of the evaporator.

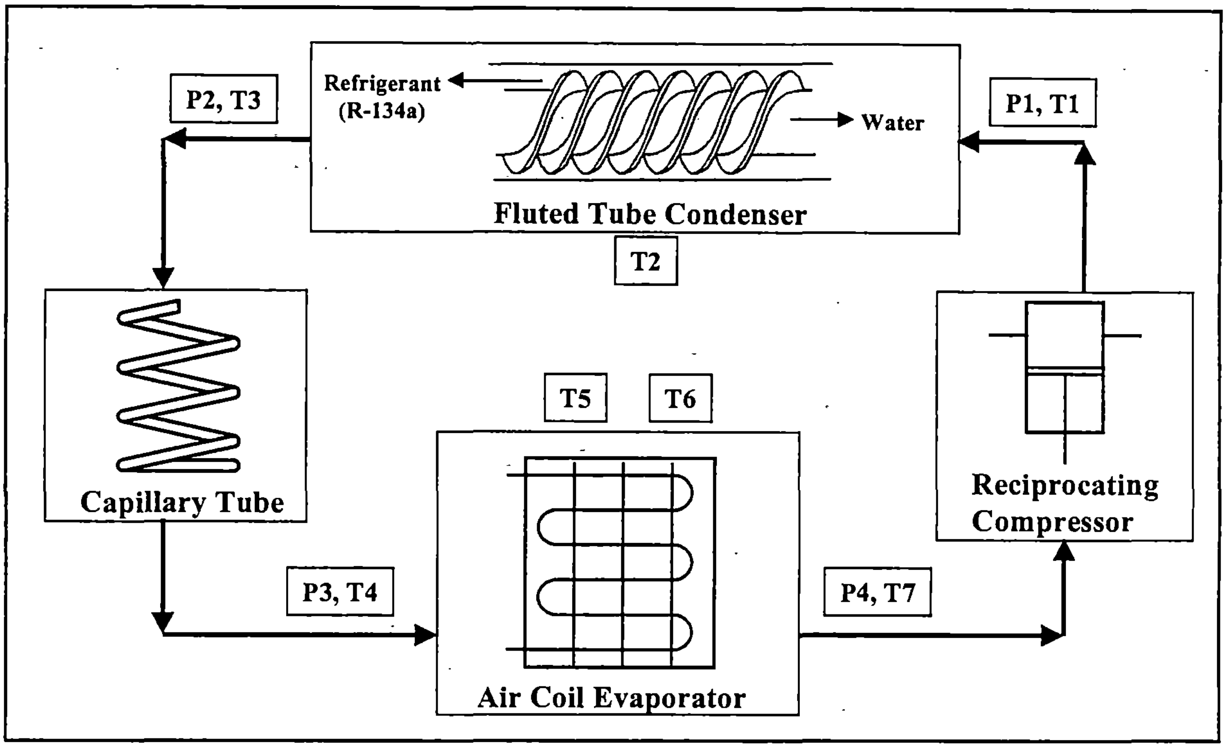

Figure 5.1: Position of measuring points on the refrigerant side

On the water side, mass flow rates as well as the inlet temperature from the tank and the outlet temperature from the heat pump were measured.

5.2.3 Experimental method

The experiments were conducted in a room where the wet-bulb temperature of the atmosphere was varied. Experiments were done at wet-bulb temperatures of 10°C, 15°C, 20°C and 25°C in order to obtain the characteristics of the micro heat pump over a wide range of conditions. At each wet-bulb temperature, measurements were taken at different inlet water temperatures. The inlet water temperature was varied between 15°C and 55°C with 5°C increments. The outlet water temperature was held constant at 60°C by manually controlling the water mass flow rate as the inlet water temperature changed. Therefore a total of 36 sets of measured data were obtained for the cycle.

5.3 *Experimental results*

A few important results that were obtained will now be discussed before the simulation and experimental results are compared.

The micro heat pump was designed to provide a nominal heating capacity of 1.2 kW at 10°C wet-bulb and 15°C inlet water temperatures. In Figure 5.2 the actual performance of the heat pump is shown by plotting the measured heating capacity normalized with the nominal capacity $(\frac{Q}{Q_n})$ for all 36 measuring points, together with curve fits based on the standard ARI equations. It can be seen that the experimental heat pump performed slightly better with a normalized capacity of just over 1 at the design condition.

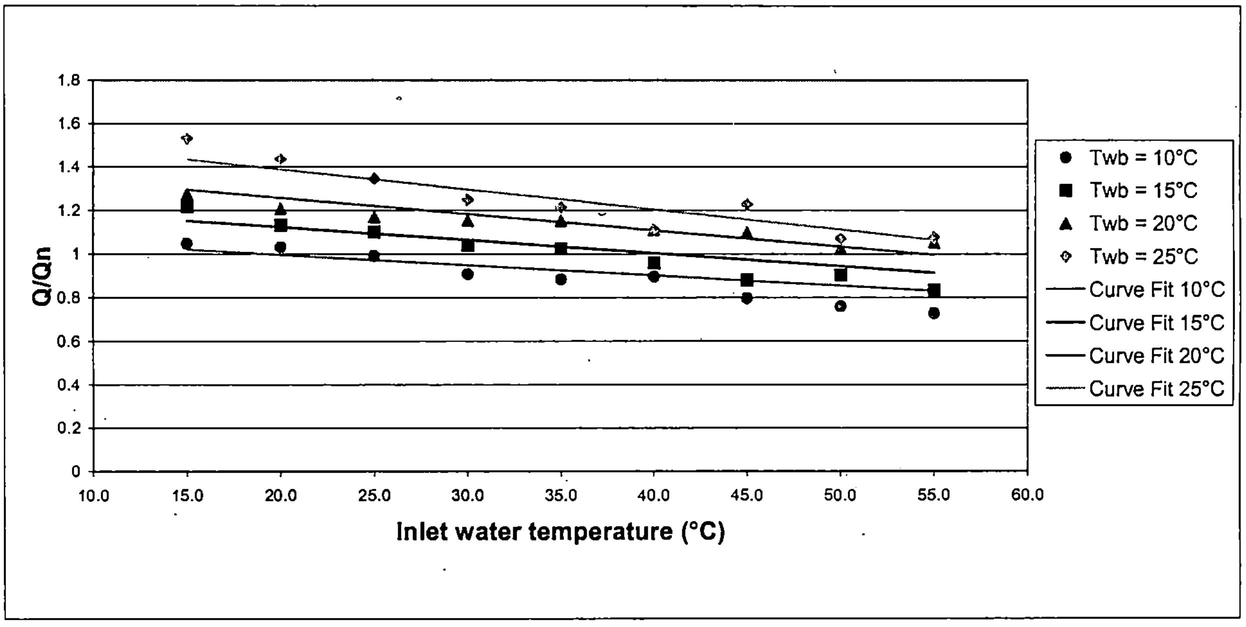

<u>Figure 5.2:</u> Q/Qn for different water temperatures

One of the most important aspects when evaluating a heat pump is the coefficient of performance (COP) of the cycle. The COP is defined by:

$$COP = \frac{\text{Heat Transfer in Condenser (W)}}{\text{Power Input of Compressor (W)}}. \qquad (5.1)$$

With a nominal capacity of 1.2 kW and a power input to the compressor of 0.6 kW, the theoretical COP given for the system was equal to 2.

As can be seen in Figure 5.3, the COP of the heat pump was above 2 for most of the working range investigated. Only at a low wet-bulb temperature of 10°C did the COP go as low as 1.5 for high inlet water temperatures. In the experiment the COP at design conditions was 2.127 compared to a design COP of 2.

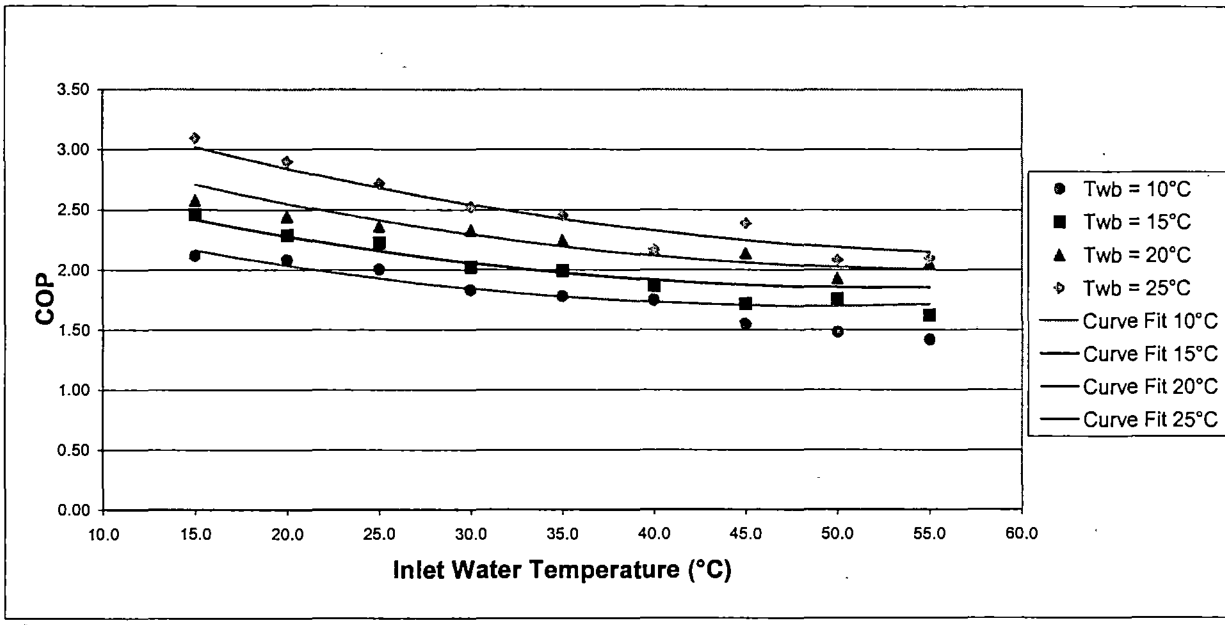

Figure 5.3: Coefficient of performance for varying temperatures

5.4 *Verification of simulation*

In this section all the results obtained with the component simulations will be verified against the experimental measured data. Only the most important results will be discussed here. Complete simulation results for each component are available in Appendix A.

5.4.1 Fluted tube condenser

A small piece of the fluted tube was cut off and the geometry of the flute was measured. The geometry used as input to the condenser model is provided in Table 5.2.

Inside diameter of outside tube	12.7-mm
Outside volumetric diameter of fluted tube	11.4-mm
Inside volumetric diameter of fluted tube	10.0-mm
Helix angle	60.82°
Flute pitch	5.0-mm
Flute depth	7.2-mm
Non-dimensional helix angle	0.6758
Non-dimensional flute depth	0.766
Non-dimensional flute pitch	0.532
Total length	3.8-m

Table 5.2: Fluted tube geometry.

Note that the mass flow rate of the refrigerant was not measured due to insufficient measuring equipment. It was decided to measure the waterside as accurately as possible to obtain the total heat transfer equal to:

$$Q = m_w.Cp_w(T_{out} - T_{in}) \tag{5.2}$$

The condenser was well insulated and both the inlet pressure and temperature and the outlet pressure and temperature of the refrigerant in the condenser was measured very accurately. A heat balance could be used to obtain the mass flow rate of the refrigerant based on the waterside heat transfer also,

$$m_r = \frac{Q}{h_{in} - h_{out}}, \tag{5.3}$$

where h is the enthalpy at the inlet and outlet.

In Figure 5.4 the heat transfer rate obtained with the simulation is plotted against the measured heat transfer rate for the 36 points. The results show an average accuracy of 97% with a maximum error of 9.5%. In general the heat transfer rate was slightly underpredicted. The two points of overprediction were found to be at high inlet water temperatures and high humidity. This resulted in high water flow rates, slightly above the measuring range of the rotameter. The apparent errors are therefore due to inaccurate measurements.

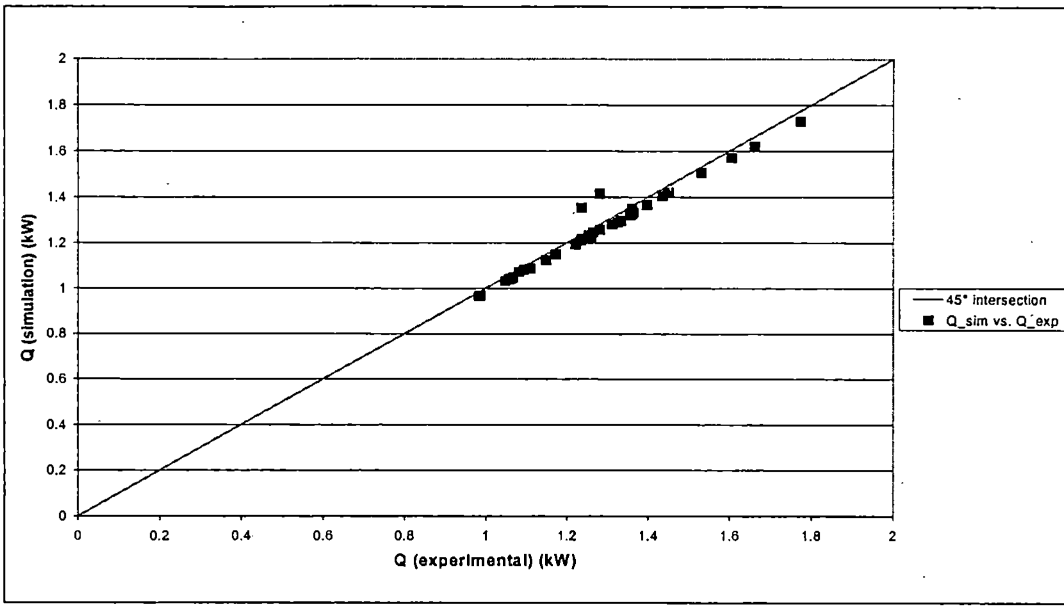

Figure 5.4: Heat transfer in condenser

In Figure 5.5 the temperature distribution through the condenser for the simulation and the experiment for the case of 10°C wet-bulb and 19.8°C inlet water temperature are compared. This indicates that the water outlet temperature is higher than the condensing temperature of the refrigerant. The possibility when using a counter-flow configuration of extracting an additional amount of energy from the refrigerant in the superheat region therefore exists.

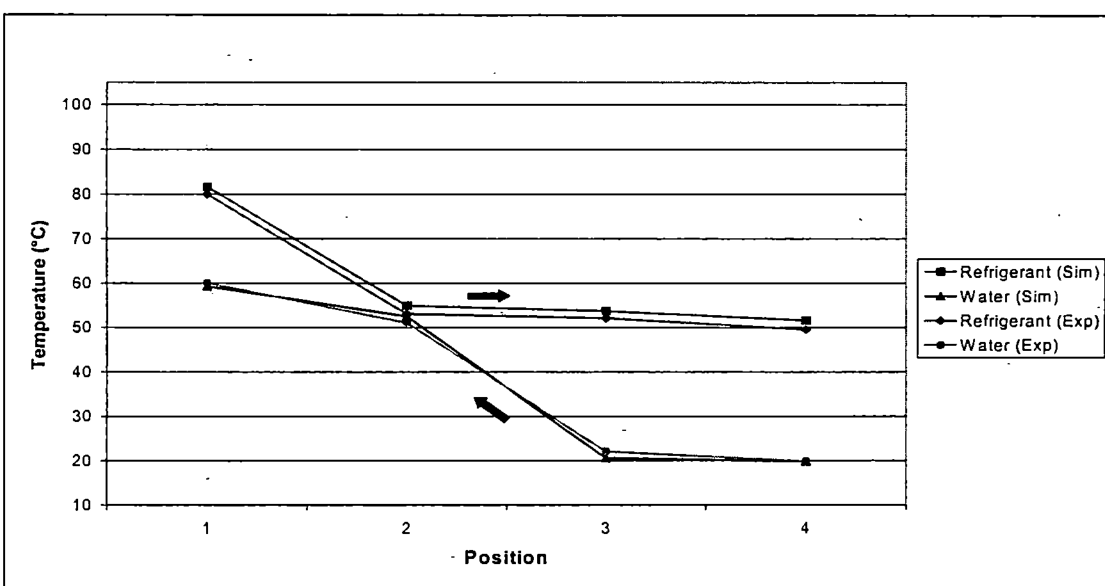

Figure 5.5: Temperature versus position in condenser

It was mentioned in Chapter 3 that the refrigerant inventory was based on the assumption that the fraction of liquid in the condenser always remains constant over any range of operating conditions. During the simulation the degree of subcool obtained from the experiments was used as input to the model, obtaining the fraction of liquid in the condenser for each simulation. Figure 5.6 shows the validity of the assumption.

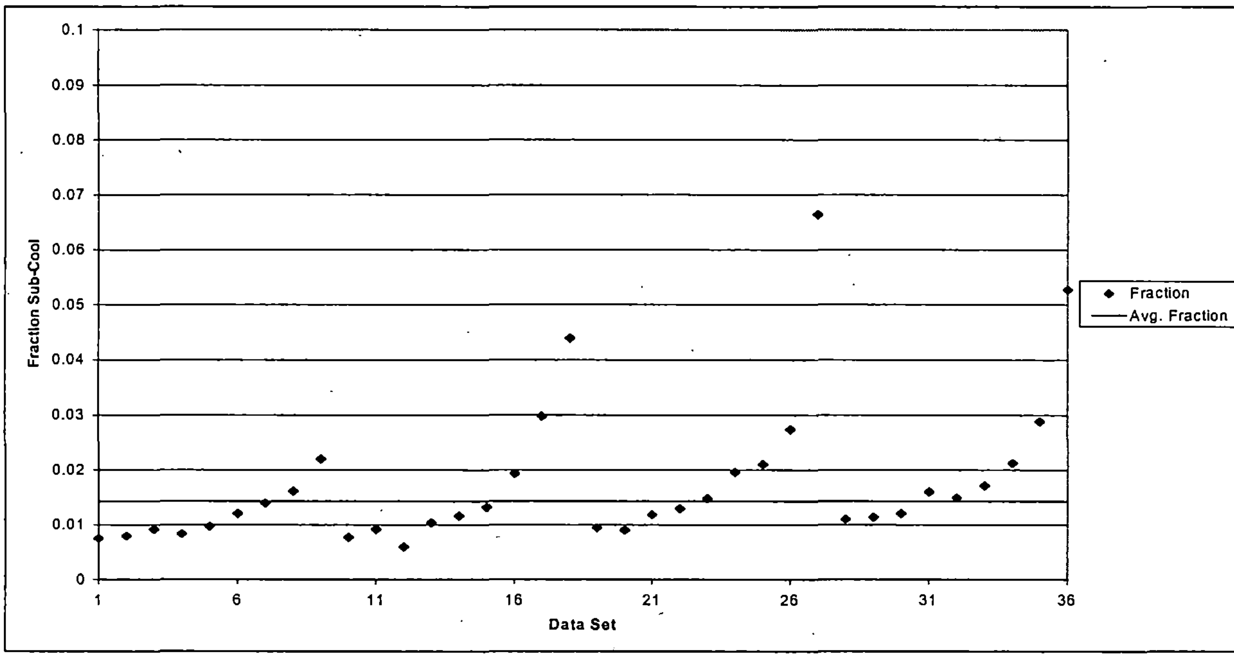

Figure 5.6: Fraction of liquid inside condenser

In Figure 5.6 the fraction of subcool is plotted for each data set. The fraction subcool bandwidth was predicted between 0.0075 and 0.03, with a few less accurate overpredictions. The values of overpredictions were found to be at high inlet water temperatures and high humidity. As stated earlier, this is due to inaccurate measurements. The results show an average fraction of 0.0143 (1.43%) for the condenser. In the above figure the trend for each wet-bulb temperature group of data points is also correct. This means that as the inlet water temperature increases, the inlet superheat temperature and pressure of the refrigerant increase, leading to an increase in the fraction of subcool in the condenser. The above figure therefore supports the assumption of a constant liquid fraction when simulating the condenser over a range of test conditions.

5.4.2 Air-cooled evaporator

The evaporator geometry in Table 5.1 is used as input to the evaporator model. The measured degree of superheat is given as a fixed input parameter to the model. A problem occurred at the set of data for 25°C wet-bulb temperature. It was found that at this temperature the evaporator was so oversized, that the intermediate temperature measurements were higher than the inlet temperature to the evaporator. This means complete evaporation took place in the first row of the evaporator. For these cases the degree of superheat was varied until the inlet temperature of the refrigerant was equal to the experimental inlet temperature.

Figure 5.7 shows the comparison between the heat transfer determined by the simulation and the heat transfer determined experimentally. The results show an average accuracy of 98% with a maximum error of 11.4%. In general the heat transfer rate was slightly underpredicted. The single less accurate point occurred at the same condition where the condenser model overpredicted. As stated earlier, this is due to an incorrect water mass flow measurement. On average the simulation also slightly underpredicts the heat transfer rate. The predicted refrigerant temperatures were on average within 1°C of the experimental temperatures.

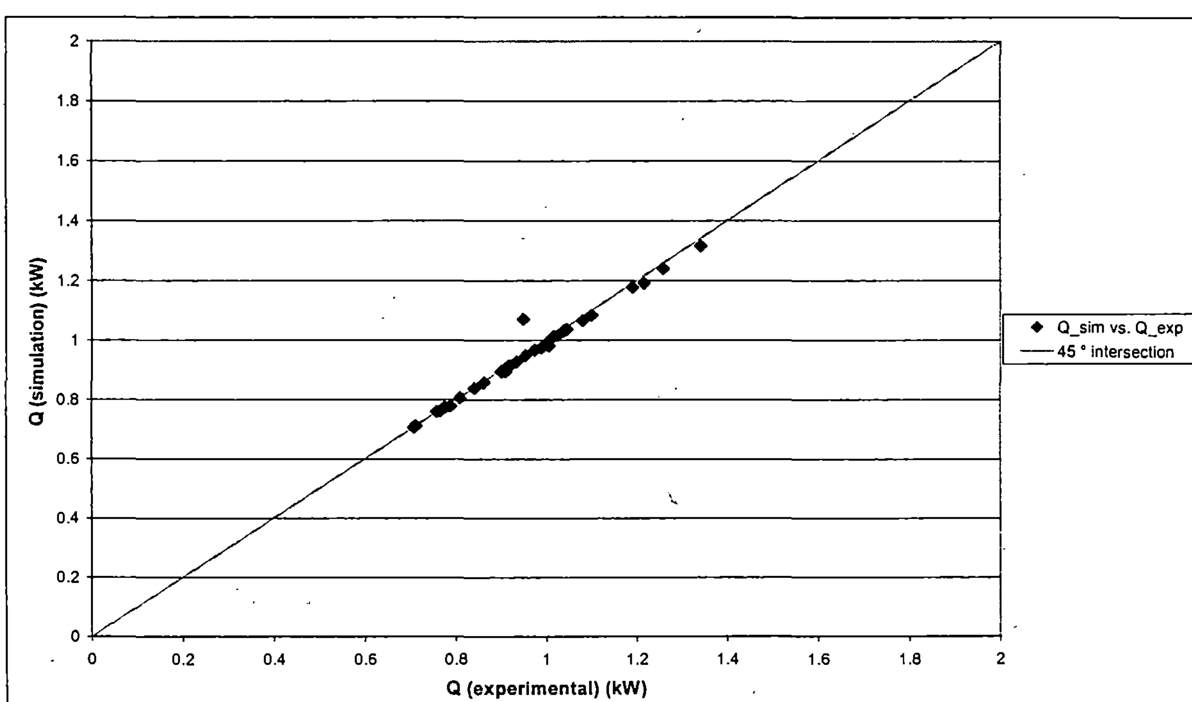

Figure 5.7: Heat transfer in evaporator

Figure 5.8 shows a typical temperature distribution through the evaporator obtained by the simulation model. Note that each block on the diagram represents a tube with eight tubes from the bottom to the top. It must be kept in mind that every tube in the evaporator can also be subdivided in the simulation model. This example is for a 10°C wet-bulb and 19.4°C dry-bulb temperature. On the refrigerant side there is a temperature drop with an increase in enthalpy up to the two-phase/superheat interface. In the superheat area the temperature increases. The air temperature change across each row differs from tube to tube due to the change in refrigerant temperature. The air temperature profile at the outlet face can therefore be determined.

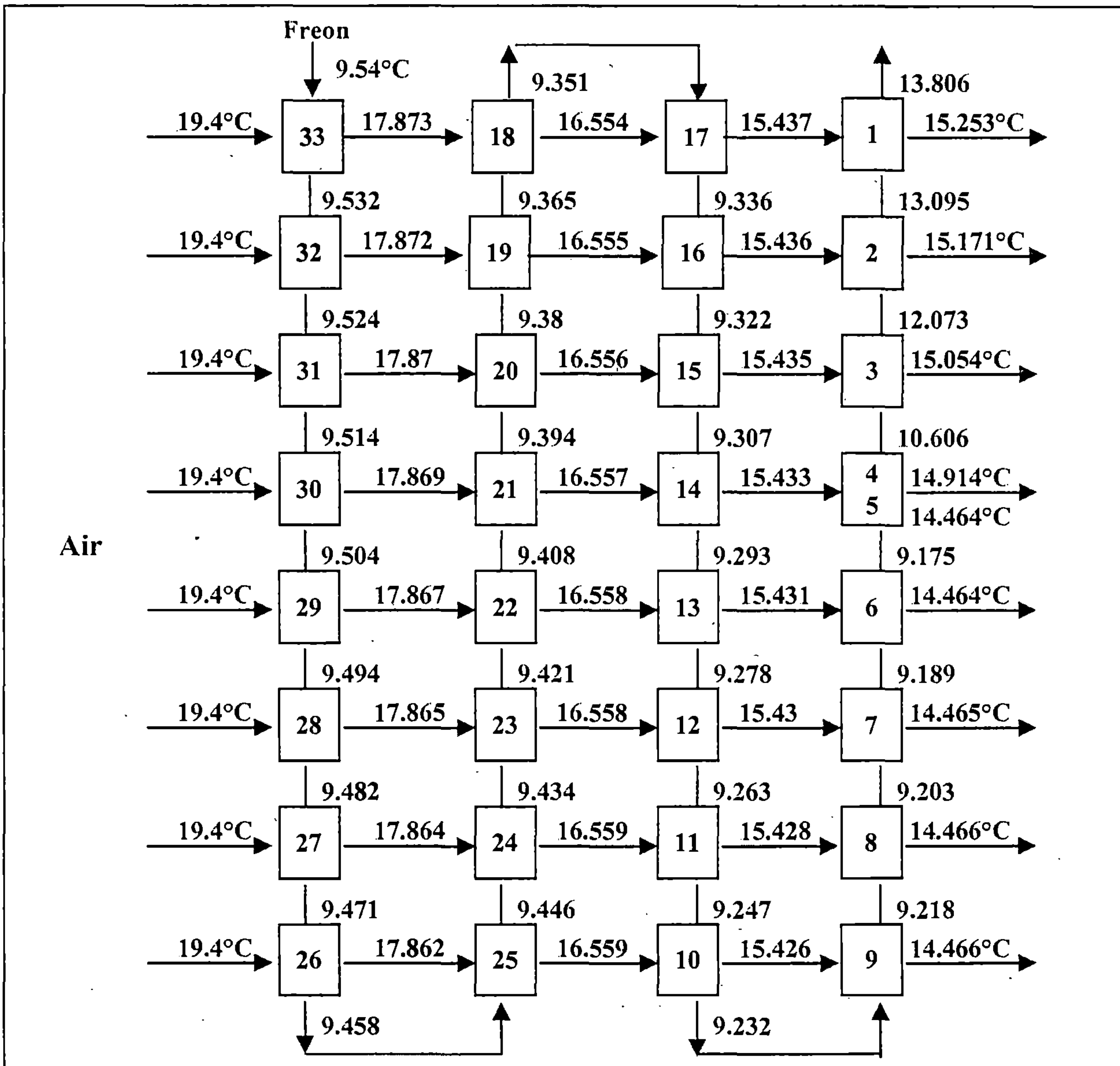

Figure 5.8: Temperature change through evaporator

5.4.3 Reciprocating compressor

When the compressor simulation was evaluated against the experimental data, it was found that the model was very inaccurate. The inaccuracy was to such a degree that the model could not be used. One of the reasons for the inaccuracy was that the theoretical isentropic efficiency and volume flow was based on a few data points supplied by the manufacturers. These data points were insufficient to obtain a valid model. It was decided to use the experimental data and obtain new coefficients for the curve fits of the isentropic efficiency and the volume flow rate. The new plots are shown in Figure 5.9.

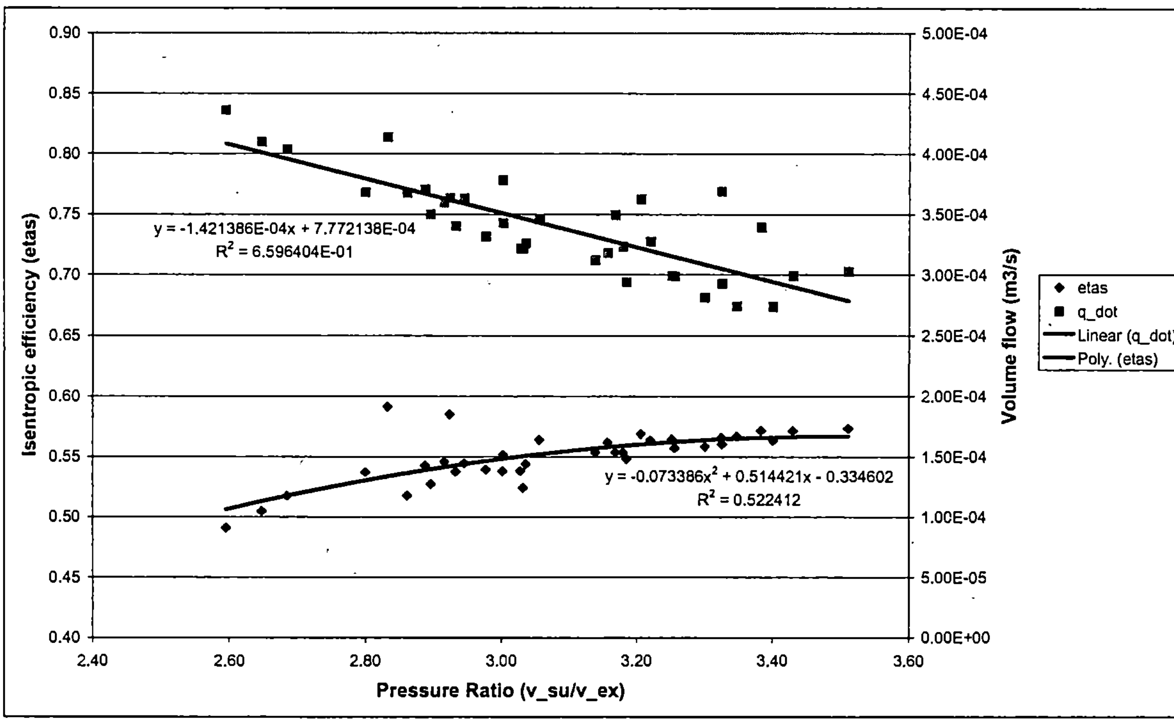

Figure 5.9: New functions for compressor simulation routine

The two curves were obtained via least square fits. The new coefficients were used in the verification of the simulation model.

In Figure 5.10 a comparison is made between the experimental and simulated mass flow rates. The simulated mass flow rates are on average 95% accurate when compared to the experimental results. The mass flow rate determined at 25°C wet-bulb and 55°C water temperature has the lowest accuracy of 87.3%.

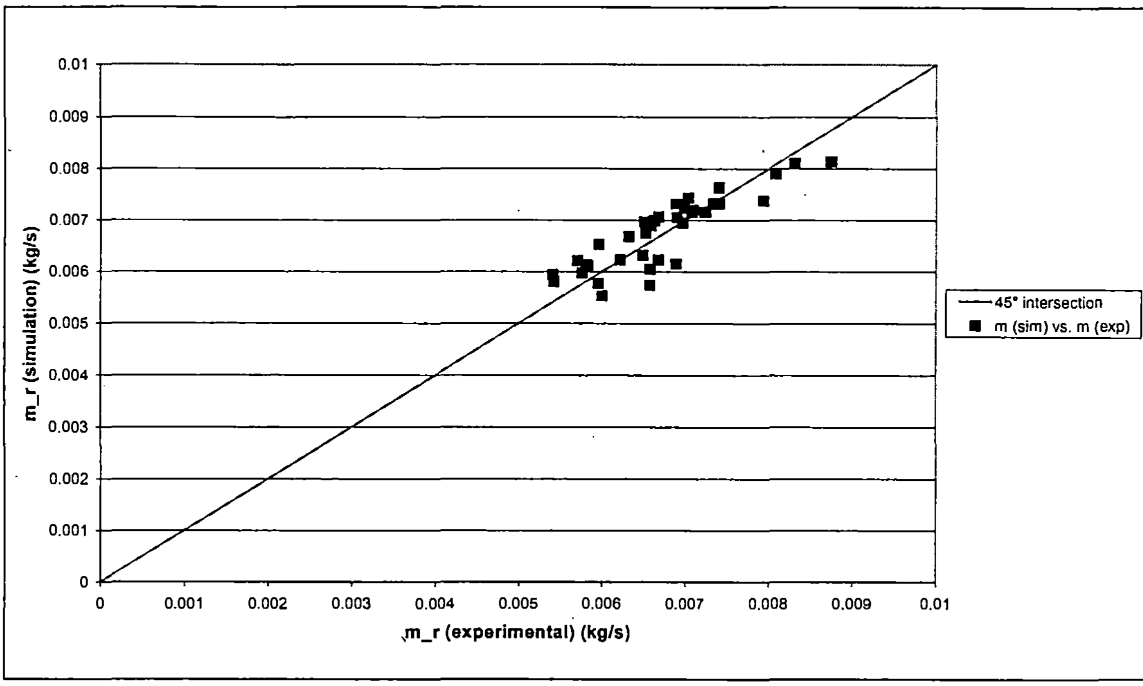

Figure 5.10: Comparison of mass flow rates

In Figure 5.11 the predicted work done on the refrigerant is evaluated. The experimental value was determined by subtracting the measured evaporator heat transfer rate (kW) from the condenser heat transfer rate (kW). The results show an average accuracy of 94.8% with a maximum error of 17.5%. The lowest accuracy of 82.5% is again at a high wet-bulb temperature with an inlet water temperature of 55°C.

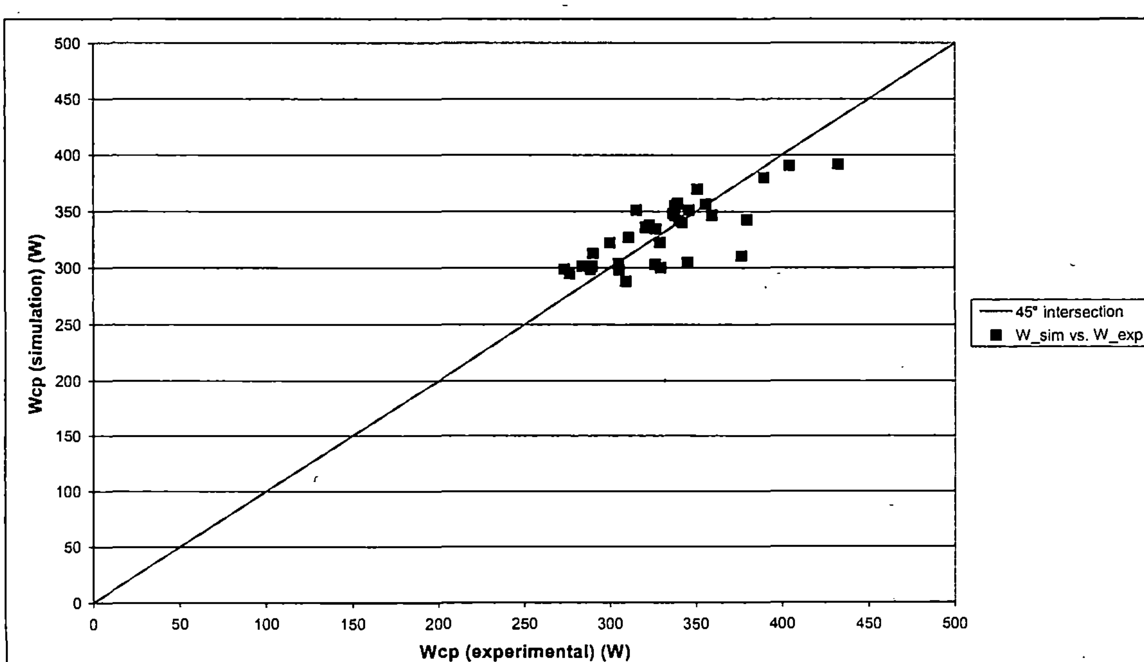

Figure 5.11: Compressor work on refrigerant

5.4.4 Capillary tube

Theoretical model of Bittle and Pate (1996)

In the simulation, the results given by Bittle and Pate were compared to results obtained in our model with the same capillary tube configuration. The simulation will be divided into two parts, as discussed in Chapter 4, namely:

- A combination of the continuity equation and the energy equation as in equation 4.18. As the quality of the refrigerant increases, the influence of the velocity increases.
- For the second approach, constant enthalpy through the two-phase region is assumed. This is an assumption that is widely used when capillary tubes are simulated.

The first approach will be discussed by means of Figures 5.12 and 5.13, which show the simulation results for a specific condition.

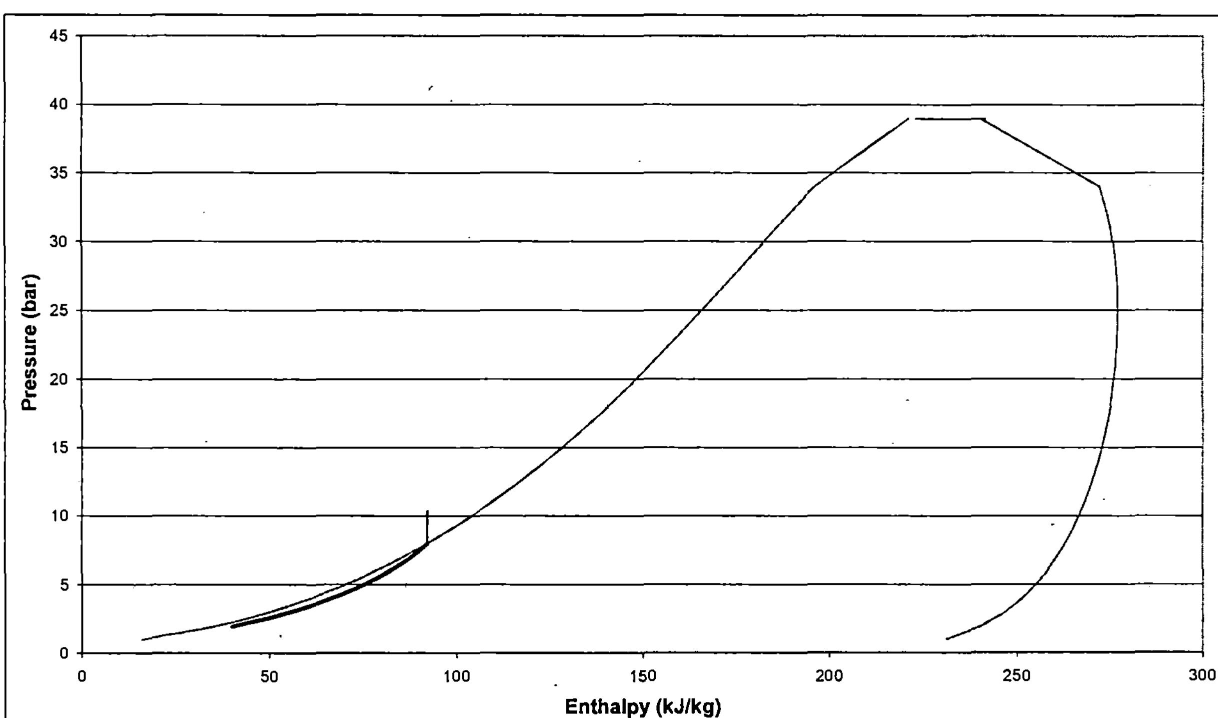

Figure 5.12: Change in the enthalpy through the capillary tube

For the first approach it was found that the enthalpy decreases as the refrigerant flows through the two-phase region. This is due to the increasing effect of the velocity in the capillary tube. As the quality of the refrigerant increases, the velocity increases because of evaporation. As shown in Figure 5.12, the simulated enthalpy drop is quite significant, contrary to the generally accepted assumption of constant enthalpy.

Another problem encountered was that as the quality of the refrigerant increased, the entropy decreased as shown in Figure 5.13. This is in conflict with the second law of thermodynamics, which states clearly that the entropy may not decrease in adiabatic flow. The results obtained by Bittle and Pate, which used this approach, did not agree with the results obtained with our simulation, even though the two models used exactly the same input data. For this reason it was decided to investigate what happens with constant enthalpy assumed through the two-phase region. It was found that in certain cases the calculated incremental length of the very last tube length was negative. However, all the equations were solved accurately. The problem discussed above could probably be ascribed to the fact that choked flow is encountered at the outlet of the capillary tube.

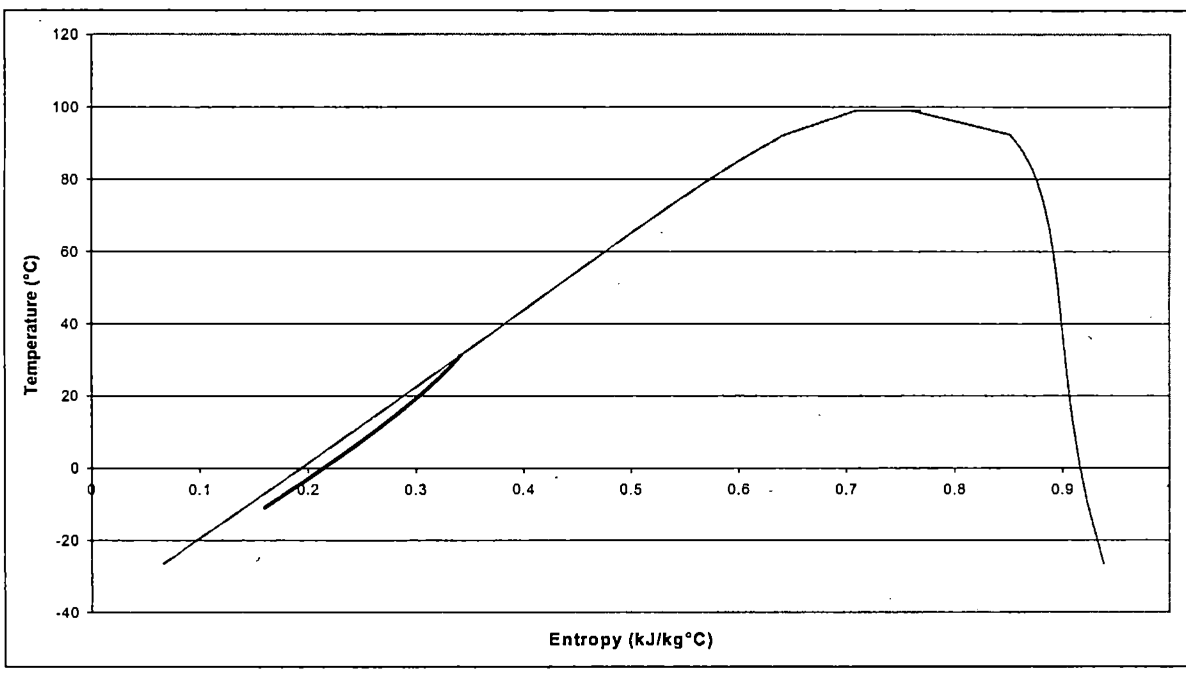

Figure 5.13: Temperature versus entropy through the capillary tube

The results provided by the capillary tube model for a specific case when simulated with constant enthalpy is shown in Figures 5.14 and 5.15. As can be seen from Figure 5.15, the entropy now increases throughout the capillary tube. This agrees with the second law of thermodynamics. With the assumption of constant enthalpy the results reported by Bittle and Pate were also obtained by us. According to our view, this shows that more research needs to be done to check the validity of their model. It seems, however, that the assumption of constant enthalpy was used to generate their results, which is in conflict with their stated governing equations.

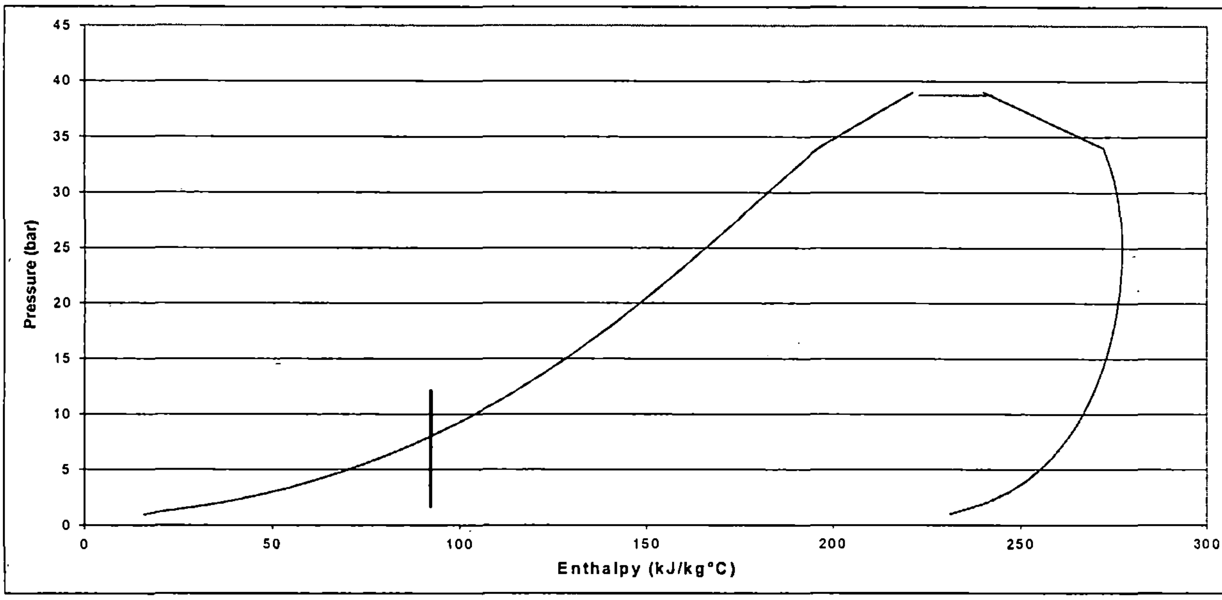

Figure 5.14: Constant enthalpy through capillary tube

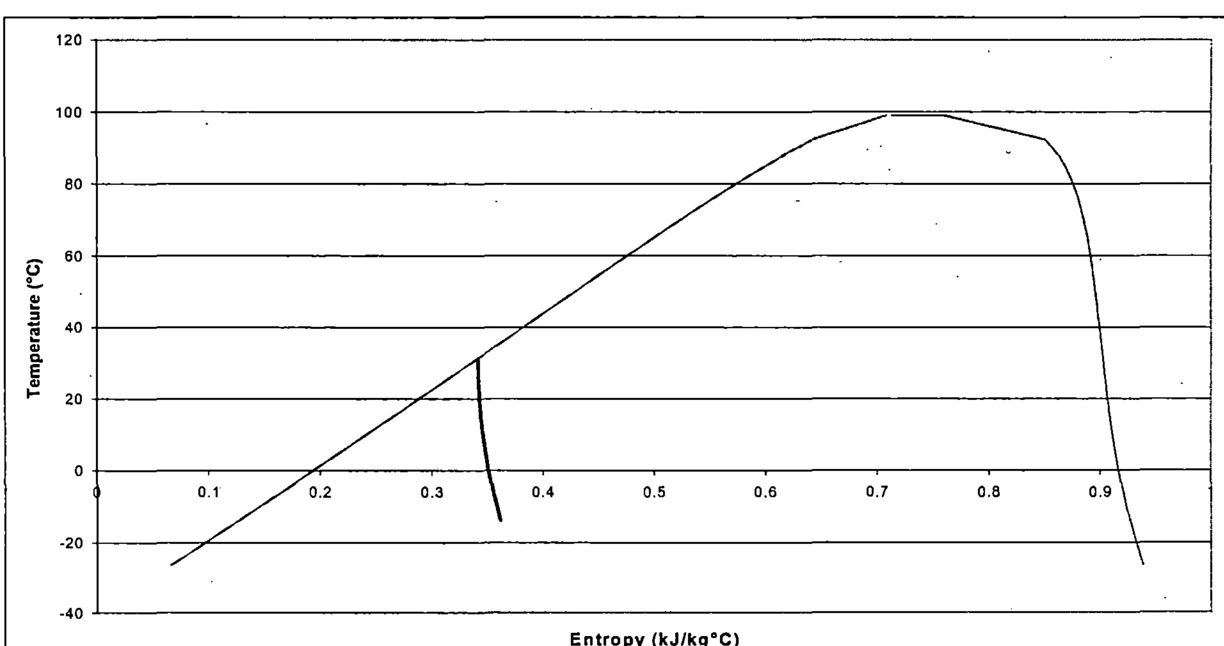

Figure 5.15: Entropy change for constant enthalpy

Figure 5.16 shows the comparison between the results obtained by Bittle and Pate (1996) and the results obtained by our simulation with decreasing entropy. The average accuracy obtained was 80.6%, with the highest accuracy being 86.5%. Due to the low accuracy this supports our statement that the results by Bittle and Pate could not have been obtained with this method.

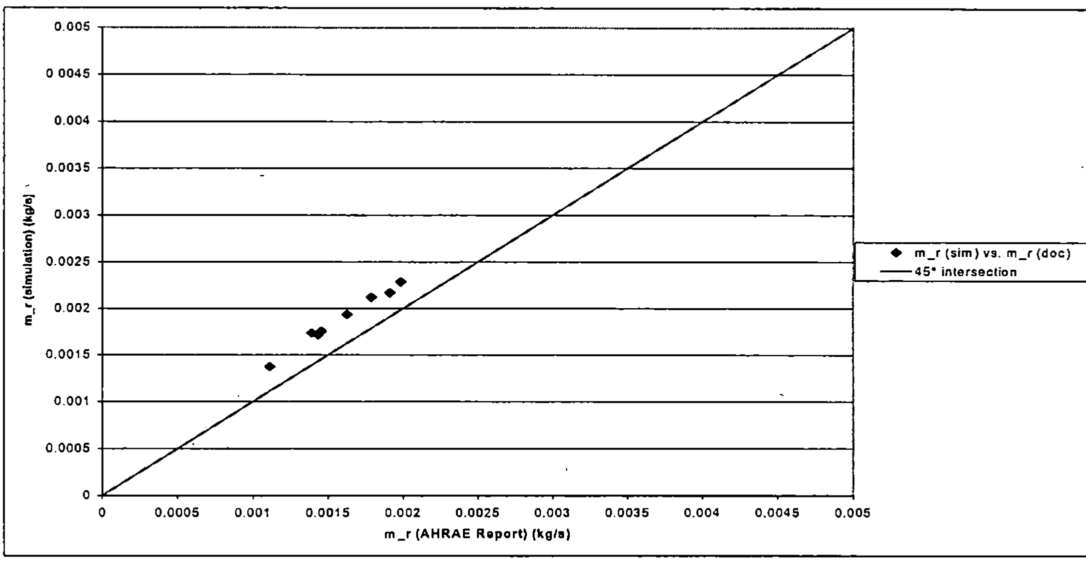

Figure 5.16: Comparison of mass flow rates for method 1 (Continuity and Energy)

The comparison with our results obtained with the assumption of constant enthalpy is shown in Figure 5.17. The average accuracy of the simulation was 95.5%, with a highest accuracy of 100%. This shows that the results by Bittle and Pate were probably obtained with the assumption of constant enthalpy.

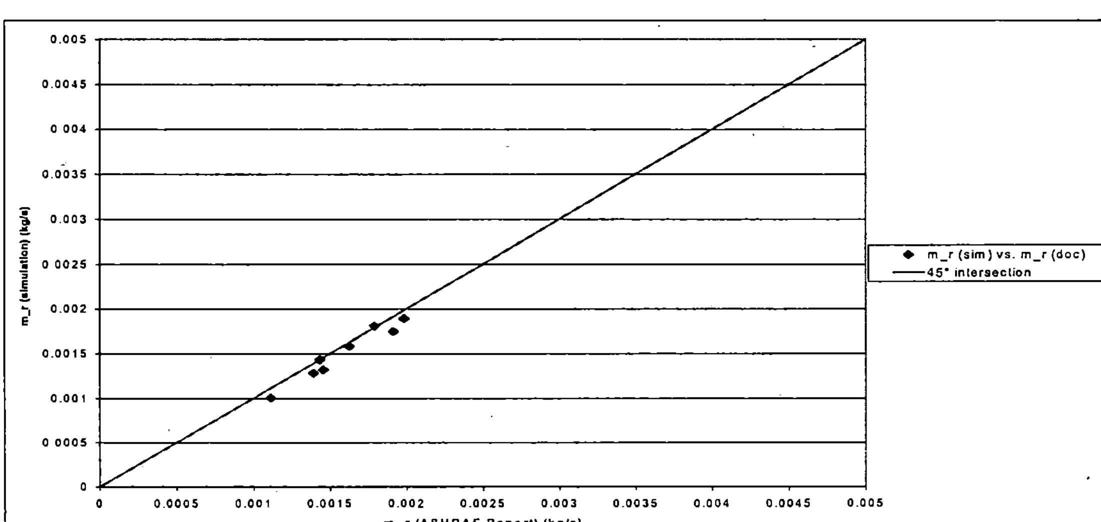

Figure 5.17: Comparison of mass flow rates for constant enthalpy

Fortunately a much simpler approach to the simulation of the capillary tube was found in a more recent publication by Bittle **et al.**, (1998), namely that of a dimensionless correlation. This will be discussed further in the next paragraph.

Dimensionless correlation of Bittle et al., (1998)

When the subcooled inlet correlation derived by Bittle **et al.**, (1998) was used to compare the predicted mass flow rate with our experimental mass flow rate, it was found that the predicted mass flow rate was almost double compared to the experimental value. A few problems could have led to this, including incorrect measurement of experimental data. It was decided that the experimental data was sufficiently accurate and that the problem was due to our operating conditions lying outside the range specified by Bittle **et al.**, in their work.

Because of the Π-groups are based on fundamental principles, the only factor which can change is the coefficients ($B, m_1, m_2, \ldots, m_7$). The coefficients which Bittle **et al.**, derived was through experimental operating conditions. It was decided to derive new coefficients based on our own experimental data. This was done with Microsoft® Excel using its built-in solver. A new subcooled inlet correlation was obtained which will be used in the simulation routine.

$$\Pi_8 = 1.8927\Pi_4^{0.7107}\Pi_1^{-0.4838}\Pi_5^{0.0459}\Pi_2^{-0.4027}\Pi_6^{1.7}\Pi_7^{0.2653} \quad (5.4)$$

$$m_r = d_c.\mu_f.(1.8927\Pi_4^{0.7107}\Pi_1^{-0.4838}\Pi_5^{0.0459}\Pi_2^{-0.4027}\Pi_6^{1.7}\Pi_7^{0.2653}) \quad (5.5)$$

With the new coefficients the simulation model provided an average accuracy of 95.6% with the largest deviation being 11.6%. The results are shown in Figure 5.18.

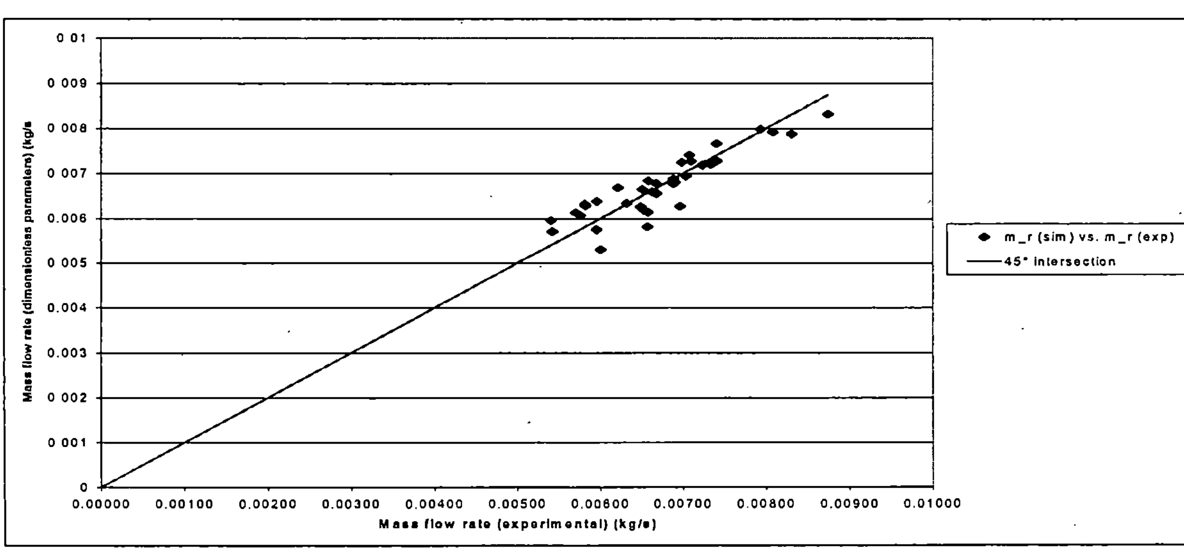

Figure 5.18: Mass flow rate prediction with dimensionless parameters

Unfortunately, the new correlation is only applicable to the range of experimental data on the micro heat pump. The validity of the correlation over a wider range of test data still has to be determined before the model can be applied over a wide range of heat pump conditions.

5.4.5 Integrated heat pump cycle

The component models were also integrated and a complete heat pump cycle simulation was done. The integrated simulation included the condenser, evaporator, compressor and dimensionless capillary tube correlation. In this part of the chapter only the most important results will be given, with detailed results provided in Appendix A. The results obtained for each component will be discussed separately.

Fluted tube condenser

In the cycle simulation the average accuracy of the heat transfer rate in the condenser was 96.9%, as shown in Figure 5.19.

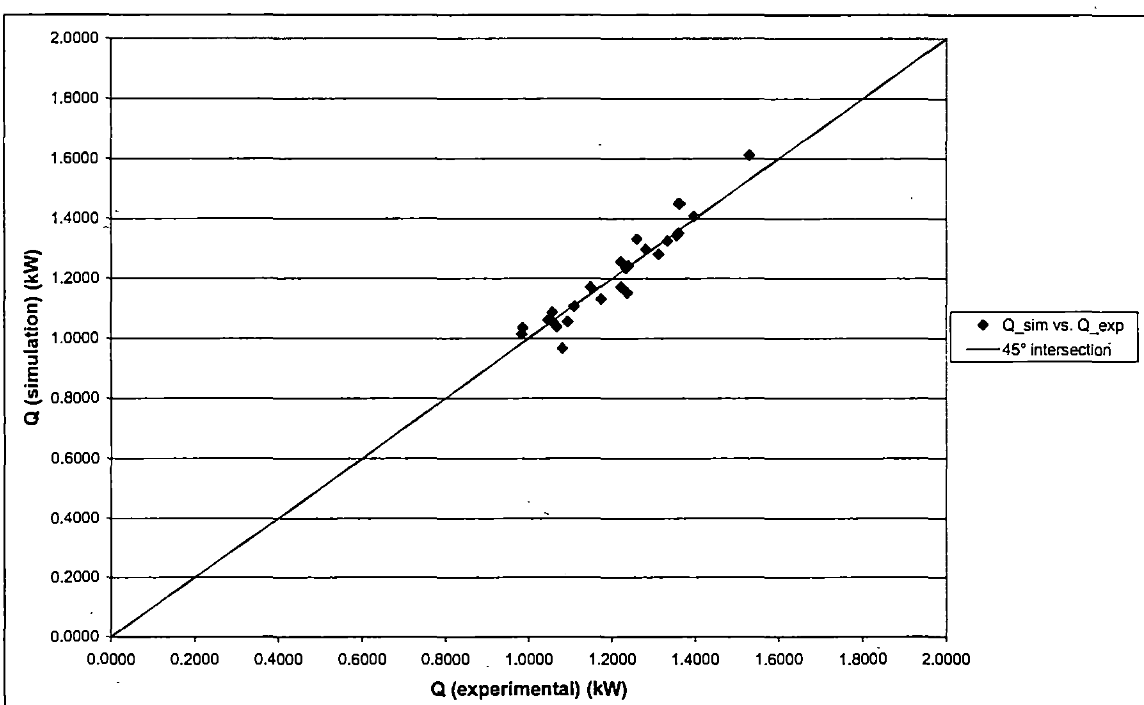

Figure 5.19: Heat transfer in condenser

Air-cooled evaporator

In the cycle simulation the average accuracy of the heat transfer rate in the evaporator was 95.9%, as shown in Figure 5.20.

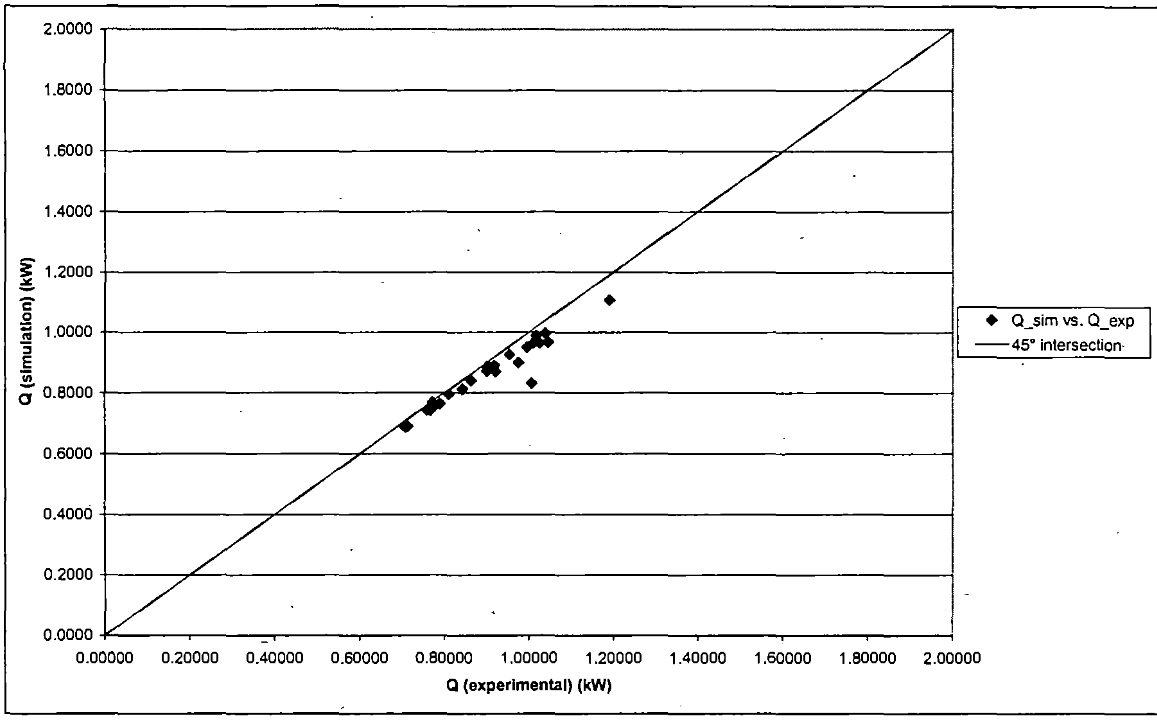

Figure 5.20: Heat transfer in evaporator

Reciprocating compressor

The accuracy of the condenser and evaporator is dependent on the accuracy of the compressor model. The compressor model is based on two curve fits to obtain the correct mass flow rates and work on the refrigerant.

The average accuracy of the mass flow rate obtained with the cycle simulation is 95.2% as shown in Figure 5.21. This means the curve fit used to predict the mass flow rate is sufficiently accurate. It must be kept in mind that the coefficients for the curve fits was based on the experimental data.

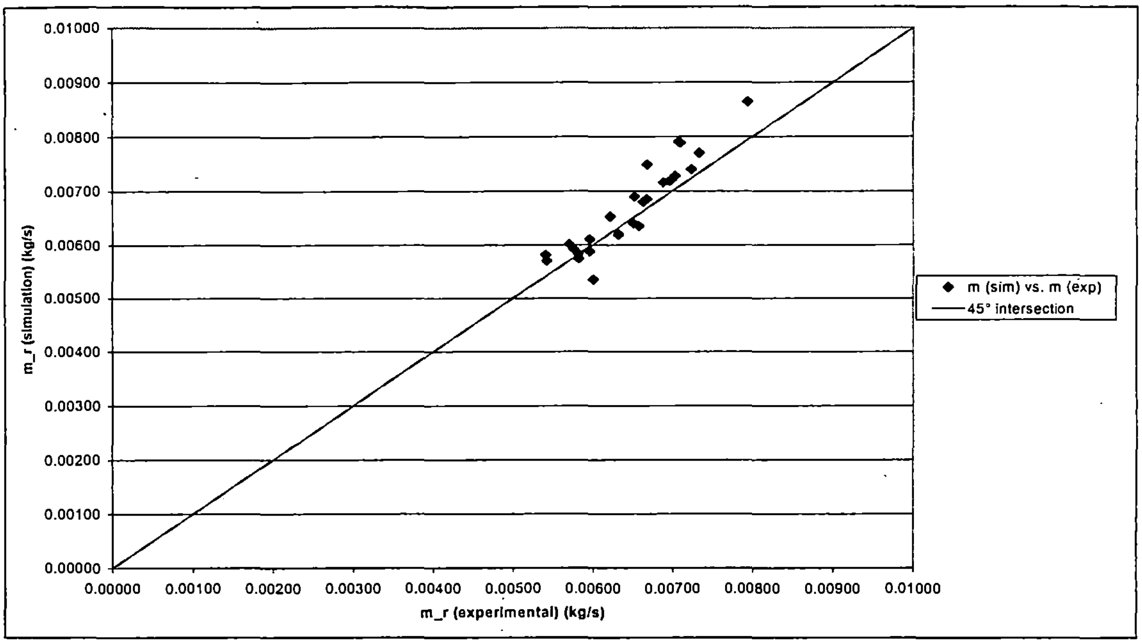

Figure 5.21: Comparison of mass flow rates

A comparison between the measured and predicted work done on the refrigerant is shown in Figure 5.22. The average accuracy is 94.9%. The cases showing larger deviations are at a high wet-bulb temperature and high inlet water temperature. This inaccuracy is dependent on the measured mass flow rate during the experimental phase. There is, however, still some room for improvement in the accuracy of the model.

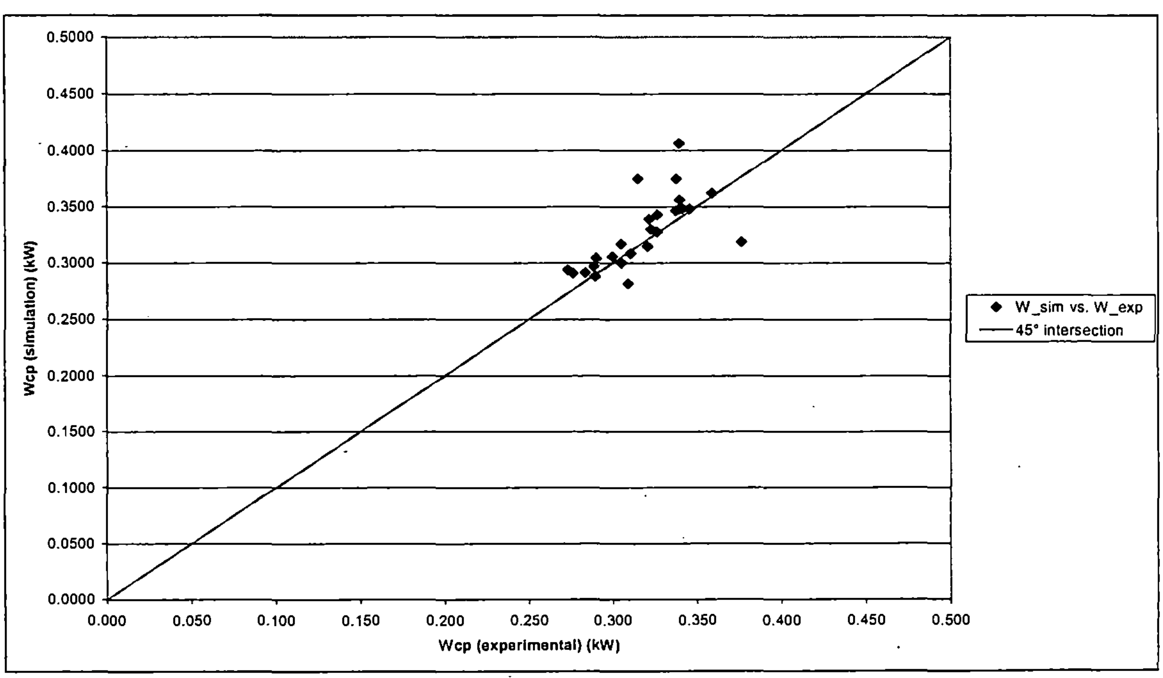

Figure 5.22: Compressor work on refrigerant

5.5 Conclusion

In this chapter the results obtained by the simulation of the different components was compared to the experimental values. The results were only given in graphical form, with complete tables available in Appendix A. The accuracy of the components when simulated on their own was very satisfactory. Both the condenser model and the evaporator model were on average within 4% of the experimental values. The accuracy of the compressor model was also satisfactory, with some room for improvement. The mass flow rate was on average 95% accurate and the work done on the refrigerant was 94.8% accurate.

No valid comparison could be obtained between the simulation and the experimental values for the theoretical capillary tube model. The most important conclusion is that Bittle and Pate (1996) also assumed constant enthalpy, contrary to the information provided in their earlier publication.

References

BITTLE, R.R., PATE, M.B. 1996. A theoretical model for predicting adiabatic capillary tube performance with alternative refrigerants. *ASHRAE Transactions*, 102(2):52-64.

BITTLE, R.R., WOLF, D.A., PATE, M.B. 1998. A generalized performance prediction method for adiabatic capillary tubes. *International Journal of Heating, Ventilating, Air-Conditioning and Refrigerating Research*, 4(1):27-43; Jan.

CHAPTER 6

CONCLUSION

CHAPTER 6
CONCLUSION

6.1 Introduction

In this chapter a summary will be provided of the most important results that were discussed in the previous chapters. From these results certain conclusions will be made, leading to recommendations for further research.

6.2 Summary

In the first chapter the background was given to why this study was regarded as important. In Chapter 2 a literature survey was conducted. It was found that various heat pump component models exist in the literature. A shortcoming of most of these models was that empirically defined equations are used, which limits the application. For the fluted tube condenser model a method for solving the geometry was found. Heat transfer and pressure drop correlations were also found and could be implemented into the model. For the air-cooled evaporator a wide range of literature was available. The model could be based on an existing method found in the literature. Heat transfer and pressure drop correlations were also found. In the case of the reciprocating compressor most of the literature reviewed made use of compressor performance data available from the manufacturers. A new model therefore had to be developed because of a lack of performance data in the case of the relevant compressor. Most of the capillary tube models found in the literature used empirical equations. A theoretical model was found where fundamental equations were used. The theoretical capillary model, however, provided doubtful results. Another capillary tube model was designed based on dimensionless correlations. This was eventually implemented in the model of this study.

In Chapter 3 the relevant theory for the four different components is derived and discussed. The way in which each simulation model was implemented is discussed in Chapter 4.

In Chapter 5 the four models were verified, using experimental data obtained from tests on the micro heat pump. Simulation results were obtained for each component separately as well as for a cycle simulation. When simulated separately, the condenser model has an average accuracy of 97.7% and the evaporator model 98%. The accuracy of the compressor model is dependent on the two curve fits used. The mass flow rate predicted is on average 95% accurate, and the refrigerant work input within 5%.

The theoretical capillary tube model was evaluated against experimental data in the literature. The model was 95.5% accurate when constant enthalpy was assumed. A dimensionless capillary tube correlation was derived to fit our experimental data. The new correlation provided results that were on average within 5%.

In the integrated cycle simulation the accuracy of the condenser model was 96.9%, and the evaporator model 95.9%. The predicted mass flow rate was on average accurate within 5% and the work input also within 5%.

6.3 Conclusion

In this study a micro heat pump simulation routine was derived and evaluated that is able to simulate the four components of the heat pump cycle. Given the environmental conditions, the simulation can simulate the response of each component in the cycle. The four components (fluted tube condenser, air-cooled evaporator, reciprocating compressor, and capillary tube) can be simulated on its own or within the integrated cycle simulation routine.

Sufficiently accurate results were obtained in all cases. Very good accuracy was obtained for the fluted tube condenser model and the air-cooled evaporator model. Results obtained with the theoretical capillary tube model showed that further work is required to validate the model. The dimensionless capillary tube correlation could also be tested against a wider range of operating conditions.

With the use of this simulation routine it is now possible to simulate the performance of the micro heat pump in different climatic and operating conditions. The condenser and evaporator designs can also be optimized. The high degree of accuracy obtained with the individual models as well as with the integrated cycle provides confidence in the simulation results. The simulation can therefore be applied as a design tool for micro heat pumps and its individual components.

6.4 *Recommendations for further research*

The following are recommended for further research:

- Further refinement of each component in the simulation routine:
  - Evaporator ⇒ Enhancing the model so that it can simulate any row arrangement and flow configuration.
  - Compressor ⇒ Inclusion of a power factor and thermal efficiency model to derive actual input power and peak demands from the refrigerant work.
  - Capillary Tube ⇒ Refinement in the stability of the solution of the theoretical model.
    ⇒ Refinement of the dimensionless correlation by testing over a wider range of operating conditions.
- More research into the theoretical capillary tube model.
- Compiling all the components into object orientated programming.
- The addition of a Microsoft® Windows based user-interface.
- Comparing the simulation routine with commercially available heat pump design tools.
- More detailed experimental measurements for validating the cycle simulation.

Appendix A

Experimental & Simulation Results

A.1 Measured Data

Condenser

Twb = 10 °C

T_in °C	P_in bar	T_cond °C	T_out °C	P_out bar
78.95	14.342	52.10	49.94	13.890
79.94	14.321	52.05	49.89	13.871
80.63	14.483	52.48	50.32	14.021
81.32	14.916	53.75	51.78	14.467
82.70	15.059	54.15	52.08	14.609
83.79	15.516	55.42	53.24	15.067
85.17	15.730	55.99	53.80	15.278
86.26	16.044	56.85	54.86	15.601
88.53	16.626	58.41	56.70	16.193

Twb = 15 °C

T_in °C	P_in bar	T_cond °C	T_out °C	P_out bar
81.71	13.775	50.22	48.08	13.254
80.32	14.005	50.94	48.50	13.494
81.51	14.627	52.83	51.36	14.144
83.98	14.824	53.36	50.99	14.327
84.18	14.747	53.13	50.77	14.248
85.07	15.236	54.54	52.16	14.748
86.45	15.531	55.37	52.49	15.052
88.42	16.115	56.99	53.90	15.651
89.31	16.428	57.87	55.27	15.986

Twb = 20 °C

T_in °C	P_in bar	T_cond °C	T_out °C	P_out bar
79.52	13.095	48.14	45.51	12.574
82.09	13.804	50.38	48.03	13.308
83.87	13.964	50.85	48.00	13.464
86.34	14.192	51.51	48.65	13.687
84.76	14.654	52.81	49.95	14.135
87.03	15.034	53.91	50.64	14.523
87.03	15.250	54.56	51.68	14.757
88.61	15.712	55.88	53.19	15.238
90.78	16.152	57.12	53.93	15.701

Twb = 25 °C

T_in °C	P_in bar	T_cond °C	T_out °C	P_out bar
87.61	13.074	47.92	44.785	12.50
87.31	13.403	48.97	46.129	12.84
85.73	13.340	48.81	45.971	12.79
85.73	13.850	50.41	47.264	13.32
86.03	14.155	51.37	48.514	13.64
88.00	14.837	53.41	50.540	14.35
90.08	14.774	53.28	50.410	14.29
91.36	15.714	55.95	53.062	15.26
95.02	16.300	57.57	54.966	15.87

Evaporator

Twb = 10°C

T_in °C	P_in bar	T_evap 1 °C	T_evap 2 °C	T_out °C	P_out bar
9.14	4.041	8.28	9.50	12.72	3.958
9.28	4.060	8.62	9.64	12.86	3.976
9.53	4.094	8.67	9.89	13.31	4.008
9.90	4.144	9.09	10.42	13.83	4.056
10.09	4.171	9.44	10.77	14.38	4.077
10.37	4.209	9.52	10.74	14.66	4.120
10.59	4.240	10.05	11.27	15.69	4.151
10.74	4.261	10.20	11.43	16.05	4.169
10.87	4.280	10.25	11.57	17.40	4.197

Twb = 15 °C

T_in °C	P_in bar	T_evap 1 °C	T_evap 2 °C	T_out °C	P_out bar
11.00	4.299	10.38	12.42	16.53	4.206
10.96	4.293	10.14	12.37	16.29	4.197
11.36	4.350	10.84	12.78	17.19	4.255
11.74	4.405	11.23	13.17	18.09	4.309
11.55	4.375	10.93	12.97	17.79	4.284
11.63	4.389	11.02	13.06	18.18	4.292
11.63	4.389	11.32	13.26	18.18	4.299
11.77	4.408	11.95	13.50	19.12	4.317
11.26	4.335	12.55	12.98	19.10	4.244

Twb = 20 °C

T_in °C	P_in bar	T_evap 1 °C	T_evap 2 °C	T_out °C	P_out bar
10.65	4.249	12.07	12.61	21.45	4.150
11.19	4.325	12.60	13.15	21.79	4.228
11.17	4.322	11.67	12.61	20.14	4.225
11.65	4.391	12.06	13.10	21.04	4.295
12.45	4.508	13.16	14.20	20.02	4.410
12.77	4.555	13.29	14.04	21.47	4.457
12.42	4.503	12.83	13.87	19.03	4.405
12.48	4.513	13.40	13.95	21.88	4.417
11.62	4.387	14.94	15.09	21.51	4.297

Twb = 25 °C

T_in °C	P_in bar	T_evap 1 °C	T_evap 2 °C	T_out °C	P_out bar
12.25	4.478	14.57	14.96	24.49	4.379
12.57	4.526	14.78	15.28	24.62	4.425
12.05	4.449	14.13	14.53	23.17	4.350
12.15	4.464	14.14	14.64	23.27	4.366
11.86	4.421	13.64	14.03	22.36	4.325
12.17	4.467	14.75	15.25	22.98	4.370
11.82	4.416	16.92	17.43	23.54	4.320
11.77	4.408	18.47	18.98	23.47	4.315
11.34	4.347	20.42	20.98	24.97	4.254

Table A.1: Experimental Conditions of Refrigerant R 134a

Twb = 10°C

T_in °C	T_out °C	m_w cm	m_w l/s
14.70	60.00	1.50	0.00667
19.80	60.00	1.90	0.00733
25.00	60.00	2.25	0.00783
29.60	60.00	2.60	0.00833
34.50	60.00	3.40	0.01000
40.50	60.00	4.90	0.01283
44.30	60.00	6.20	0.01500
48.90	60.00	9.50	0.02117
53.70	60.00	19.20	0.04100

Twb = 15 °C

T_in °C	T_out °C	m_w cm	m_w l/s
15.50	60.00	2.10	0.00750
19.40	60.00	2.30	0.00800
26.00	60.00	2.80	0.00900
29.90	60.00	3.30	0.00983
35.00	60.00	4.30	0.01167
39.50	60.00	5.40	0.01367
44.10	60.00	7.10	0.01667
49.90	60.00	11.50	0.02500
54.50	60.00	22.00	0.04750

Twb = 20 °C

T_in °C	T_out °C	m_w cm	m_w l/s
13.80	60.00	2.30	0.00792
21.00	60.00	2.60	0.00833
25.10	60.00	3.10	0.00933
30.10	60.00	3.90	0.01083
35.50	60.00	5.10	0.01300
40.00	60.00	6.60	0.01567
45.20	60.00	9.10	0.02033
49.70	60.00	13.20	0.02833
54.50	60.00	27.60	0.06000

Twb = 25 °C

T_in °C	T_out °C	m_w cm	m_w l/s
15.40	60.00	3.20	0.00950
20.30	60.00	3.50	0.01000
24.60	60.00	3.90	0.01083
30.30	60.00	4.40	0.01167
35.20	60.00	5.50	0.01383
40.00	60.00	6.60	0.01583
44.60	60.00	10.20	0.02267
50.10	60.00	13.80	0.02983
55.10	60.00	28.00	0.06117

Table A.2: Measured Water Conditions through Condenser

Twb = 10 °C

Tdb_in °C	Twb_in °C	Rh_in %	Tdb_out °C	Twb_out °C	Rh_out %
18.72	10.52	38.20	14.20	9.25	55.40
19.08	11.31	41.50	14.48	9.95	59.20
19.40	11.62	41.90	14.72	10.08	58.60
19.68	11.86	42.00	15.16	10.59	59.70
20.08	11.93	40.50	15.60	10.39	55.10
20.72	10.98	31.90	16.40	10.27	49.10
21.12	11.51	33.30	17.12	10.27	44.90
21.68	11.19	29.20	18.16	10.80	42.90
22.44	11.56	28.30	20.20	11.44	36.90

Twb = 15 °C

Tdb_in °C	Twb_in °C	Rh_in %	Tdb_out °C	Twb_out °C	Rh_out %
25.48	13.26	26.30	20.00	12.50	44.49
25.36	13.99	30.20	18.00	12.00	52.10
24.96	14.15	32.40	19.00	13.00	53.27
26.36	17.07	41.90	19.50	13.00	50.43
26.08	15.25	33.80	19.50	14.00	57.28
25.68	14.67	32.40	19.80	14.00	55.52
25.00	14.47	33.90	20.70	14.50	53.77
25.72	17.17	45.10	20.80	12.50	40.57
24.96	13.48	29.10	20.00	14.00	54.37

Twb = 20 °C

Tdb_in °C	Twb_in °C	Rh_in %	Tdb_out °C	Twb_out °C	Rh_out %
30.84	19.20	35.70	24.00	18.50	61.31
30.84	20.46	41.30	21.00	19.50	87.85
28.80	17.12	33.20	21.50	17.50	69.47
29.92	20.68	45.80	22.00	20.00	84.31
29.00	17.86	35.90	21.00	17.00	69.13
30.12	20.05	42.00	22.00	19.50	80.57
28.92	17.54	34.70	22.50	18.00	66.71
29.60	19.36	40.70	24.50	20.00	68.06
29.52	18.05	35.00	24.50	17.50	52.62

Twb = 25 °C

Tdb_in °C	Twb_in °C	Rh_in %	Tdb_out °C	Twb_out °C	Rh_out %
36.60	22.54	32.00	25.00	19.00	59.02
35.92	23.66	38.10	24.50	21.50	78.07
33.60	22.70	41.60	24.50	22.50	85.09
32.84	24.01	50.20	25.50	22.50	78.50
31.76	23.62	52.70	24.50	22.00	81.55
31.84	23.77	53.10	24.50	23.00	88.71
33.80	24.13	47.10	26.50	20.50	60.19
33.16	23.34	45.90	24.50	21.00	74.67
34.20	25.01	49.60	34.50	25.50	50.66

Table A.3: Measured Air Change over Evaporator

Twb = 10°C

Current A	Volts V	Power W	Q W	COP
2.7	220	594	1263.568	2.127
2.7	220	594	1233.443	2.077
2.7	220	594	1147.113	1.931
2.7	220	594	1059.947	1.784
2.7	220	594	1066.920	1.796
2.8	220	616	1047.046	1.700
2.8	220	616	985.332	1.600
2.8	220	616	983.031	1.596
2.8	220	616	1080.727	1.754

Twb = 15°C

Current A	Volts V	Power W	Q W	COP
2.7	220	594	1396.410	2.351
2.7	220	594	1358.963	2.288
2.7	220	594	1280.304	2.155
2.8	220	616	1238.394	2.010
2.8	220	616	1220.333	1.981
2.8	220	616	1172.217	1.903
2.8	220	616	1108.760	1.800
2.8	220	616	1056.460	1.715
2.8	220	616	1093.070	1.774

Twb = 20°C

Current A	Volts V	Power W	Q W	COP
2.7	220	594	1530.298	2.576
2.7	220	594	1359.800	2.289
2.7	220	594	1362.868	2.294
2.8	220	616	1355.267	2.200
2.8	220	616	1332.604	2.163
2.8	220	616	1310.987	2.128
2.8	220	616	1259.105	2.044
2.8	220	616	1221.031	1.982
2.8	220	616	1235.300	2.005

Twb = 25°C

Current A	Volts V	Power W	Q W	COP
2.7	220	594	1772.761	2.984
2.7	220	594	1661.048	2.796
2.7	220	594	1604.564	2.701
2.7	220	594	1449.756	2.441
2.7	220	594	1435.391	2.416
2.8	220	616	1324.933	2.151
2.8	220	616	1280.500	2.079
2.8	220	616	1235.744	2.006
2.8	220	616	1254.015	2.036

Table A.4: COP of the Micro Heat Pump

A.2 Simulated Data

A.2.1 Fluted Tube Condenser

Refrigerant: (R 134a)

Twb = 10°C

T_r1 (°C)	P_r1 (kPa)	h_r1 (kJ/kg)	T_r2 (°C)	P_r2 (kPa)	h_r2 (kJ/kg)	T_r3 (°C)	P_r3 (kPa)	h_r3 (kJ/kg)	T_r4 (°C)	P_r4 (kPa)	h_r4 (kJ/kg)	Q kW
80.508	1538.438	302.997	54.573	1476.201	272.54	53.308	1431.194	125.343	51.148	1430.986	121.991	**1.24714**
81.613	1545.521	304.151	54.867	1486.77	272.639	53.679	1444.288	125.922	51.579	1444.085	122.657	**1.21056**
82.238	1557.696	304.666	55.397	1506.057	272.814	54.357	1468.445	126.982	52.199	1468.247	123.618	**1.12431**
82.535	1574.442	304.725	56.162	1534.191	273.064	55.252	1500.774	128.386	53.283	1500.602	125.304	**1.04244**
84.004	1596.178	306.072	56.753	1556.216	273.252	55.86	1523.021	129.343	53.787	1522.82	126.09	**1.04749**
84.885	1627.995	306.565	57.765	1594.449	273.567	56.916	1562.288	131.01	54.734	1562.041	127.572	**1.03136**
86.144	1641.917	307.813	58.336	1616.366	273.741	57.583	1587.543	132.069	55.396	1587.288	128.612	**0.96948**
87.177	1670.187	308.569	59.13	1647.133	273.978	58.394	1618.575	133.359	56.4	1618.278	130.194	**0.96679**
89.082	1703.071	310.294	59.928	1678.535	274.209	59.084	1645.326	134.462	57.374	1644.854	131.737	**1.07134**

Twb = 15°C

T_r1 (°C)	P_r1 (kPa)	h_r1 (kJ/kg)	T_r2 (°C)	P_r2 (kPa)	h_r2 (kJ/kg)	T_r3 (°C)	P_r3 (kPa)	h_r3 (kJ/kg)	T_r4 (°C)	P_r4 (kPa)	h_r4 (kJ/kg)	Q kW
83.734	1518.989	307.044	53.769	1447.44	272.267	52.331	1397.12	123.822	50.187	1396.884	120.507	**1.36732**
82.38	1540.896	305.117	54.467	1472.377	272.504	53.095	1423.662	125.01	51.109	1423.438	121.93	**1.32628**
83.229	1580.561	305.429	55.721	1517.926	272.92	54.482	1472.917	127.177	53.01	1472.748	124.877	**1.25845**
85.368	1580.619	307.919	56.043	1529.759	273.026	54.914	1488.446	127.854	52.548	1488.177	124.159	**1.21833**
85.879	1595.67	308.27	56.666	1552.969	273.224	55.592	1513.201	128.921	53.227	1512.91	125.216	**1.19168**
86.454	1622.328	308.503	57.45	1582.492	273.47	56.454	1545.049	130.28	54.078	1544.733	126.544	**1.14998**
87.702	1643.793	309.62	58.263	1613.543	273.719	57.38	1579.848	131.747	54.503	1579.43	127.21	**1.08716**
89.362	1680.93	310.99	59.356	1656.027	274.043	58.564	1625.175	133.632	55.474	1624.577	128.736	**1.03885**
90.189	1708.115	311.536	60.085	1684.764	274.254	59.256	1652.075	134.737	56.166	1650.829	129.825	**1.08118**

Twb = 20°C

T_r1 (°C)	P_r1 (kPa)	h_r1 (kJ/kg)	T_r2 (°C)	P_r2 (kPa)	h_r2 (kJ/kg)	T_r3 (°C)	P_r3 (kPa)	h_r3 (kJ/kg)	T_r4 (°C)	P_r4 (kPa)	h_r4 (kJ/kg)	Q kW
82.909	1542.764	305.696	54.106	1459.426	272.383	52.434	1400.705	123.983	49.801	1400.363	119.914	**1.50484**
84.707	1563.788	307.428	55.095	1495.033	272.715	53.733	1446.165	126.005	51.383	1445.889	122.353	**1.35105**
86.119	1557.422	309.169	54.989	1491.144	272.68	53.678	1444.235	125.92	50.828	1443.894	121.496	**1.33248**
88.383	1570.122	311.594	55.588	1513.063	272.877	54.338	1467.765	126.952	51.482	1467.398	122.507	**1.32171**
86.765	1609.395	309.081	56.785	1557.407	273.262	55.573	1512.526	128.892	52.71	1512.103	124.412	**1.29822**
88.747	1629.751	311.077	57.476	1583.499	273.478	56.334	1540.583	130.09	53.063	1540.042	124.96	**1.28235**
88.852	1658.539	310.741	58.478	1621.857	273.784	57.425	1581.556	131.818	54.549	1581.004	127.283	**1.2255**
89.896	1667.276	311.84	58.753	1632.457	273.866	57.754	1594.039	132.341	55.065	1593.407	128.092	**1.19437**
92.25	1727.727	313.696	60.325	1694.388	274.321	59.171	1648.75	134.602	55.978	1646.689	129.529	**1.35363**

Twb = 25°C

T_r1 (°C)	P_r1 (kPa)	h_r1 (kJ/kg)	T_r2 (°C)	P_r2 (kPa)	h_r2 (kJ/kg)	T_r3 (°C)	P_r3 (kPa)	h_r3 (kJ/kg)	T_r4 (°C)	P_r4 (kPa)	h_r4 (kJ/kg)	Q kW
90.345	1516.653	314.684	52.694	1409.722	271.895	50.71	1341.999	121.315	47.71	1341.529	116.713	**1.72829**
89.918	1537.831	313.873	53.756	1446.987	272.263	51.993	1385.425	123.297	49.153	1384.993	118.919	**1.62008**
88.89	1568.467	312.209	54.738	1482.131	272.596	53.072	1422.844	124.974	50.233	1422.394	120.578	**1.57137**
88.456	1585.206	311.443	55.809	1521.151	272.949	54.416	1470.564	127.074	51.27	1470.095	122.179	**1.41947**
88.7	1612.104	311.303	56.68	1553.495	273.229	55.331	1503.645	128.51	52.475	1503.168	124.046	**1.40443**
89.911	1626.492	312.497	57.371	1579.508	273.446	56.219	1536.312	129.909	53.349	1535.837	125.407	**1.29092**
92.453	1661.226	314.962	58.209	1611.439	273.703	56.925	1562.639	131.025	54.055	1561.956	126.509	**1.41528**
92.62	1669.289	315.038	58.797	1634.153	273.879	57.802	1595.868	132.417	54.914	1595.146	127.855	**1.21482**
96.123	1720.733	318.449	60.262	1691.866	274.303	59.296	1653.667	134.802	56.692	1652.316	130.657	**1.23379**

Table A.5: Simulation Results of Condenser

Tw_in (°C)	Tw_1 (°C)	Tw_2 (°C)	Tw_out (°C)
14.7	15.53	51.87	59.39
19.8	20.51	52.42	59.27
25.0	25.64	53.21	59.23
29.6	30.11	54.23	59.51
34.5	34.95	54.97	59.54
40.5	40.87	56.17	59.71
44.3	44.60	56.81	59.75
48.9	49.09	57.70	59.82
53.7	53.80	58.81	60.10

Tw_in (°C)	Tw_1 (°C)	Tw_2 (°C)	Tw_out (°C)
15.5	16.27	50.95	59.07
19.4	20.07	51.97	59.02
26.0	26.43	53.40	59.42
29.9	30.50	53.90	59.52
35.0	35.49	54.73	59.41
39.5	39.91	55.74	59.61
44.1	44.49	56.62	59.69
49.9	50.17	57.82	59.83
54.5	54.65	58.82	59.94

Tw_in (°C)	Tw_1 (°C)	Tw_2 (°C)	Tw_out (°C)
13.8	14.80	51.07	59.21
21.0	21.77	52.49	59.76
25.1	25.91	52.60	59.23
30.1	30.79	53.30	59.27
35.5	36.08	54.74	59.37
40.0	40.54	55.61	59.56
45.2	45.56	56.71	59.61
49.7	49.93	57.69	59.78
54.5	54.65	58.74	59.89

Tw_in (°C)	Tw_1 (°C)	Tw_2 (°C)	Tw_out (°C)
15.4	16.41	49.48	58.88
20.3	21.17	50.76	59.02
24.6	25.40	52.11	59.28
30.3	31.05	53.46	59.37
35.2	35.78	54.54	59.47
40.0	40.47	55.42	59.49
44.6	44.96	56.25	59.52
50.1	50.34	57.69	59.83
55.1	55.21	58.79	59.92

Table A.6: Simulated Water Change through Condenser

A.2.2 Air-Cooled Evaporator

Refrigerant: (R 134a)

T_r7 °C	p_r7 kPa	h_r7 kJ/kg	T_r8 °C	p_r8 kPa	h_r8 kJ/kg	T_r9 °C	p_r9 kPa	h_r9 kJ/kg	Q kW
8.211	390.804	120.406	7.682	383.852	250.863	12.115	383.229	255.036	**0.9279**
8.816	398.880	120.312	8.349	392.645	251.227	12.782	392.068	255.413	**0.9010**
9.678	410.611	121.042	9.313	405.616	251.750	13.948	405.071	256.148	**0.8390**
10.520	422.327	123.284	10.231	418.259	252.246	14.968	417.741	256.762	**0.7757**
10.131	416.862	123.666	9.824	412.615	252.027	14.763	412.182	256.722	**0.7742**
10.474	421.685	125.174	10.183	417.591	252.221	15.324	417.183	257.116	**0.7597**
10.887	427.481	126.436	10.640	424.007	252.467	16.285	423.621	257.854	**0.7112**
11.415	435.050	127.873	11.181	431.673	252.759	17.028	431.263	258.354	**0.7074**
10.698	424.829	131.013	10.395	420.568	252.335	17.544	419.904	259.152	**0.7690**

T_r7 °C	p_r7 kPa	h_r7 kJ/kg	T_r8 °C	p_r8 kPa	h_r8 kJ/kg	T_r9 °C	p_r9 kPa	h_r9 kJ/kg	Q kW
10.653	424.188	117.493	10.144	417.037	252.199	16.295	416.386	258.06	**1.0306**
10.765	425.769	118.182	10.271	418.827	252.268	16.416	418.196	258.13	**1.0134**
11.184	431.712	122.490	10.751	425.566	252.527	17.104	424.942	258.60	**0.9490**
12.188	446.240	121.954	11.830	441.018	253.107	18.688	440.472	259.69	**0.9133**
11.289	433.227	121.647	10.923	427.987	252.621	17.780	427.487	259.17	**0.8953**
11.416	435.057	123.844	11.080	430.218	252.705	18.239	429.712	259.55	**0.8575**
11.602	437.741	124.333	11.309	433.511	252.827	18.167	433.086	259.39	**0.8051**
12.860	456.176	126.529	12.619	452.614	253.529	19.781	452.203	260.43	**0.7630**
12.034	443.971	128.708	11.746	439.809	253.062	18.296	439.437	259.35	**0.7780**

T_r7 °C	p_r7 kPa	h_r7 kJ/kg	T_r8 °C	p_r8 kPa	h_r8 kJ/kg	T_r9 °C	p_r9 kPa	h_r9 kJ/kg	Q kW
12.333	448.394	113.615	11.804	440.647	253.093	21.184	439.541	262.110	**1.1780**
13.389	464.127	116.584	13.013	458.439	253.739	22.196	457.667	262.619	**1.0366**
11.837	441.119	117.390	11.412	435.003	252.883	19.886	434.263	261.005	**1.0165**
12.988	458.055	118.364	12.610	452.483	253.524	21.589	451.734	262.186	**1.0051**
12.842	455.898	120.336	12.447	450.079	253.437	19.312	449.539	260.053	**0.9820**
13.917	472.126	121.424	13.574	466.931	254.037	21.750	466.302	261.968	**0.9680**
13.879	471.552	123.036	13.551	466.582	254.025	19.754	466.166	260.039	**0.9149**
14.419	479.879	125.418	14.134	475.460	254.334	22.612	474.852	262.585	**0.8940**
13.414	464.505	126.520	12.997	458.194	253.730	19.566	457.624	260.083	**0.9813**

T_r7 °C	p_r7 kPa	h_r7 kJ/kg	T_r8 °C	p_r8 kPa	h_r8 kJ/kg	T_r9 °C	p_r9 kPa	h_r9 kJ/kg	Q kW
12.652	453.101	112.487	12.01	443.623	253.204	22.255	441.961	263.075	**1.316**
12.832	455.757	114.475	12.281	447.617	253.348	23.115	445.955	263.799	**1.2405**
12.016	443.702	114.288	11.451	435.564	252.904	20.696	434.268	261.779	**1.1913**
12.201	446.436	116.226	11.76	440.008	253.069	21.76	438.821	262.68	**1.0841**
11.405	434.895	118.166	10.941	428.231	252.63	20.941	426.976	262.2	**1.0662**
12.131	445.401	121.244	11.753	439.911	253.066	21.753	438.941	262.67	**0.9756**
12.106	445.039	121.061	11.646	438.364	253.008	22.646	437.078	263.572	**1.0705**
12.250	447.160	125.231	11.934	442.522	253.163	23.934	441.534	264.695	**0.9048**
13.900	471.866	128.497	13.604	467.375	254.052	24.604	466.537	264.723	**0.8947**

Table A.7: Simulation Results of Evaporator

A.2.3 Reciprocating Compressor

T_r10 (°C)	P_r10 (kPa)	h_r10 (kJ/kg)	s_r10 (kJ/kg)	T_r11 (°C)	P_r11 (kPa)	h_r11 (kJ/kg)	s_r11 (kJ/kg)	m_r (kg/s)	Wcp (W)	Efficiency
12.715	395.8	255.245	924.944	79.858	1434.2	304.029	987.635	0.00615	300.026	0.560
12.855	397.6	255.326	924.901	79.767	1432.1	303.961	987.546	0.00623	302.856	0.559
13.309	400.8	255.663	925.491	80.399	1448.3	304.406	988.004	0.00623	303.734	0.560
13.831	405.6	256.023	925.887	81.747	1491.6	305.216	988.239	0.00613	301.589	0.562
14.379	407.7	256.483	927.103	82.539	1505.9	305.885	989.438	0.00611	301.606	0.563
14.661	412.0	256.630	926.858	83.750	1551.6	306.521	989.183	0.00598	298.319	0.565
15.690	415.1	257.521	929.379	85.150	1573	307.791	991.798	0.00594	298.650	0.565
16.045	416.9	257.809	930.067	86.286	1604.4	308.602	992.721	0.00580	294.563	0.566
17.396	419.7	259.017	933.752	89.222	1662.6	311.114	997.321	0.00553	287.905	0.567

T_r10 (°C)	P_r10 (kPa)	h_r10 (kJ/kg)	s_r10 (kJ/kg)	T_r11 (°C)	P_r11 (kPa)	h_r11 (kJ/kg)	s_r11 (kJ/kg)	m_r (kg/s)	Wcp (W)	Efficiency
16.528	420.6	258.167	930.678	80.304	1377.5	305.473	994.387	0.00733	346.538	0.539
16.285	419.7	257.961	930.119	80.658	1400.5	305.492	993.313	0.00716	340.099	0.544
17.191	425.5	258.666	931.567	82.700	1462.7	306.783	993.918	0.00695	334.279	0.551
18.088	430.9	259.376	933.105	83.717	1482.4	307.620	995.332	0.007	337.819	0.551
17.786	428.4	259.154	932.760	83.406	1474.7	307.390	995.049	0.00697	335.986	0.552
18.175	429.2	259.504	933.827	85.026	1523.6	308.457	995.755	0.00668	326.913	0.557
18.175	429.9	259.485	933.647	85.751	1553.1	308.813	995.475	0.00653	321.908	0.560
19.116	431.7	260.336	936.272	88.192	1611.5	310.718	998.299	0.00621	312.628	0.564
19.103	424.4	260.516	938.115	89.864	1642.8	312.185	1001.097	0.00577	297.913	0.566

T_r10 (°C)	P_r10 (kPa)	h_r10 (kJ/kg)	s_r10 (kJ/kg)	T_r11 (°C)	P_r11 (kPa)	h_r11 (kJ/kg)	s_r11 (kJ/kg)	m_r (kg/s)	Wcp (W)	Efficiency
21.445	415.0	262.986	948.197	84.689	1309.5	311.419	1014.389	0.00738	357.246	0.526
21.785	422.8	263.111	947.308	86.002	1380.4	311.813	1011.827	0.00720	350.887	0.538
20.140	422.5	261.553	942.002	84.573	1396.4	309.961	1005.905	0.00715	346.231	0.541
21.037	429.5	262.227	943.137	85.539	1419.2	310.693	1006.839	0.00724	351.047	0.541
20.023	441.0	260.960	936.866	84.588	1465.4	308.888	999.632	0.00743	355.958	0.544
21.469	445.7	262.225	940.443	86.695	1503.4	310.693	1002.888	0.00732	354.867	0.547
19.030	440.5	260.021	933.731	84.992	1525.0	308.395	995.519	0.00707	341.896	0.553
21.882	441.7	262.724	942.798	89.120	1571.2	312.433	1004.750	0.00675	335.376	0.558
21.507	429.7	262.671	944.628	91.029	1615.2	313.986	1007.213	0.00605	310.486	0.565

T_r10 (°C)	P_r10 (kPa)	h_r10 (kJ/kg)	s_r10 (kJ/kg)	T_r11 (°C)	P_r11 (kPa)	h_r11 (kJ/kg)	s_r11 (kJ/kg)	m_r (kg/s)	Wcp (W)	Efficiency
24.491	437.9	265.318	952.338	86.548	1307.4	313.510	1020.306	0.00813	391.615	0.509
24.616	442.5	265.325	951.583	87.016	1340.3	313.542	1018.678	0.00810	390.650	0.514
23.165	435.0	264.121	948.719	85.742	1334.0	312.219	1015.327	0.00790	380.047	0.518
23.268	436.6	264.180	948.651	86.734	1385.0	312.565	1013.678	0.00764	369.561	0.530
22.361	432.5	263.415	946.716	86.684	1415.5	312.042	1010.759	0.00733	356.514	0.539
22.979	437.0	263.893	947.600	88.566	1483.7	313.139	1010.579	0.00706	347.866	0.548
23.537	432.0	264.551	950.702	89.427	1477.4	314.217	1013.860	0.00690	342.522	0.550
23.471	431.5	264.500	950.613	91.752	1571.4	315.490	1013.221	0.00632	322.417	0.561
24.968	425.4	266.078	957.068	95.655	1630.0	319.198	1021.074	0.00574	304.957	0.566

Table A.8: Simulation Results of Compressor

A.2.5 Integrated Micro Heat Pump Cycle

Twb = 10°C

p_r1 (kPa)	T_r1 (°C)	h_r1 (kJ/kg)	p_r2 (kPa)	T_r2 (°C)	h_r2 (kJ/kg)	p_r3 (kPa)	T_r3 (°C)	h_r3 (kJ/kg)	p_r4 (kPa)	T_r4 (°C)	h_r4 (kJ/kg)
1575.588	81.780	303.827	1515.218	55.647	272.896	1471.356	54.438	127.109	1471.138	52.282	123.747
1607.439	83.055	304.770	1553.018	56.667	273.225	1513.094	55.589	128.916	1512.880	53.431	125.534
1580.159	83.607	305.876	1539.712	56.310	273.111	1506.203	55.401	128.620	1506.032	53.432	125.535
1586.808	84.075	306.310	1547.441	56.518	273.177	1514.805	55.636	128.990	1514.607	53.563	125.740
1644.060	85.804	307.376	1609.205	58.151	273.685	1575.871	57.275	131.580	1575.613	55.093	128.136
1681.234	86.771	307.906	1650.687	59.221	274.004	1618.819	58.400	133.369	1618.538	56.213	129.899
1690.091	87.539	308.670	1665.198	59.589	274.111	1634.434	58.804	134.014	1634.115	56.810	130.843
1669.769	89.706	311.575	1651.258	59.235	274.008	1623.364	58.517	133.557	1622.946	56.807	130.839

Twb = 15°C

p_r1 (kPa)	T_r1 (°C)	h_r1 (kJ/kg)	p_r2 (kPa)	T_r2 (°C)	h_r2 (kJ/kg)	p_r3 (kPa)	T_r3 (°C)	h_r3 (kJ/kg)	p_r4 (kPa)	T_r4 (°C)	h_r4 (kJ/kg)
1572.748	83.234	305.567	1498.079	55.179	272.743	1444.953	53.698	125.951	1444.696	51.554	122.618
1569.901	82.640	304.924	1500.487	55.244	272.764	1450.672	53.860	126.204	1450.386	51.415	122.404
1602.643	84.373	306.395	1544.983	56.452	273.156	1498.242	55.183	128.277	1498.064	53.711	125.971
1604.050	85.445	307.625	1551.792	56.634	273.214	1509.172	55.482	128.747	1508.891	53.116	125.043
1589.302	85.326	307.728	1541.644	56.362	273.128	1502.761	55.307	128.472	1502.474	52.942	124.771
1608.565	86.527	308.816	1569.795	57.115	273.367	1533.421	56.142	129.787	1533.114	53.766	126.056
1658.629	87.263	308.860	1624.835	58.556	273.807	1589.990	57.647	132.171	1589.560	54.770	127.629
1702.667	88.835	310.006	1673.344	59.796	274.171	1639.986	58.948	134.243	1639.352	55.858	129.339
1701.369	88.658	309.816	1680.573	59.980	274.224	1648.416	59.163	134.588	1647.483	56.564	130.454

Twb = 20°C

p_r1 (kPa)	T_r1 (°C)	h_r1 (kJ/kg)	p_r2 (kPa)	T_r2 (°C)	h_r2 (kJ/kg)	p_r3 (kPa)	T_r3 (°C)	h_r3 (kJ/kg)	p_r4 (kPa)	T_r4 (°C)	h_r4 (kJ/kg)
1635.658	87.450	309.456	1536.471	56.223	273.083	1473.645	54.502	127.209	1473.257	51.859	123.090
1660.999	87.801	309.458	1577.694	57.323	273.431	1524.140	55.891	129.391	1523.824	53.541	125.706
1669.031	87.287	308.718	1594.573	57.768	273.568	1541.163	56.349	130.115	1540.751	53.499	125.641
1592.354	86.896	309.510	1533.462	56.143	273.058	1486.200	54.851	127.756	1485.813	51.995	123.301
1634.686	85.606	307.300	1580.795	57.405	273.456	1533.828	56.153	129.804	1533.382	53.290	125.314
1770.858	89.241	309.371	1719.397	60.950	274.496	1676.064	59.865	135.714	1675.535	56.594	130.502
1717.543	86.537	307.007	1675.191	59.843	274.185	1627.858	58.634	133.742	1627.209	55.758	129.182
1689.347	89.106	310.548	1651.414	59.239	274.009	1609.461	58.158	132.983	1608.781	55.469	128.727
1692.968	88.641	309.934	1667:254	59.642	274.126	1630.702	58.707	133.860	1628.859	55.514	128.799

Table A.9: Refrigerant Properties through Condenser with Cycle Simulation

Twb = 10°C

p_r7 (kPa)	T_r7 (°C)	h_r7 (kJ/kg)	p_r8 (kPa)	T_r8 (°C)	h_r8 (kJ/kg)	p_r9 (kPa)	T_r9 (°C)	h_r9 (kJ/kg)
417.778	10.196	123.662	411.934	9.775	252.000	411.463	14.007	256.025
412.382	9.807	125.588	407.407	9.444	251.821	406.866	14.079	256.222
402.439	9.081	125.382	397.890	8.742	251.441	397.539	13.479	255.916
403.405	9.152	125.740	398.863	8.815	251.480	398.507	13.754	256.148
415.215	10.014	128.118	410.987	9.705	251.963	410.619	15.219	257.198
415.389	10.026	129.899	411.702	9.758	251.991	411.386	15.403	257.350
417.982	10.211	130.826	414.334	9.950	252.095	413.994	15.797	257.653
419.504	10.319	130.860	415.150	10.009	252.127	414.496	17.158	258.931

Twb = 15°C

p_r7 (kPa)	T_r7 (°C)	h_r7 (kJ/kg)	p_r8 (kPa)	T_r8 (°C)	h_r8 (kJ/kg)	p_r9 (kPa)	T_r9 (°C)	h_r9 (kJ/kg)
438.516	11.656	122.618	431.729	11.185	252.761	431.101	17.336	258.652
418.964	10.281	121.335	411.844	9.768	251.996	411.235	15.913	257.838
438.636	11.664	126.028	432.568	11.243	252.792	432.031	17.388	258.677
431.301	11.155	124.933	425.806	10.768	252.537	425.240	17.626	259.087
418.532	10.250	124.736	413.110	9.860	252.046	412.457	16.717	258.567
420.422	10.385	126.029	415.472	10.032	252.139	414.774	17.191	258.954
422.236	10.514	125.353	417.920	10.206	252.233	417.327	17.064	258.766
429.727	11.046	129.324	425.875	10.773	252.539	425.392	17.935	259.377
431.598	11.176	130.469	427.302	10.874	252.594	426.883	17.424	258.851

Twb = 20°C

p_r7 (kPa)	T_r7 (°C)	h_r7 (kJ/kg)	p_r8 (kPa)	T_r8 (°C)	h_r8 (kJ/kg)	p_r9 (kPa)	T_r9 (°C)	h_r9 (kJ/kg)
457.533	12.952	122.918	450.289	12.462	253.445	448.936	21.842	262.501
447.056	12.243	125.695	441.262	11.847	253.116	440.227	21.030	261.945
449.570	12.413	125.254	443.810	12.023	253.210	442.869	20.497	261.366
434.570	11.382	123.335	428.749	10.977	252.650	427.677	19.956	261.244
442.164	11.909	124.472	436.215	11.496	252.928	435.458	18.361	259.515
446.360	12.196	130.420	440.831	11.817	253.100	440.022	19.993	260.956
457.181	12.928	129.182	452.088	12.584	253.510	451.528	18.757	259.466
450.445	12.472	125.418	445.772	12.156	253.281	444.909	20.634	261.444
454.642	12.756	128.812	450.009	12.443	253.434	449.545	19.012	259.764

Table A.10: Refrigerant Properties through Evaporator with Cycle Simulation

A.3 Comparison between Experimental & Simulated Results

A.3.1 Fluted Tube Condenser

Experimental
Refrigerant: (R 134a)

Twb = 10 °C

T_in (°C)	P_in bar	T_cond (°C)	T_out (°C)	P_out bar	Q (kW)
78.947	14.342	52.10	49.940	13.890	**1.2636**
79.935	14.321	52.05	49.894	13.871	**1.2334**
80.627	14.483	52.48	50.322	14.021	**1.1471**
81.318	14.916	53.75	51.781	14.467	**1.0599**
82.701	15.059	54.15	52.077	14.609	**1.0669**
83.788	15.516	55.42	53.238	15.067	**1.0470**
85.170	15.730	55.99	53.803	15.278	**0.9853**
86.257	16.044	56.85	54.856	15.601	**0.9830**
88.529	16.626	58.41	56.700	16.193	**1.0807**

Twb = 15 °C

T_in (°C)	P_in bar	T_cond (°C)	T_out (°C)	P_out bar	Q (kW)
81.707	13.775	50.22	48.076	13.254	**1.3964**
80.324	14.005	50.94	48.495	13.494	**1.3590**
81.51	14.627	52.83	51.358	14.144	**1.2803**
83.979	14.824	53.36	50.994	14.327	**1.2384**
84.177	14.747	53.13	50.765	14.248	**1.2203**
85.066	15.236	54.54	52.164	14.748	**1.1722**
86.448	15.531	55.37	52.493	15.052	**1.1088**
88.424	16.115	56.99	53.9	15.651	**1.0565**
89.313	16.428	57.87	55.271	15.986	**1.0931**

Twb = 20 °C

T_in (°C)	P_in bar	T_cond (°C)	T_out (°C)	P_out bar	Q (kW)
79.522	13.095	48.14	45.507	12.574	**1.5303**
82.09	13.804	50.38	48.03	13.308	**1.3598**
83.868	13.964	50.85	48	13.464	**1.3629**
86.337	14.192	51.51	48.654	13.687	**1.3553**
84.757	14.654	52.81	49.947	14.135	**1.3326**
87.029	15.034	53.91	50.639	14.523	**1.3110**
87.029	15.250	54.56	51.684	14.757	**1.2591**
88.609	15.712	55.88	53.191	15.238	**1.2210**
90.782	16.152	57.12	53.927	15.701	**1.2353**

Twb = 25 °C

T_in (°C)	P_in bar	T_cond (°C)	T_out (°C)	P_out bar	Q (kW)
87.609	13.074	47.92	44.785	12.504	**1.7728**
87.313	13.403	48.97	46.129	12.843	**1.6610**
85.733	13.340	48.81	45.971	12.791	**1.6046**
85.733	13.850	50.41	47.264	13.316	**1.4498**
86.029	14.155	51.37	48.514	13.641	**1.4354**
88.004	14.837	53.41	50.54	14.346	**1.3249**
90.079	14.774	53.28	50.41	14.288	**1.2805**
91.363	15.714	55.95	53.062	15.263	**1.2357**
95.018	16.300	57.57	54.966	15.870	**1.2540**

Simulation
Refrigerant: (R 134a)

T_r1 (°C)	P_r1 (kPa)	T_r2 (°C)	P_r2 (kPa)	T_r3 (°C)	P_r3 (kPa)	T_r4 (°C)	P_r4 (kPa)	Q kW
80.508	1538.438	54.573	1476.201	53.308	1431.194	51.148	1430.986	**1.24714**
81.613	1545.521	54.867	1486.77	53.679	1444.288	51.579	1444.085	**1.21056**
82.238	1557.696	55.397	1506.057	54.357	1468.445	52.199	1468.247	**1.12431**
82.535	1574.442	56.162	1534.191	55.252	1500.774	53.283	1500.602	**1.04244**
84.004	1596.178	56.753	1556.216	55.86	1523.021	53.787	1522.82	**1.04749**
84.885	1627.995	57.765	1594.449	56.916	1562.288	54.734	1562.041	**1.03136**
86.144	1641.917	58.336	1616.366	57.583	1587.543	55.396	1587.288	**0.96948**
87.177	1670.187	59.13	1647.133	58.394	1618.575	56.4	1618.278	**0.96679**
89.082	1703.071	59.928	1678.535	59.084	1645.326	57.374	1644.854	**1.07134**

T_r1 (°C)	P_r1 (kPa)	T_r2 (°C)	P_r2 (kPa)	T_r3 (°C)	P_r3 (kPa)	T_r4 (°C)	P_r4 (kPa)	Q kW
83.734	1518.989	53.769	1447.44	52.331	1397.12	50.187	1396.884	**1.36732**
82.38	1540.896	54.467	1472.377	53.095	1423.662	51.109	1423.438	**1.32628**
83.229	1580.561	55.721	1517.926	54.482	1472.917	53.01	1472.748	**1.25845**
85.368	1580.619	56.043	1529.759	54.914	1488.446	52.548	1488.177	**1.21833**
85.879	1595.67	56.666	1552.969	55.592	1513.201	53.227	1512.91	**1.19168**
86.454	1622.328	57.45	1582.492	56.454	1545.049	54.078	1544.733	**1.14998**
87.702	1643.793	58.263	1613.543	57.38	1579.848	54.503	1579.43	**1.08716**
89.362	1680.93	59.356	1656.027	58.564	1625.175	55.474	1624.577	**1.03885**
90.189	1708.115	60.085	1684.764	59.256	1652.075	56.166	1650.829	**1.08118**

T_r1 (°C)	P_r1 (kPa)	T_r2 (°C)	P_r2 (kPa)	T_r3 (°C)	P_r3 (kPa)	T_r4 (°C)	P_r4 (kPa)	Q kW
82.909	1542.764	54.106	1459.426	52.434	1400.705	49.801	1400.363	**1.50484**
84.707	1563.788	55.095	1495.033	53.733	1446.165	51.383	1445.889	**1.35105**
86.119	1557.422	54.989	1491.144	53.678	1444.235	50.828	1443.894	**1.33248**
88.383	1570.122	55.588	1513.063	54.338	1467.765	51.482	1467.398	**1.32171**
86.765	1609.395	56.785	1557.407	55.573	1512.526	52.71	1512.103	**1.29822**
88.747	1629.751	57.476	1583.499	56.334	1540.583	53.063	1540.042	**1.28235**
88.852	1658.539	58.478	1621.857	57.425	1581.556	54.549	1581.004	**1.2255**
89.896	1667.276	58.753	1632.457	57.754	1594.039	55.065	1593.407	**1.19437**
92.25	1727.727	60.325	1694.388	59.171	1648.75	55.978	1646.689	**1.35363**

T_r1 (°C)	P_r1 (kPa)	T_r2 (°C)	P_r2 (kPa)	T_r3 (°C)	P_r3 (kPa)	T_r4 (°C)	P_r4 (kPa)	Q kW
90.345	1516.653	52.694	1409.722	50.71	1341.999	47.71	1341.529	**1.72829**
89.918	1537.831	53.756	1446.987	51.993	1385.425	49.153	1384.993	**1.62008**
88.89	1568.467	54.738	1482.131	53.072	1422.844	50.233	1422.394	**1.57137**
88.456	1585.206	55.809	1521.151	54.416	1470.564	51.27	1470.095	**1.41947**
88.7	1612.104	56.68	1553.495	55.331	1503.645	52.475	1503.168	**1.40443**
89.911	1626.492	57.371	1579.508	56.219	1536.312	53.349	1535.837	**1.29092**
92.453	1661.226	58.209	1611.439	56.925	1562.639	54.055	1561.956	**1.41528**
92.62	1669.289	58.797	1634.153	57.802	1595.868	54.914	1595.146	**1.21482**
96.123	1720.733	60.262	1691.866	59.296	1653.667	56.692	1652.316	**1.23379**

Table A.11: Comparison of Experimental & Simulation Results for Condenser

A.3.2 Air-Cooled Evaporator

Experimental
Refrigerant: (R 134a)
Twb = 10°C

T_in °C	P_in bar	X_in %	T_evap °C	T_out °C	P_out bar	Q kW
9.144	4.041	30.99	8.282	12.715	3.958	**0.93373**
9.284	4.060	30.86	8.623	12.855	3.976	**0.90639**
9.533	4.094	31.08	8.674	13.309	4.008	**0.84138**
9.897	4.144	32.07	9.094	13.831	4.056	**0.77578**
10.092	4.171	32.16	9.440	14.379	4.077	**0.77764**
10.365	4.209	33.00	9.520	14.661	4.120	**0.75866**
10.586	4.240	33.34	10.045	15.690	4.151	**0.71238**
10.736	4.261	34.10	10.198	16.045	4.169	**0.70720**
10.870	4.280	35.60	10.247	17.396	4.197	**0.77186**

Twb = 15°C

T_in °C	P_in bar	X_in %	T_evap °C	T_out °C	P_out bar	Q kW
11.004	4.299	28.36	10.377	16.528	4.206	**1.0378**
10.962	4.293	28.75	10.140	16.285	4.197	**1.0167**
11.362	4.35	30.83	10.838	17.191	4.255	**0.9536**
11.744	4.405	30.29	11.230	18.088	4.309	**0.9162**
11.546	4.375	30.25	10.929	17.786	4.284	**0.8995**
11.633	4.389	31.36	11.016	18.175	4.292	**0.8619**
11.633	4.389	31.62	11.317	18.175	4.299	**0.8097**
11.765	4.408	32.71	11.954	19.116	4.317	**0.7668**
11.257	4.335	34.16	12.553	19.103	4.244	**0.7888**

Twb = 20°C

T_in °C	P_in bar	X_in %	T_evap °C	T_out °C	P_out bar	Q kW
10.650	4.249	26.52	12.065	21.445	4.150	**1.1908**
11.187	4.325	27.77	12.602	21.785	4.228	**1.0447**
11.166	4.322	28.21	11.666	20.140	4.225	**1.0253**
11.647	4.391	28.44	12.058	21.037	4.295	**1.0102**
12.450	4.508	29.01	13.158	20.023	4.410	**0.9944**
12.768	4.555	29.40	13.293	21.469	4.457	**0.9743**
12.416	4.503	30.47	12.827	19.030	4.405	**0.9198**
12.484	4.513	31.70	13.404	21.882	4.417	**0.9001**
11.619	4.387	32.79	14.938	21.507	4.297	**1.0052**

Twb = 25°C

T_in °C	P_in bar	X_in %	T_evap °C	T_out °C	P_out bar	Q kW
12.246	4.478	24.95	14.573	24.491	4.379	**1.3418**
12.572	4.526	25.81	14.782	24.616	4.425	**1.2582**
12.047	4.449	26.03	14.131	23.165	4.350	**1.2159**
12.150	4.464	27.03	14.138	23.268	4.366	**1.0997**
11.855	4.421	28.21	13.639	22.361	4.325	**1.0801**
12.171	4.467	29.66	14.752	22.979	4.370	**0.9889**
11.820	4.416	29.77	16.921	23.537	4.320	**0.9489**
11.765	4.408	32.02	18.472	23.471	4.315	**0.9075**
11.341	4.347	33.85	20.420	24.968	4.254	**0.9096**

Simulation
Refrigerant: (R 134a)
Twb = 10°C

T_r7 °C	p_r7 kPa	T_r8 °C	p_r8 kPa	T_r9 °C	p_r9 kPa	Q kW
8.211	390.804	7.682	383.852	12.115	383.229	**0.9279**
8.816	398.880	8.349	392.645	12.782	392.068	**0.9010**
9.678	410.611	9.313	405.616	13.948	405.071	**0.8390**
10.52	422.327	10.231	418.259	14.968	417.741	**0.7757**
10.131	416.862	9.824	412.615	14.763	412.182	**0.7742**
10.474	421.685	10.183	417.591	15.324	417.183	**0.7597**
10.887	427.481	10.640	424.007	16.285	423.621	**0.7112**
11.415	435.050	11.181	431.673	17.028	431.263	**0.7074**
10.698	424.829	10.395	420.568	17.544	419.904	**0.7690**

Twb = 15°C

T_r7 °C	p_r7 kPa	T_r8 °C	p_r8 kPa	T_r9 °C	p_r9 kPa	Q kW
10.653	424.188	10.144	417.037	16.295	416.386	**1.0306**
10.765	425.769	10.271	418.827	16.416	418.196	**1.0134**
11.184	431.712	10.751	425.566	17.104	424.942	**0.9490**
12.188	446.24	11.830	441.018	18.688	440.472	**0.9133**
11.289	433.227	10.923	427.987	17.780	427.487	**0.8953**
11.416	435.057	11.080	430.218	18.239	429.712	**0.8575**
11.602	437.741	11.309	433.511	18.167	433.086	**0.8051**
12.860	456.176	12.619	452.614	19.781	452.203	**0.7630**
12.034	443.971	11.746	439.809	18.296	439.437	**0.7780**

Twb = 20°C

T_r7 °C	p_r7 kPa	T_r8 °C	p_r8 kPa	T_r9 °C	p_r9 kPa	Q kW
12.333	448.394	11.804	440.647	21.184	439.541	**1.1780**
13.389	464.127	13.013	458.439	22.196	457.667	**1.0366**
11.837	441.119	11.412	435.003	19.886	434.263	**1.0165**
12.988	458.055	12.610	452.483	21.589	451.734	**1.0051**
12.842	455.898	12.447	450.079	19.312	449.539	**0.9820**
13.917	472.126	13.574	466.931	21.750	466.302	**0.9680**
13.879	471.552	13.551	466.582	19.754	466.166	**0.9149**
14.419	479.879	14.134	475.460	22.612	474.852	**0.8940**
13.414	464.505	12.997	458.194	19.566	457.624	**0.9813**

Twb = 25°C

T_r7 °C	p_r7 kPa	T_r8 °C	p_r8 kPa	T_r9 °C	p_r9 kPa	Q kW
12.652	453.101	12.010	443.623	22.255	441.961	**1.3160**
12.832	455.757	12.281	447.617	23.115	445.955	**1.2405**
12.016	443.702	11.451	435.564	20.696	434.268	**1.1913**
12.201	446.436	11.760	440.008	21.760	438.821	**1.0841**
11.405	434.895	10.941	428.231	20.941	426.976	**1.0662**
12.131	445.401	11.753	439.911	21.753	438.941	**0.9756**
12.106	445.039	11.646	438.364	22.646	437.078	**1.0705**
12.250	447.160	11.934	442.522	23.934	441.534	**0.9048**
13.900	471.866	13.604	467.375	24.604	466.537	**0.8947**

Table A.12: Comparison of Experimental & Simulation Results for Evaporator

A.3.3 Reciprocating Compressor

Experimental
Refrigerant: (R 134a)

Twb = 10°C

T_in (°C)	P_in (bar)	T_out (°C)	P_out (bar)	m_r (kg/s)	Wcp (W)
12.715	3.958	78.947	79.804	0.00689	**329.606**
12.855	3.976	79.935	80.792	0.00667	**326.339**
13.309	4.008	80.627	81.484	0.00621	**305.014**
13.831	4.056	81.318	82.175	0.00581	**283.789**
14.379	4.077	82.701	83.558	0.00582	**289.555**
14.661	4.120	83.788	84.645	0.00576	**288.733**
15.690	4.151	85.170	86.027	0.00541	**273.220**
16.045	4.169	86.257	87.114	0.00542	**276.341**
17.396	4.197	88.529	89.386	0.00600	**309.167**

Twb = 15°C

T_in (°C)	P_in (bar)	T_out (°C)	P_out (bar)	m_r (kg/s)	Wcp (W)
16.528	4.206	81.707	82.564	0.00733	**359.185**
16.285	4.197	80.324	81.181	0.00724	**341.889**
17.191	4.255	81.51	82.367	0.00697	**326.637**
18.088	4.309	83.979	84.836	0.00663	**322.877**
17.786	4.284	84.177	85.034	0.00651	**320.685**
18.175	4.292	85.066	85.923	0.00632	**310.770**
18.175	4.299	86.448	87.305	0.00596	**299.882**
19.116	4.317	88.424	89.281	0.00570	**290.062**
19.103	4.244	89.313	90.170	0.00595	**305.147**

Twb = 20°C

T_in (°C)	P_in (bar)	T_out (°C)	P_out (bar)	m_r (kg/s)	Wcp (W)
21.445	4.150	79.522	80.379	0.00793	**339.389**
21.785	4.228	82.090	82.947	0.00710	**315.292**
20.140	4.225	83.868	84.725	0.00708	**337.811**
21.037	4.295	86.337	87.194	0.00699	**345.857**
20.023	4.410	84.757	85.614	0.00703	**339.485**
21.469	4.457	87.029	87.886	0.00689	**337.583**
19.030	4.405	87.029	87.886	0.00668	**339.993**
21.882	4.417	88.609	89.466	0.00652	**321.707**
21.507	4.297	90.782	91.639	0.00657	**376.451**

Twb = 25°C

T_in (°C)	P_in (bar)	T_out (°C)	P_out (bar)	m_r (kg/s)	Wcp (W)
24.491	4.379	87.609	88.466	0.00874	**432.494**
24.616	4.425	87.313	88.170	0.00831	**404.217**
23.165	4.350	85.733	86.590	0.00808	**389.457**
23.268	4.366	85.733	86.590	0.00740	**350.718**
22.361	4.325	86.029	86.886	0.00740	**355.560**
22.979	4.370	88.004	88.861	0.00690	**336.585**
23.537	4.320	90.079	90.936	0.00658	**379.527**
23.471	4.315	91.363	92.220	0.00649	**329.026**
24.968	4.254	95.018	95.875	0.00657	**345.167**

Simulation

Twb = 10°C

T_r10 (°C)	P_r10 (kPa)	T_r11 (°C)	P_r11 (kPa)	m_r (kg/s)	Wcp (W)	Efficiency
12.715	395.8	79.858	1434.2	0.00615	**300.026**	0.560
12.855	397.6	79.767	1432.1	0.00623	**302.856**	0.559
13.309	400.8	80.399	1448.3	0.00623	**303.734**	0.560
13.831	405.6	81.747	1491.6	0.00613	**301.589**	0.562
14.379	407.7	82.539	1505.9	0.00611	**301.606**	0.563
14.661	412.0	83.750	1551.6	0.00598	**298.319**	0.565
15.690	415.1	85.150	1573	0.00594	**298.650**	0.565
16.045	416.9	86.286	1604.4	0.00580	**294.563**	0.566
17.396	419.7	89.222	1662.6	0.00553	**287.905**	0.567

Twb = 15°C

T_r10 (°C)	P_r10 (kPa)	T_r11 (°C)	P_r11 (kPa)	m_r (kg/s)	Wcp (W)	Efficiency
16.528	420.6	80.304	1377.5	0.00733	**346.538**	0.539
16.285	419.7	80.658	1400.5	0.00716	**340.099**	0.544
17.191	425.5	82.700	1462.7	0.00695	**334.279**	0.551
18.088	430.9	83.717	1482.4	0.007	**337.819**	0.551
17.786	428.4	83.406	1474.7	0.00697	**335.986**	0.552
18.175	429.2	85.026	1523.6	0.00668	**326.913**	0.557
18.175	429.9	85.751	1553.1	0.00653	**321.908**	0.560
19.116	431.7	88.192	1611.5	0.00621	**312.628**	0.564
19.103	424.4	89.864	1642.8	0.00577	**297.913**	0.566

Twb = 20°C

T_r10 (°C)	P_r10 (kPa)	T_r11 (°C)	P_r11 (kPa)	m_r (kg/s)	Wcp (W)	Efficiency
21.445	415.0	84.689	1309.5	0.00738	**357.246**	0.526
21.785	422.8	86.002	1380.4	0.00720	**350.887**	0.538
20.140	422.5	84.573	1396.4	0.00715	**346.231**	0.541
21.037	429.5	85.539	1419.2	0.00724	**351.047**	0.541
20.023	441.0	84.588	1465.4	0.00743	**355.958**	0.544
21.469	445.7	86.695	1503.4	0.00732	**354.867**	0.547
19.030	440.5	84.992	1525.0	0.00707	**341.896**	0.553
21.882	441.7	89.120	1571.2	0.00675	**335.376**	0.558
21.507	429.7	91.029	1615.2	0.00605	**310.486**	0.565

Twb = 25°C

T_r10 (°C)	P_r10 (kPa)	T_r11 (°C)	P_r11 (kPa)	m_r (kg/s)	Wcp (W)	Efficiency
24.491	437.9	86.548	1307.4	0.00813	**391.615**	0.509
24.616	442.5	87.016	1340.3	0.00810	**390.650**	0.514
23.165	435.0	85.742	1334.0	0.00790	**380.047**	0.518
23.268	436.6	86.734	1385.0	0.00764	**369.561**	0.530
22.361	432.5	86.684	1415.5	0.00733	**356.514**	0.539
22.979	437.0	88.566	1483.7	0.00706	**347.866**	0.548
23.537	432.0	89.427	1477.4	0.00690	**342.522**	0.550
23.471	431.5	91.752	1571.4	0.00632	**322.417**	0.561
24.968	425.4	95.655	1630.0	0.00574	**304.957**	0.566

Table A.13: Comparison of Experimental & Simulation Results for Compressor

A.3.4 Capillary Tube

Continuity & Energy Equations:

Data from ASHRAE Report (RP-762): **Simulation**

Inside Diameter (mm)	Length (m)	T_in °C	P_in (kPa)	P_out (kPa)	Sub-Cooling (°C)	Mass Flow Rate (kg/s)	Mass Flow Rate (kg/s)	Accuracy (%)
0.8636	3.302	31.16	1205.7	172.37	1.11	0.001982	0.002286	0.8466
0.8636	3.302	24.01	1034.7	193.05	1.11	0.001789	0.002118	0.8162
0.8636	3.302	23.672	861.78	199.95	6.67	0.001433	0.001717	0.8016
0.8636	3.302	30.028	1034.4	193.05	6.67	0.001624	0.001936	0.8079
0.8636	3.302	34.95	1206.9	172.37	6.67	0.001911	0.002170	0.8646
0.7874	2.413	43.839	1207.4	179.26	15.00	0.001454	0.001755	0.7931
0.7874	2.413	43.789	1206.4	186.16	15.00	0.001390	0.001736	0.7512
0.7874	2.413	31.094	862.67	172.37	15.00	0.001113	0.001372	0.7666

Table A.14: Simulation of Capillary Tube with Continuity & Energy Equations

Constant Enthalpy:

Data from ASHRAE Report (RP-762): **Simulation**

Inside Diameter (mm)	Length (m)	T_in °C	P_in (kPa)	P_out (kPa)	Sub-Cooling (°C)	Mass Flow Rate (kg/s)	Mass Flow Rate (kg/s)	Accuracy (%)
0.8636	3.302	31.16	1205.7	172.37	1.11	0.001982	0.001891	0.9540
0.8636	3.302	24.01	1034.7	193.05	1.11	0.001789	0.001808	0.9893
0.8636	3.302	23.672	861.78	199.95	6.67	0.001433	0.001433	1.0000
0.8636	3.302	30.028	1034.4	193.05	6.67	0.001624	0.001582	0.9742
0.8636	3.302	34.95	1206.9	172.37	6.67	0.001911	0.001746	0.9136
0.7874	2.413	43.839	1207.4	179.26	15.00	0.001454	0.001321	0.9087
0.7874	2.413	43.789	1206.4	186.16	15.00	0.001390	0.001283	0.9229
0.7874	2.413	31.094	862.67	172.37	15.00	0.001113	0.001003	0.9016

Table A.15: Simulation of Capillary Tube with Constant Enthalpy

A.3.5 Micro Heat Pump Cycle

Experiment

Twb = 10°C

Q_cond (kW)	Q_evap (kW)	Wcp (kW)	m_r (kg/s)
1.2334	0.90639	0.326	0.00667
1.1471	0.84138	0.305	0.00621
1.0599	0.77578	0.284	0.00581
1.0669	0.77764	0.290	0.00582
1.0470	0.75866	0.289	0.00576
0.9853	0.71238	0.273	0.00541
0.9830	0.70720	0.276	0.00542
1.0807	0.77186	0.309	0.00600

Twb = 15°C

Q_cond (kW)	Q_evap (kW)	Wcp (kW)	m_r (kg/s)
1.3964	1.0378	0.359	0.00733
1.3590	1.0167	0.342	0.00724
1.2803	0.9536	0.327	0.00697
1.2384	0.9162	0.323	0.00663
1.2203	0.8995	0.321	0.00651
1.1722	0.8619	0.311	0.00632
1.1088	0.8097	0.300	0.00596
1.0565	0.7668	0.290	0.00570
1.0931	0.7888	0.305	0.00595

Twb = 20°C

Q_cond (kW)	Q_evap (kW)	Wcp (kW)	m_r (kg/s)
1.5303	1.1908	0.339	0.00793
1.3598	1.0447	0.315	0.00710
1.3629	1.0253	0.338	0.00708
1.3553	1.0102	0.346	0.00699
1.3326	0.9944	0.339	0.00703
1.3110	0.9743	0.338	0.00689
1.2591	0.9198	0.340	0.00668
1.2210	0.9001	0.322	0.00652
1.2353	1.0052	0.376	0.00657

Simulation

Twb = 10°C

Q_cond (kW)	Q_evap (kW)	Wcp (kW)	Efficiency (%)	m_r (kg/s)
1.2339	0.8820	0.3275	55.374	0.00685
1.1697	0.8121	0.3168	55.623	0.00653
1.0507	0.7584	0.2911	56.272	0.00583
1.0375	0.7590	0.2881	56.392	0.00574
1.0600	0.7427	0.2968	56.494	0.00591
1.0341	0.6895	0.2937	56.578	0.00581
1.0141	0.6867	0.2909	56.649	0.00570
0.9663	0.7685	0.2815	56.676	0.00535

Twb = 15°C

Q_cond (kW)	Q_evap (kW)	Wcp (kW)	Efficiency (%)	m_r (kg/s)
1.4068	0.9961	0.3619	53.228	0.00770
1.3500	0.9883	0.3483	53.077	0.00740
1.2968	0.9255	0.3430	54.814	0.00719
1.2408	0.8895	0.3299	55.417	0.00680
1.1710	0.8712	0.3146	55.819	0.00640
1.1304	0.8401	0.3084	56.201	0.00619
1.1061	0.7951	0.3058	56.358	0.00610
1.0858	0.7423	0.3043	56.538	0.00601
1.0553	0.7639	0.2999	56.636	0.00588

Twb = 20°C

Q_cond (kW)	Q_evap (kW)	Wcp (kW)	Efficiency (%)	m_r (kg/s)
1.6113	1.1069	0.4059	50.101	0.00864
1.4506	0.9674	0.3751	52.647	0.00789
1.4486	0.9637	0.3747	52.869	0.00791
1.3430	0.9649	0.3481	54.245	0.00721
1.3244	0.9494	0.3477	54.652	0.00728
1.2801	0.8992	0.3465	55.018	0.00716
1.3312	0.8703	0.3559	54.854	0.00749
1.2549	0.8869	0.3389	55.693	0.00690
1.1511	0.8318	0.3188	56.544	0.00635

__Table A.16:__ Comparison of Heat Transfer and Mass Flow for Cycle Simulation

Tw_in (°C)	Tw_int1 (°C)	Tw_int2 (°C)	Tw_out (°C)	Ta_in (°C)	Ta_out (°C)
19.8	20.551	53.123	60.034	19.080	16.024
25.0	25.674	54.421	60.705	19.400	14.881
29.6	30.116	54.270	59.748	19.680	15.484
34.5	34.946	54.746	59.296	20.080	15.885
40.5	40.879	56.535	60.246	20.720	17.061
44.3	44.621	57.639	60.777	21.120	17.938
48.9	49.104	58.124	60.348	21.680	17.882
53.7	53.785	58.162	59.333	22.440	18.896

Tw_in (°C)	Tw_int1 (°C)	Tw_int2 (°C)	Tw_out (°C)	Ta_in (°C)	Ta_out (°C)
15.5	16.317	52.288	60.332	25.480	20.860
19.4	20.240	52.627	59.733	25.360	19.895
26.0	26.440	54.094	60.439	24.960	20.092
29.9	30.512	54.384	60.070	26.360	20.206
35.0	35.485	54.446	58.982	26.080	19.016
39.5	39.903	55.431	59.264	25.680	18.910
44.1	44.497	56.892	59.959	25.000	19.582
49.9	50.182	58.222	60.280	25.720	19.883
54.5	54.622	58.756	59.810	24.960	19.689

Tw_in (°C)	Tw_int1 (°C)	Tw_int2 (°C)	Tw_out (°C)	Ta_in (°C)	Ta_out (°C)
13.8	14.875	52.931	62.420	30.840	23.118
21.0	21.835	54.461	62.622	30.840	22.065
25.1	26.007	55.083	62.207	28.800	22.114
30.1	30.805	53.799	59.567	29.920	20.948
35.5	36.101	55.321	59.849	29.000	20.240
40.0	40.686	58.946	63.535	30.120	21.798
45.2	45.601	57.962	60.850	28.920	20.890
49.7	49.948	58.159	60.287	29.600	21.350
54.5	54.628	58.179	59.085	29.520	21.848

Table A.17: Water and Air Change for Cycle Simulation

APPENDIX B

SAMPLE CALCULATIONS

B.1 Fluted tube condenser

In this section sample calculations are conducted to show how the simulation operates for each of the three regions (subcool, two-phase, and superheat) in the condenser. The condenser is divided into 4 sections for the purpose of the calculations. All the results shown below are for the last iteration of the condenser simulation. The sample calculations is based on the geometry given in Table 5.2 and the following set of test conditions:

$m_w = 0.0075$ kg/s

$T_{w,in} = 15.5$ °C

$m_r = 0.00725$ kg/s

$h_{su} = 307.0443$ kJ/kg

$dT_{sub} = 2.144$ °C

For the last iteration the estimated temperature at working point 2 is given by

$$T_{r2} = \frac{T_{r,\,top} + T_{r,\,bottom}}{2} = (54.6962 + 54.6958)/2 = 54.696 \text{ °C}$$

The total outside area is divided into 4 equal sections (n):

$A_o[i] = 0.1361/4 = 0.03402$ m

Divide n sections into m = n+2 areas to incorporate subcool/two-phase interface and superheat/two-phase interface. The 6 areas are given in Table B.1 as divided from the superheated inlet.

Area	Size (m)
A[1]	0.03402
A[2]	0.00213
A[3]	0.0319
A[4]	0.03402
A[5]	0.03294
A[6]	0.00108

Table B.1: Size of divided areas.

Determine the overall heat transfer coefficient (U) and the pressure drop (Δp) for each area using the following equations. The calculations will only be shown for one area in each region (superheat, two-phase, subcool) along with the calculation on the waterside and conduction through the wall.

Conduction through tube wall

Ratio of outside volumetric diameter to inside volumetric diameter is given by

$$b_c = \frac{D_{vo}}{D_{vi}} = 0.0114/0.01 = 1.14.$$

Wall thickness is determined by

$$\text{wall} = 0.5(D_{vo} - D_{vi}) = 0.5(0.0114 - 0.01) = 0.0007 \text{ m}.$$

The tube wall resistance is calculated by

$$R_m = \frac{\text{wall}}{Kt} + \frac{b_c}{hl} = \frac{0.0007}{393} + \frac{1.14}{1.0x10^7} = 1.895x10^{-6}.$$

Water side conditions

$$c_p, \mu, k = f(T_w)$$

Prandtl number is given by

$$P_r = \frac{c_p.\mu}{k} = \frac{4184(0.000656)}{0.614} = 4.4702.$$

The inside cross-sectional area is calculated by

$$A_i = \frac{\pi D_{hi}^2}{4} = \frac{\pi(0.01)^2}{4} = 7.834x10^{-5} \text{ m}^2.$$

The mass flux is given by

$$G_w = \frac{m_w}{A_i} = \frac{0.0075}{7.834x10^{-5}} = 95.493 \text{ kg/(s.m}^2\text{)}.$$

The Reynolds number is calculated with the mass flux:

$$Rey_w = \frac{G.D_{hi}}{\mu} = \frac{95.493(0.01)}{0.000656} = 1455.685.$$

$Rey_w < 5000$, thus the Nusselt number and friction factor is given by:

$$Nu = 0.014.Rey^{0.842}\left(e^*\right)^{-0.067}\left(p^*\right)^{-0.293}\left(\theta^*\right)^{-0.705} Pr^{0.4}$$

$$= 18.9498$$

$$\text{fric} = 0.554\frac{64}{\text{Rey}_w - 45}(e^*)^{0.384}(p^*)^{-1.454+2.083(e^*)}(\theta^*)^{-2.426}$$

$$= 0.0537.$$

The inside heat transfer coefficient is determined by

$$h_i = \frac{Nu.k}{D_{hi}} = \frac{18.9498(0.614)}{0.01} = 1163.517 \text{ W/(m}^2\text{.K)}.$$

The water side resistance is given by

$$R_r = \frac{b_c}{h_i} = \frac{1.14}{1163.517} = 0.0009798.$$

To determine the water pressure drop the velocity is given by

$$V = \frac{G}{\rho} = \frac{95.493}{992.2} = 0.09624 \text{ m/s}.$$

Length of section is determined by

$$l_c = \frac{A[i]}{A_{tot}}L = \frac{0.03402}{0.13609}(3.8) = 0.95 \text{ m}.$$

The pressure drop on the water side is then given by

$$\Delta p_w = \frac{\rho V^2}{2}.\frac{\text{fric.lc}}{D_{hi}} = \frac{992.2(0.09624)^2}{2}.\frac{0.05369(0.95)}{0.01} = 23.436 \text{ Pa}.$$

Refrigerant side conditions

The cross-sectional area is determined by

$$A_{cr} = \frac{\pi(D_o^2 - D_{vo}^2)}{4} = \frac{\pi(0.0127^2 - 0.0114^2)}{4} = 2.4607\text{e-}5 \text{ m}^2.$$

The annulus hydraulic diameter is calculated by

$$D_{ho} = D_o - D_{vo} = 0.0127 - 0.0114 = 0.0013 \text{ m}.$$

Parameter d_{coil} used in friction factor calculation:

$$d_{coil} = \frac{D_{hi}}{\sin\left(\theta^*.\frac{\pi}{2}\right)} = 0.01145 \text{ m}$$

Superheat Region

The inlet temperature to the section is given by

$$T_{su} = f(p_{su}, h_{su}) = f(1.546\text{x}10^6, 0.307\text{x}10^6) = 84.12 \text{ °C}$$

The inlet specific volume to the section is given by

$$v_{su} = f(p_{su}, h_{su}) = 0.0153 \text{ m}^3/\text{kg}$$

The inlet viscosity to the section is given by

$$\mu_{su} = f(T_{su}) = 1.839x10^{-5} \text{ kg/(s.m)}$$

The inlet thermal conductivity of the section is given by

$$k_{su} = f(T_{su}) = 0.0222 \text{ W/(m.K)}$$

The inlet density is calculated by

$$\rho_{su} = \frac{1}{v_{su}} = 65.22 \text{ kg/m}^3$$

The outlet properties of the section are calculated in the same way as the inlet properties.

$$T_{ex} = f(1.484x10^6, 0.2733x10^6) = 55.319°C$$

$$v_{ex} = 0.0132 \text{ m}^3/\text{kg}$$

$$\mu_{ex} = 1.427x10^{-5} \text{ kg/(s.m)}$$

$$k_{ex} = 0.0175 \text{ W/(m.K)}$$

$$\rho_{ex} = 75.679 \text{ kg/m}^3$$

The specific heat for the section is given by

$$cp_r = \frac{h_{su} - h_{ex}}{T_{su} - T_{ex}} = \frac{307044.3 - 273266.0}{84.12 - 55.32} = 1172.82 \text{ J/(kg.K)}$$

The average viscosity for the section is given by

$$\mu_r = \frac{\mu_{su} + \mu_{ex}}{2} = 1.633x10^{-5} \text{ kg/(s.m)}$$

The average thermal conductivity for the section is given by

$$k_r = \frac{k_{su} + k_{ex}}{2} = 0.0199 \text{ W/(m.K)}$$

The average density for the section is given by

$$\rho_r = \frac{\rho_{su} + \rho_{ex}}{2} = 70.449 \text{ kg/m}^3$$

Prandtl number is given by

$$P_r = \frac{c_p.\mu}{k} = 0.963$$

Mass flux is determined by

$$G_r = \frac{m_r}{A_{cr}} = 294.673 \text{ kg/(s.m}^2)$$

The velocity for the section is given by

$$V = \frac{G_r}{\rho_r} = 4.182 \text{ m/s}$$

The Reynolds number is calculated by

$$Rey_r = \frac{G_r.D_{ho}}{\mu_r} = 23453.186$$

The Nusselt number is determined by

$$Nu = 0.023.Rey_{liq}{}^{0.8}.Pr^{0.3} = 71.28$$

The outside heat transfer coefficient is given by

$$h_o = Nu.\frac{k_r}{D_{ho}} = 1090.658 \text{ W/(m}^2\text{.K)}$$

The friction factor is determined by

$$fsc = 0.079.Rey_r{}^{-0.25} + 0.075\left(\frac{D_{ho}}{d_{coil}}\right)^{0.5} = 0.0089$$

$$ff = fsc + 17.5782.Rey_r{}^{-0.3137}\left(\frac{D_{ho}}{d_{coil}}\right)^{0.3621}\left(\frac{e}{D_{ho}}\right)^{0.6885} = 0.0343$$

$$ff = ff{*}4 = 0.1373$$

The influence of the friction on the pressure drop is given by

$$y = \log_{10}\left(\frac{e}{3.7(D_{ho})} + \frac{5.74}{Rey_r{}^{0.9}}\right) = -2.1607$$

$$ratio = \frac{ff}{\left(\frac{1}{4.y^2}\right)} = 2.5634$$

$$ratio = 0.25(ratio-1)+1 = 1.3908$$

Influence of friction on outside heat transfer coefficient is given by

$$h_o = 1.15(h_o.ratio) = 1744.471 \text{ W/(m}^2\text{.K)}$$

The overall heat transfer coefficient is given by

$$U = \frac{1}{\frac{1}{h_o} + R_r + R_m} = 643.119 \text{ W/(m}^2\text{.K)}$$

The pressure drop on the refrigerant side is determined by

$$\Delta p = \frac{ff.l_c.\rho_r.V^2}{2.D_{ho}} = 61800.484 \text{ Pa}$$

Two-phase region

The inlet pressure and enthalpy for the section are

$$p_{su} = 1.4806x10^6 \text{ Pa}$$

$$h_{su} = 272.581x10^3 \text{ kJ/kg}$$

Inlet quality of the section is a function of the enthalpy.

$$x_{su} = \frac{h_{su} - h_{liq}}{h_{vap} - h_{liq}} = 1.0$$

The inlet temperature is given by

$$T_{su} = f(p_{su}) = 54.696 \text{ °C}$$

The specific volume at the inlet is determined by means of the quality.

$$\nu_{su} = (1-x_{su}).\nu_{liq} + x_{su}.\nu_{vap} = 0.0132 \text{ m}^3\text{/kg}$$

The inlet viscosity is given by

$$\mu_{su} = (1-x_{su}).\ \mu_{liq} + x_{su}.\ \mu_{vap} = 1.422x10^{-5} \text{ kg/(s.m)}$$

The thermal conductivity at the inlet is given by

$$k_{su} = (1-x_{su}).k_{liq} + x_{su}.k_{vap} = 0.0175 \text{ W/(m.K)}$$

The inlet density is calculated from

$$\rho_{su} = \frac{1}{\nu_{su}} = 75.801 \text{ kg/m}^3$$

The outlet pressure and enthalpy for the section are

$$p_{ex} = 1.434x10^6 \text{ Pa}$$

$$h_{ex} = 253.305 \text{ kJ/kg}$$

The outlet properties of the section are calculated in the same way as the inlet conditions of the section.

$$x_{ex} = 0.8716$$

$$T_{ex} = 53.377 \text{ °C}$$

$$\nu_{ex} = 0.012 \text{ m}^3\text{/kg}$$

$$\mu_{ex} = 3.1697x10^{-5} \text{ kg/(s.m)}$$

$$k_{ex} = 0.0239 \text{ W/(m.K)}$$

$$\rho_{ex} = 83.038 \text{ kg/m}^3$$

The average temperature is calculated from

$$T_r = \frac{T_{su} + T_{ex}}{2} = 54.036 \text{ °C}$$

The average pressure is given by

$$p_r = f(T_r) = 1.457x10^6 \text{ Pa}$$

The average quality is given by

$$x_r = \frac{x_{su} + x_{ex}}{2} = 0.9358$$

The liquid viscosity at the average temperature is

$$\mu_{liq} = f(T_r) = 14.988\text{x}10^{-5}\ \text{kg/(s.m)}$$

The vapour viscosity at the average temperature is

$$\mu_{vap} = f(T_r) = 1.4163\text{x}10^{-5}\ \text{kg/(s.m)}$$

The viscosity relation at the average quality is given by

$$\mu_r = \frac{\mu_{vap}}{\mu_{liq}} = 0.0945$$

The liquid specific volume at the average temperature is

$$v_{liq} = f(T_r) = 92.249\text{x}10^{-5}\ \text{m}^3/\text{kg}$$

The vapour specific volume at the average temperature is

$$v_{vap} = f(T_r) = 0.0134\ \text{m}^3/\text{kg}$$

The liquid density at the average temperature is

$$\rho_{liq} = \frac{1}{v_{liq}} = 1084.02\ \text{kg/m}^3$$

The vapour density at the average temperature is

$$\rho_{vap} = \frac{1}{v_{vap}} = 74.424\ \text{kg/m}^3$$

The density relation at the average temperature is given by

$$\rho_r = \frac{\rho_{vap}}{\rho_{liq}} = 0.0687$$

The mass flux is determined by means of

$$G_r = \frac{m_r}{A_{cr}} = 294.637\ \text{kg/(s.m}^2)$$

The liquid Reynolds number is given by

$$Rey_{liq} = \frac{G_r.D_{ho}}{\mu_{liq}} = 2555.572$$

The vapour Reynolds number is given by

$$Rey_{vap} = \frac{G_r.D_{ho}}{\mu_{vap}} = 27044.11$$

The Reynolds number at the average temperature is given by

$$\mathrm{Rey_r} = \mathrm{Rey_{liq}} + \left(\frac{\mu_{vap}}{\rho_{iq}}\right)\left(\frac{\rho_{iq}}{\rho_{vap}}\right)^{0.5} .\mathrm{Rey_{vap}} = 12308.83$$

The liquid specific heat is determined by

$$c_{p,liq} = f(T_r) = 1603.33 \text{ J/(kg.K)}$$

The thermal conductivity at the average temperature is given by

$$k_{liq} = f(T_r) = 0.0685 \text{ W/(m.K)}$$

The liquid Prandtl number is determined from

$$\mathrm{Pr_{liq}} = \frac{\mu_{liq}.C_{p,\,liq}}{k_{liq}} = 3.5065$$

The reduced pressure is calculated by

$$pr = \frac{p_r}{p_{crit}} = 0.359$$

The liquid outside heat transfer coefficient is determined by

$$ho_{liq} = 0.023.\mathrm{Rey_{liq}}^{0.8}.\mathrm{Pr}^{0.4}.\frac{k_{liq}}{D_{ho}} = 1065.663 \text{ W/(m}^2\text{.K)}$$

The correlation of Shah (1979:548) was then implemented to obtain the outside two-phase heat transfer coefficient.

$$ho_{tpc} = ho_{liq}\left[(1-x_r)^{0.8} + \frac{3.8.x_r^{0.76}(1-x_r)^{0.04}}{pr^{0.38}}\right] = 5209.157 \text{ W/(m}^2\text{.K)}$$

The two-phase pressure drop is determined by a technique used by Christensen and Srinivasan (1991:82)

$$\Delta p = 0.09.\mathrm{Rey_{vap}}^{-0.2}.x_r^{1.8}\left[1 + 2.85\left(\mu_r^{-0.1}\left(\frac{1-x}{x}\right)^{0.9}\rho_r^{0.5}\right)^{0.523}\right]^2.\frac{G^2}{\rho_{vap}D_{ho}} = 19.661 \text{ kPa}$$

The friction factor is determined with the technique described by Das (1993:972).

$$fsc = 0.079.\mathrm{Rey_{vap}}^{-0.25} + 0.075\left(\frac{D_{ho}}{d_{coil}}\right)^{0.5} = 0.00869$$

$$ff = fsc + 17.5782.\mathrm{Rey_{vap}}^{-0.3137}\left(\frac{D_{ho}}{d_{coil}}\right)^{0.3621}\left(\frac{e}{D_{ho}}\right)^{0.6885} = 0.0329$$

To determine the influence of the friction on the pressure drop, the following equations are used.

$$ff = ff^*4 = 0.1319$$

$$y = \ln\left(\frac{e}{3.7(D_{ho})} + \frac{5.74}{Rey_{vap}^{\ 0.9}}\right) = -2.129$$

$$ratio = \frac{ff}{\left(\frac{0.25}{y^2}\right)} = 2.3915$$

The pressure drop is multiplied by the ratio.

$$\Delta p = \Delta p * ratio = 47.0215 \text{ kPa}$$

The outside heat transfer coefficient is also multiplied by the ratio.

$$ratio = 0.25(ratio\text{-}1)+1 = 1.349$$

$$h_o = 1.15(h_o)(ratio) = 8074.506 \text{ W/(m}^2\text{.K)}$$

The overall heat transfer coefficient for the section is given by

$$U = \frac{1}{\frac{1}{h_o} + R_r + R_m} = 905.544 \text{ W/(m}^2\text{.K)}$$

Subcooled region

The inlet temperature is a function of the enthalpy

$$T_{su} = f(h_{su}) = f(121.2827x10^3) = 50.69 \text{ °C}$$

The inlet viscosity is a function of the temperature

$$\mu_{su} = f(T_{su}) = 15.638x10^{-5} \text{ kg/(s.m)}$$

The inlet conductivity is a function of the temperature

$$k_{su} = f(T_{su}) = 0.0701 \text{ W/(m.K)}$$

The inlet specific volume is a function of the temperature

$$\nu_{su} = f(T_{su}) = 9.091x10^{-4} \text{ m}^3\text{/kg}$$

The inlet density is given by

$$\rho_{su} = \frac{1}{\nu_{su}} = 1099.99 \text{ kg/m}^3$$

The inlet velocity is given by

$$V_{su} = \frac{m_r}{\rho_{su}.A_{cr}} = 0.2679 \text{ m/s}$$

The outlet temperature is a function of the enthalpy

$$T_{ex} = f(h_{ex}) = f(117.989x10^3) = 48.546 \text{ °C}$$

The outlet viscosity is a function of the temperature

$$\mu_{ex} = f(T_{ex}) = 16.0622 \times 10^{-5}\ kg/(s.m)$$

The outlet conductivity is a function of the temperature

$$k_{ex} = f(T_{ex}) = 0.0711\ W/(m.K)$$

The outlet specific volume is a function of the temperature

$$\nu_{ex} = f(T_{ex}) = 9.01 \times 10^{-4}\ m^3/kg$$

The outlet density is given by

$$\rho_{ex} = \frac{1}{\nu_{ex}} = 1109.93\ kg/m^3$$

The outlet velocity is given by

$$V_{ex} = \frac{m_r}{\rho_{ex}.A_{cr}} = 0.2655\ m/s$$

The specific heat for the section is given by

$$c_p = \frac{h_{su} - h_{ex}}{T_{su} - T_{ex}} = 1536.194\ J/(kg.K)$$

The viscosity for the section is given by

$$\mu_r = \frac{\mu_{su} + \mu_{ex}}{2} = 15.85 \times 10^{-5}\ kg/(s.m)$$

The thermal conductivity of the section is given by

$$k_r = \frac{k_{su} + k_{ex}}{2} = 0.0706\ W/(m.K)$$

The density for the section is given by

$$\rho_r = \frac{\rho_{su} + \rho_{ex}}{2} = 1104.962\ kg/m^3$$

The average velocity for the section is given by

$$V_r = \frac{V_{su} + V_{ex}}{2} = 0.2667\ m/s$$

Prandtl number is given by

$$P_r = \frac{c_p.\mu_r}{k_r} = 3.4503$$

Mass flux is determined by

$$G_r = \frac{m_r}{A_{cr}} = 294.637 \text{ kg/(s.m}^2)$$

The Reynolds number is calculated by

$$Rey_r = \frac{G_r.D_{ho}}{\mu_r} = 2416.509$$

The Nusselt number is determined by

$$Nu = 0.023.Rey_{liq}^{0.8}.Pr^{0.3} = 16.968$$

The outside heat transfer coefficient is given by

$$h_o = Nu.\frac{k_r}{D_{ho}} = 921.138 \text{ W/(m}^2\text{.K)}$$

The friction factor is determined by

$$fsc = 0.079.Rey_r^{-0.25} + 0.075\left(\frac{D_{ho}}{d_{coil}}\right)^{0.5} = 0.0138$$

$$ff = fsc + 17.5782.Rey_r^{-0.3137}\left(\frac{D_{ho}}{d_{coil}}\right)^{0.3621}\left(\frac{e}{D_{ho}}\right)^{0.6885} = 0.0656$$

$$ff = ff^{*}4 = 0.2625$$

The influence of the friction on the pressure drop is given by

$$y = \log_{10}\left(\frac{e}{3.7(D_{ho})} + \frac{5.74}{Rey_r^{0.9}}\right) = -1.9428$$

$$ratio = \frac{ff}{\left(\frac{1}{4.y^2}\right)} = 3.9619$$

$$ratio = 0.25(ratio-1)+1 = 1.7405$$

Influence of friction on outside heat transfer coefficient is given by

$$h_o = 1.15(h_o.ratio) = 1843.706 \text{ W/(m}^2\text{.K)}$$

The overall heat transfer coefficient is given by

$$U = \frac{1}{\frac{1}{h_o} + R_f + R_m} = 656.138 \text{ W/(m}^2\text{.K)}$$

The pressure drop on the refrigerant side is determined by

$$\Delta p = \frac{ff.l_c.\rho_r.V^2}{2.D_{ho}} = 239.139 \text{ Pa}$$

In the next table the calculated values for each section is given:

Section	Area (m^2)	U ($W/m^2.K$)	Δp (kPa)
A[1]	0.034023	643.1189	61.8005
A[2]	0.002126	629.6893	3.4587
A[3]	0.031896	904.544	47.0215
A[4]	0.034023	897.616	58.5619
A[5]	0.032944	843.3249	33.7340
A[6]	0.00108	656.1385	0.23914

Table B.2: Calculated values for each section

The pressure at each interface between the new areas:

$p[1] = 1.54588 \text{x} 10^6$ Pa

$p[2] = 1.48408 \text{x} 10^6$ Pa

$p[3] = 1.48062 \text{x} 10^6$ Pa

$p[4] = 1.4336 \text{x} 10^6$ Pa

$p[5] = 1.37504 \text{x} 10^6$ Pa

$p[6] = 1.3413 \text{x} 10^6$ Pa

$p[7] = 1.3411 \text{x} 10^6$ Pa

The pressures at the four main interfaces are

$p_{r1} = 1.54588 \text{x} 10^6$ Pa (Inlet of condenser)

$p_{r2} = 1.48062 \text{x} 10^6$ Pa (Superheat/two-phase interface)

$p_{r3} = 1.3413 \text{x} 10^6$ Pa (Two-phase/subcool interface)

$p_{r4} = 1.3411 \text{x} 10^6$ Pa (Outlet of condenser)

The temperature at the inlet of the condenser is calculated with the new pressure and the fixed enthalpy.

$$T_{r1} = f(p_{r1}, h_{r1}) = f(1.54588 \text{x} 10^6, 307.044 \text{x} 10^3) = 84.12°C$$

The temperature at the interface between the subcool and two-phase regions is determined from the pressure.

$$T_{r3} = f(p_{r3}) = 50.69°C$$

The enthalpies at the two interfaces is given by

$h_{r2} = f(p_{r2}) = 272.581$ kJ/kg (saturated vapour)

$h_{r3} = f(p_{r3}) = 121.282$ kJ/kg (saturated liquid)

The outlet refrigerant temperature of the condenser is

$$T_{r4} = T_{r3} - dT_{sub} = 50.69 - 2.144 = 48.546\ °C$$

The outlet refrigerant enthalpy of the condenser is

$$h_{r4} = f(T_{r4}) = 117.988\ kJ/kg$$

Check that the outlet refrigerant temperature is higher than the inlet water temperature.

$$T_{r4} = 48.546\ °C > 15.5\ °C = T_{l4}$$

Subcool region

Determine the interface temperatures and enthalpies and the new subcool area. From Table B.2 it can be seen that there is only one subcool area. When the condenser is divided into more areas the subcool area will be subdivided into smaller areas. The simulation works backward from the outlet of the condenser towards the inlet.

The specific heat of the refrigerant is determined from

$$cp_r = \frac{h_{r3} - h_{r4}}{T_{r3} - T_{r4}} = \frac{121.282x10^3 - 117.988x10^3}{50.69 - 48.55} = 1536.193\ J/(kg.K)$$

The heat transfer is determined from

$$Q = m_r(h_{r3} - h_{r4}) = 0.00725(121.282x10^3 - 117.988x10^3) = 23.879\ W$$

Determine the minimum and maximum $(m.c_p)$ value for the water and the refrigerant

$$(m.c_p)_{min} = m_r.c_{pr} = 0.00725(1536.193) = 11.137$$

$$(m.c_p)_{max} = m_l.c_{pl} = 0.0075(4184.0) = 31.38$$

The ratio of the minimum to the maximum value is

$$(m.c_p)_{ratio} = \frac{(m.c_p)_{min}}{(m.c_p)_{max}} = 0.355$$

The maximum heat transfer is calculated from

$$Q_{max} = (m.c_p)_{min}.(T_{r3} - T_{l4}) = 11.137(50.69 - 15.5) = 391.92\ W$$

The efficiency in the subcool region is

$$\eta = \frac{Q}{Q_{max}} = 0.0609$$

The number of transfer units for counterflow is determined as

$$NTU = 0.0636$$

The new subcool area is determined from

$$A_{scc} = \frac{NTU(m.c_p)_{min}}{U} = \frac{0.0636(11.137)}{656.13} = 0.00108$$

The change in the water temperature over the section is given by

$$T_{l3} = T_{l4} + \frac{Q}{m_l.c_{pl}} = 16.26\ °C$$

Two-phase region

In the two-phase region one of the intermediate sections will be discussed as well as the last section before the refrigerant is in the superheat area.

Intermediate section

Assign an estimated value to the specific heat of the section.

$$c_{pr} = \frac{h_{r2} - h_{r3}}{T_{r2} - T_{r3}} = \frac{272.581x10^3 - 121.282x10^3}{54.696 - 50.689} = 37763.03\ J/(kg.K)$$

Iterate to find correct c_p value as follows.

Determine the minimum and maximum $(m.c_p)$ value for the water and the refrigerant

$$(m.c_p)_{min} = m_l.c_{pl} = 0.0075(4184.0) = 31.38$$

$$(m.c_p)_{max} = m_r.c_{pr} = 0.00725(37763.03) = 1273.782$$

The ratio of the minimum to the maximum value is

$$(m.c_p)_{ratio} = \frac{(m.c_p)_{min}}{(m.c_p)_{max}} = 0.1146$$

The temperature at the outlet of the section is determined from the pressure

$$T_{ex} = f(p_{ex}) = f(1.375x10^6) = 51.687\ °C$$

The inlet temperature to the section is $T_{r3} = 50.69$ °C.

The number of transfer units for the section is given by

$$NTU = \frac{U[5].A[5]}{(m.c_p)_{min}} = \frac{843.325(0.0329)}{31.38} = 0.885$$

The effectiveness for the counterflow arrangement of the section is determined by

$$\eta = \frac{1 - \exp\left(-Ntu\left(1 - \left(\dot{m}Cp\right)_{ratio}\right)\right)}{1 - \left(\dot{m}Cp\right)_{ratio}.\exp\left(-Ntu\left(1 - \left(\dot{m}Cp\right)_{ratio}\right)\right)} = 0.573$$

The maximum heat transfer is calculated from

$$Q_{max} = (m.c_p)_{min}.(T_{ex} - T_{l3}) = 31.38(51.687 - 16.261) = 1111.679\ W$$

The heat transfer is

$$Q = \eta.Q_{max} = 0.573(1111.679) = 637.408\ W$$

The enthalpy at the outlet of the section is given by

$$h_{ex} = h_{r3} + \frac{Q}{m_r} = 121.282x10^3 + \frac{637.408}{0.00725} = 209.201 \text{ kJ/kg}$$

The change in the specific heat is determined by

$$\Delta c_{pr} = \frac{h_{ex} - h_{r3}}{T_{ex} - T_{r3}} - c_{pr} = 50355.58 \text{ J/(kg.K)}$$

Determine the error for the specific heat calculation

$$\text{error} = \frac{\Delta c_{pr}}{c_{pr}} = 1.333$$

New iteration value for c_{pr} is

$$c_{pr} = c_{pr} + 0.5(\Delta c_{pr}) = 62940.822 \text{ J/(kg.K)}$$

The routine is iterated until the specific heat value converges resulting in the following solutions:

$$Q = 646.387 \text{ W}$$

$$\eta = 0.581$$

$$h_{ex} = 210.439 \text{ kJ/kg}$$

$$T_{l,ex} = T_{l3} + \frac{Q}{m_l.c_{pl}} = 36.86 \text{ °C}$$

Two-phase/superheat interface

For the last area in the two-phase region at the two-phase/superheat interface the routine determines the size of the area to comply with the refrigerant properties.

The specific heat for the section is given by

$$c_p = \frac{h_{r2} - h_{su}}{T_{r2} - T_{su}} = \frac{272.581x10^3 - 253.304x10^3}{54.696 - 53.377} = 14608.534 \text{ J/(kg.K)}$$

Determine the minimum and maximum $(m.c_p)$ value for the water and the refrigerant

$$(m.c_p)_{min} = m_l.c_{pl} = 0.0075(4184.0) = 31.38$$

$$(m.c_p)_{max} = m_r.c_{pr} = 0.00725(14608.534) = 105.912$$

The ratio of the minimum to the maximum value is

$$(m.c_p)_{ratio} = \frac{(m.c_p)_{min}}{(m.c_p)_{max}} = 0.2963$$

The heat transfer is determined from

$$Q = m_r(h_{r2} - h_{su}) = 0.00725(272.582x10^3 - 253.304x10^3) = 139.762 \text{ W}$$

The maximum heat transfer is calculated from

$$Q_{max} = (m.c_p)_{min}.(T_{r3} - T_{l,su}) = 31.38(54.696 - 46.763) = 248.938 \text{ W}$$

The efficiency for the last section in the two-phase region is

$$\eta = \frac{Q}{Q_{max}} = 0.561$$

The number of transfer units for counterflow is determined as

$$NTU = 0.9194$$

The size of the last two-phase area is

$$A = \frac{NTU(m.c_p)_{min}}{U} = \frac{0.9194(31.38)}{904.544} = 0.0319 \text{ m}^2$$

The water temperature leaving the area is

$$T_{l2} = T_{l,su} + \frac{Q}{m_l.c_{pl}} = 46.763 + \frac{139.762}{0.0075(4184)} = 51.217 \text{ °C}$$

Superheat region

In the superheat region one of the intermediate sections will be discussed as well as the last section which is at the refrigerant inlet of the condenser from the compressor.

The total superheat area is equal to the total area of the condenser minus the determined subcool and two-phase areas.

$$A_{shc} = A_{tot} - A_{scc} - A_{tpc} = 0.1361 - 0.00108 - 0.09886 = 0.03615 \text{ m}^2$$

Intermediate section

Assign an estimated value to the specific heat of the refrigerant

$$c_{pr} = f(T_{r2}) = 1276.05 \text{ J/(kg.K)}$$

Determine the minimum and maximum $(m.c_p)$ value for the water and the refrigerant

$$(m.c_p)_{min} = m_r.c_{pr} = 0.00725(1276.05) = 9.251$$

$$(m.c_p)_{max} = m_l.c_{pl} = 0.0075(4184.0) = 31.38$$

The ratio of the minimum to the maximum value is

$$(m.c_p)_{ratio} = \frac{(m.c_p)_{min}}{(m.c_p)_{max}} = 0.2948$$

The number of transfer units for the section is given by

$$NTU = \frac{U[2].A[2]}{(m.c_p)_{min}} = \frac{629.689(0.00213)}{9.251} = 0.1447$$

The effectiveness for the counterflow arrangement of the section is determined by

$$\eta = \frac{1 - \exp\left(-Ntu\left(1 - \left(\dot{m}Cp\right)_{ratio}\right)\right)}{1 - \left(\dot{m}Cp\right)_{ratio}.\exp\left(-Ntu\left(1 - \left(\dot{m}Cp\right)_{ratio}\right)\right)} = 0.1322$$

The heat transfer is determined from

$$Q = \eta \frac{(m.c_p)_{min}}{1 - \frac{\eta.(m.c_p)_{min}}{m_r.c_{pr}}}(T_{r2} - T_{l2}) = 4.905 \text{ W}$$

The enthalpy at the outlet of the section is given by

$$h_{ex} = h_{r2} + \frac{Q}{m_r} = 272.582\text{x}10^3 + \frac{4.905}{0.00725} = 273.258 \text{ kJ/kg}$$

The refrigerant temperature at the outlet of the section is a function of the pressure and the enthalpy.

$$T_{ex} = f(p_{ex}, h_{ex}) = f(1.4841\text{x}10^6, 273.258\text{x}10^3) = 55.313 \text{ °C}$$

The change in the specific heat is determined by

$$\Delta c_{pr} = \frac{h_{ex} - h_{r2}}{T_{ex} - T_{r2}} - c_{pr} = -178.669 \text{ J/(kg.K)}$$

Determine the error for the specific heat calculation

$$\text{error} = \frac{\Delta c_{pr}}{c_{pr}} = 0.14$$

New iteration value for c_{pr} is

$$c_{pr} = c_{pr} + 0.5(\Delta c_{pr}) = 1186.715 \text{ J/(kg.K)}$$

The routine is iterated until the specific heat value converges resulting in the following solutions:

$$Q = 4.9613 \text{ W}$$

$$\eta = 0.1512$$

$$h_{ex} = 273.266 \text{ kJ/kg}$$

$$T_{l,ex} = T_{l2} + \frac{Q}{m_l.c_{pl}} = 51.376 \text{ °C}$$

Section at condenser inlet

The last section must be equal to the total superheat area minus the intermediate areas calculated thus far.

$$A = A_{shc} - A_{sum} = 0.03615 - 0.00213 = 0.034 \text{ m}^2$$

The inlet enthalpy of the condenser is fixed as discussed in Chapter 4.

An estimated value is determined for the specific heat of the refrigerant for the last section

$$c_{pr} = \frac{h_{r1} - h_{su}}{T_{r1} - T_{su}} = \frac{307.044x10^3 - 273.266x10^3}{84.12 - 55.32} = 1172.82 \text{ J/(kg.K)}$$

The fixed heat transfer for the section is given by

$$Q = m_r(h_{r1} - h_{su}) = 0.00725(307.044x10^3 - 273.266x10^3) = 244.893 \text{ W}$$

Determine the minimum and maximum $(m.c_p)$ value for the water and the refrigerant

$$(m.c_p)_{min} = m_r.c_{pr} = 0.00725(1172.82) = 8.503$$

$$(m.c_p)_{max} = m_l.c_{pl} = 0.0075(4184.0) = 31.38$$

The ratio of the minimum to the maximum value is

$$(m.c_p)_{ratio} = \frac{(m.c_p)_{min}}{(m.c_p)_{max}} = 0.255$$

The number of transfer units for the section is given by

$$NTU = \frac{U[1].A[1]}{(m.c_p)_{min}} = \frac{643.119(0.034)}{8.503} = 2.573$$

The effectiveness for the counterflow arrangement of the section is determined by

$$\eta = \frac{1 - \exp\left(-Ntu\left(1 - \left(\dot{m}Cp\right)_{ratio}\right)\right)}{1 - \left(\dot{m}Cp\right)_{ratio}.\exp\left(-Ntu\left(1 - \left(\dot{m}Cp\right)_{ratio}\right)\right)} = 0.883$$

The maximum heat transfer for the section is

$$Q_{max} = \frac{Q}{\eta} = 277.191 \text{ W}$$

The temperature at the inlet to the condenser is

$$T_{r1} = \frac{Q_{max}}{(m.c_p)_{min}} + T_{l,su} = \frac{277.191}{8.503} + 51.375 = 83.975 \text{ °C}$$

The change in the specific heat is determined by

$$\Delta c_{pr} = \frac{h_{r1} - h_{su}}{T_{r1} - T_{su}} - c_{pr} = 5.95 \text{ J/(kg.K)}$$

Determine the error for the specific heat calculation

$$\text{error} = \frac{\Delta c_{pr}}{c_{pr}} = 0.005$$

New iteration value for c_{pr} is

$$c_{pr} = c_{pr} + 0.5(\Delta c_{pr}) = 1175.796 \text{ J/(kg.K)}$$

The cycle is iterated until the specific heat for the section converges yielding the following solutions.

$$T_{r1} = 83.918 \text{ °C}$$

$$\eta = 0.8828$$

The change in the value of T_{r1} is monitored to determine if the value of T_{r2} should be moved up or down until T_{r1} converges.

$$\Delta T_{r1} = Tr_1 - T_{r1,old} = 83.918 - 84.12 = -0.202$$

The outlet water temperature of the condenser is calculated from

$$T_{l1} = T_{1,su} + \frac{Q}{m_l.c_{pl}} = 59.179 \text{ °C}$$

The condenser model is iterated until T_{r1} converges and all the area solutions are satisfied for the three regions (superheat, two-phase, subcool) on the refrigerant side. The solutions shown in Appendix A are found after convergence of the model.

B.2 Air-cooled evaporator

In this section sample calculations are conducted to show how the simulation operates for each of the two regions (two-phase and superheat) in the evaporator. The evaporator consists of eight tubes high and four rows deep. The evaporator is thus divided into 32 sections for the purpose of the calculations, with each section representing one tube. All the results shown below are for the last iteration of the evaporator simulation. The sample calculations is based on the geometry given in Table 5.1 and the following set of test conditions:

$$m_a = 0.72 \text{ kg/s}$$

$$T_{a,in} = 19.4 \text{ °C}$$

$$m_r = 0.00621 \text{ kg/s}$$

$$h_{su} = 121.004 \text{ kJ/kg}$$

$$dT_{sup} = 4.635 \text{ °C}$$

For the last iteration the estimated temperature at working point 8 is given by

$$T_{r8} = \frac{T_{r,\,top} + T_{r,\,bot}}{2} = \frac{7.454 + 6.903}{2} = 7.178\ °C$$

The superheat area is given by

$$A_{she} = f_{she}.A_{tot} = 0.0613(0.35814) = 0.02195\ m^2$$

Two-phase area is then the rest of the area

$$A_{tpe} = A_{tot} - A_{she} = 0.33619\ m^2$$

The total outside area of the evaporator is divided into n section.

$$n = r.k = 8(4) = 32$$

$$A_o[i] = A_{tot}/32 = m^2$$

The area is then divided to include the two-phase/superheat interface.

$$m = n + 1 = 32 + 1 = 33$$

After the calculations were performed it was found that the second area got divided into two areas to incorporate the two-phase/superheat interface.

$$A[2] = 0.01075\ m^2$$

$$A[3] = 0.00044\ m^2$$

The air mass flow rate is then determined for each of the 33 sections.

$$m_a[1] = m_{a,tot}.\frac{A[1]}{A_{tot}} = 0.72(\frac{0.01119}{0.35814}) = 0.022496\ kg/s$$

The pressures at the three main interfaces are determined and given by

$p_{r7} = 0.38305x10^6$ Pa	(Inlet of the evaporator)
$p_{r8} = 0.3773x10^6$ Pa	(Two-phase/superheat interface)
$p_{r9} = 0.37694x10^6$ Pa	(Outlet of evaporator)

The temperature at the inlet of the evaporator is calculated from the pressure.

$$T_{r7} = f(p_{r7}) = 7.621\ °C$$

The enthalpy at the two-phase/superheat interface is a function of the temperature

$$h_{r8} = f(T_{r8}) = 250.588\ kJ/kg$$

The temperature at the evaporator outlet is determined with the degree of superheat.

$$T_{r9} = T_{r8} + dT_{sup} = 11.813\ °C$$

The enthalpy at the outlet of the evaporator is a function of the pressure and temperature.

$$h_{r9} = f(p_{r9}, T_{r9}) = 254.931 \text{ kJ/kg}$$

Superheat region

In the superheat region the interface temperatures and enthalpies and new superheat area are determined. The calculations for the section at the outlet of the evaporator and the section at the superheat/two-phase interface will be shown. The calculations for the intermediate sections work the same as the section at the outlet of the evaporator. The simulation works backward from the outlet of the evaporator towards the inlet.

Section at evaporator outlet

To determine which tube's outlet air temperature is the inlet air temperature of this section the index is determined as follows.

$$i = 2.r = 2(8) = 16$$

Assign an estimated value to the refrigerant specific heat of the section.

$$c_{pr} = f(T_{r9}) = 938.114 \text{ J/(kg.K)}$$

The specific heat of the air is a function of the outlet air of the tube in front.

$$c_{pa} = f(T_{ae}[j+i] = f(T_{ae}[17]) = f(15.705) = 1005.33 \text{ J/(kg.K)}$$

Determine the minimum and maximum $(m.c_p)$ value for the refrigerant and the air.

$$(m.c_p)_{min} = m_r.c_{pr} = 0.00621(938.114) = 5.826$$

$$(m.c_p)_{max} = m_a\, c_{pa} = 0.0225(1005.33) = 22.62$$

The ratio of the minimum to the maximum value is

$$(m.c_p)_{ratio} = \frac{(m.c_p)_{min}}{(m.c_p)_{max}} = 0.258$$

The number of transfer units for the section is given by

$$NTU = \frac{U.A}{(m.c_p)_{min}} = \frac{219.95(0.01119)}{5.826} = 0.4226$$

The effectiveness for the crossflow layout of the section is determined by

$$\eta = 1 - e^{\frac{1-e^{-NTU.(m.c_p)_{ratio}}}{(m.c_p)_{ratio}}} = 0.33$$

The heat transfer is given by

$$Q = \frac{\eta.(m.c_p)_{min}}{1 - \frac{\eta.(m.c_p)_{min}}{m_r.c_{pr}}}.(T_{ae}[17] - T_{r9}) = 11.167 \text{ W}$$

The enthalpy at the inlet of the section is given by

$$h_{r,su} = h_{r9} - \frac{Q}{m_r} = 253.133 \text{ kJ/kg}$$

The temperature at the inlet of the section is a function of the pressure and the enthalpy

$$T_{r,su} = f(p_{r,su}, hr_{,su}) = f(0.3771\text{x}10^6, 253.133\text{x}10^3) = 9.895 \text{ °C}$$

The change in the specific heat is determined by

$$\Delta c_{pr} = abs(\frac{h_{r9} - h_{su}}{T_{r9} - T_{su}}) - c_{pr} = -0.719 \text{ J/(kg.K)}$$

Determine the error for the specific heat calculation

$$error = \frac{\Delta c_{pr}}{c_{pr}} = 0.000766$$

New iteration value for c_{pr} is

$$c_{pr} = c_{pr} + 0.5(\Delta c_{pr}) = 937.467 \text{ J/(kg.K)}$$

The routine is iterated until the specific heat value converges solving for the conditions at the inlet of the section. The outlet air temperature for the section of the dry coil is given by

$$T_{ae} = T_{ai} - \frac{Q}{m_a.c_{pa}} = 15.2117 \text{ °C}$$

Two-phase/superheat interface

For the last section in the superheat region the routine determines the size of the area to comply with the refrigerant properties.

The section has a fixed specific heat value.

$$c_{pr} = abs(\frac{h_{ex} - h_{r8}}{T_{ex} - T_{r8}}) = abs(\frac{253.133\text{x}10^3 - 250.587\text{x}10^3}{9.895 - 7.178}) = 936.946 \text{ J/(kg.K)}$$

The heat transfer is also fixed.

$$Q_{fixed} = m_r.(h_{ex} - h_{r8}) = 15.807 \text{ W}$$

Assign a value to the maximum and a minimum size that the area can be.

$$A_{top} = A_{tot} = 0.35814 \text{ m}^2$$

$$A_{bot} = 0$$

The first estimated value for the area is

$$A = \frac{A_{top} + A_{bot}}{2} = 0.17907 \text{ m}^2$$

The air mass flow rate for the section is determined by

$$m_a = m_{a,tot}.\frac{A}{A_{tot}} = 0.36 \text{ kg/s}$$

Determine the minimum and maximum $(m.c_p)$ value for the refrigerant and the air.

$$(m.c_p)_{min} = m_r.c_{pr} = 0.00621(936.946) = 5.818$$

$$(m.c_p)_{max} = m_a.c_{pa} = 0.36(1005.33) = 361.919$$

The ratio of the minimum to the maximum value is

$$(m.c_p)_{ratio} = \frac{(m.c_p)_{min}}{(m.c_p)_{max}} = 0.0161$$

The number of transfer units for the section is given by

$$NTU = \frac{U.A}{(m.c_p)_{min}} = 0.4066$$

The effectiveness for the crossflow layout of the section is determined by

$$\eta = 1 - e^{\frac{1-e^{-NTU.(m.c_p)_{ratio}}}{(m.c_p)_{ratio}}} = 0.9984$$

The heat transfer is given by

$$Q = \frac{\eta.(m.c_p)_{min}}{1 - \frac{\eta.(m.c_p)_{min}}{m_r.c_{pr}}}.(T_{ae}[j+i] - T[j]) = 20622.214 \text{ W}$$

The change in the heat transfer is determined by

$$\Delta Q = Q - Q_{fixed} = 20606.407 \text{ W}$$

If ΔQ is greater than zero the maximum area (A_{top}) is assigned the value of A, else A_{bot} is assigned the value of A. An error value monitors the convergence of the heat transfer.

$$\text{error} = \frac{\Delta Q}{Q} = 0.999$$

The routine is iterated until the heat transfer converges and the correct area is then obtained.

$$A = 0.01067 \text{ m}^2$$

Two-phase region

The calculations for the area at the two-phase/superheat interface are shown below as well as the calculations at the inlet section of the evaporator from the capillary tube.

Two-phase/superheat interface

The routine starts by assigning an estimated value to the refrigerant specific heat of the section.

$$c_{pr} = abs(\frac{h_{r8} - h_{r7}}{T_{r8} - T_{r7}}) = abs(\frac{250.587x10^3 - 121.004x10^3}{7.178 - 7.621}) = 293060.05 \text{ J/(kg.K)}$$

Determine the minimum and maximum $(m.c_p)$ value for the refrigerant and the air.

$$(m.c_p)_{min} = m_a.c_{pa} = 0.000879(1005.33) = 0.8836$$

$$(m.c_p)_{max} = m_r.c_{pr} = 0.00621(293060.05) = 1819.903$$

The ratio of the minimum to the maximum value is

$$(m.c_p)_{ratio} = \frac{(m.c_p)_{min}}{(m.c_p)_{max}} = 0.000486$$

The refrigerant inlet temperature for the section is a function of the pressure.

$$T_{su} = f(p_{su}) = f(377.3115x10^3) = 7.179 \text{ °C}$$

The number of transfer units for the section is given by

$$NTU = \frac{U.A}{(m.c_p)_{min}} = 0.1237$$

The effectiveness for the crossflow layout of the section is determined by

$$\eta = \frac{1 - e^{-(m.c_p)_{ratio}.(1-e^{-NTU})}}{(m.c_p)_{ratio}} = 0.1163$$

The maximum heat transfer for the section is given by

$$Q_{max} = (m.c_p)_{min}.(T_{ae}[j+i] - T_{r8}) = 0.8836(15.704 - 7.178) = 7.533 \text{ W}$$

The heat transfer is calculated with the aid of the maximum heat transfer

$$Q = \eta.Q_{max} = 0.8765 \text{ W}$$

The enthalpy at the inlet of the section is given by

$$h_{su} = h_{r8} - \frac{Q}{m_r} = 250.446 \text{ kJ/kg}$$

The change in the specific heat is determined by

$$\Delta c_{pr} = abs(\frac{h_{r8} - h_{su}}{T_{r8} - T_{su}}) - c_{pr} = -71565.474 \text{ J/(kg.K)}$$

Determine the error for the specific heat calculation

$$error = \frac{\Delta c_{pr}}{c_{pr}} = 0.244$$

New iteration value for c_{pr} is

$$c_{pr} = c_{pr} + 0.5(\Delta c_{pr}) = 235807.671 \text{ J/(kg.K)}$$

The routine is iterated until the specific heat value converges resulting in the following solutions:

$Q = 0.8765$ W

$h_{su} = 250.446$ kJ/kg

Inlet section of the evaporator

The routine starts by assigning an estimated value to the refrigerant specific heat of the section. The value is equal to the specific heat of the previous section.

$c_{pr} = 509430.143$ J/(kg.K)

Determine the minimum and maximum ($m.c_p$) value for the refrigerant and the air.

$(m.c_p)_{min} = m_a.c_{pa} = 0.0225(1005.473) = 22.623$

$(m.c_p)_{max} = m_r.c_{pr} = 0.00621(509430.143) = 3163.561$

The ratio of the minimum to the maximum value is

$$(m.c_p)_{ratio} = \frac{(m.c_p)_{min}}{(m.c_p)_{max}} = 0.00715$$

The refrigerant inlet temperature for the section is a function of the pressure

$T_{su} = f(p_{su}) = f(383.053x10^3) = 7.621$ °C

The number of transfer units for the section with area equal to $0.01119m^2$ is given by

$$NTU = \frac{U.A}{(m.c_p)_{min}} = 0.1237$$

The effectiveness for the crossflow layout of the section is determined by

$$\eta = \frac{1 - e^{-(m.c_p)_{ratio}.(1-e^{-NTU})}}{(m.c_p)_{ratio}} = 0.1163$$

The maximum heat transfer for the section is given by

$Q_{max} = (m.c_p)_{min}.(T_{ai} - T_{su}) = 22.623(19.4 - 7.6114) = 266.694$ W

The heat transfer is calculated with the aid of the maximum heat transfer

$Q = \eta.Q_{max} = 31.013$ W

The enthalpy at the inlet of the section is given by

$$h_{r7} = h_{ex} - \frac{Q}{m_r} = 125.995x10^3 - \frac{31.013}{0.00621} = 121.001 \text{ kJ/kg}$$

The change in the specific heat is determined by

$$\Delta c_{pr} = abs(\frac{h_{ex} - h_{r7}}{T_{ex} - T_{r7}}) - c_{pr} = 34407.051 \text{ J/(kg.K)}$$

Determine the error for the specific heat calculation

$$\text{error} = \frac{\Delta c_{pr}}{c_{pr}} = 0.0675$$

New iteration value for c_{pr} is

$$c_{pr} = c_{pr} + 0.5(\Delta c_{pr}) = 536955.784 \text{ J/(kg.K)}$$

The routine is iterated until the specific heat value converges resulting in the following solutions:

$$Q = 31.014 \text{ W}$$

$$h_{su} = 121.0007 \text{ kJ/kg}$$

The change in the enthalpy at working point 7 is monitored to determine if the estimated temperature value at working point 8 should increase or decrease.

$$\Delta h = h_{r7,fixed} - h_{r7,new} = 121.0041 - 121.0007 = 0.0034 \text{ kJ/kg}$$

If Δh is positive the temperature at working point 8 is moved down. The evaporator model is iterated until the enthalpy at the inlet of the evaporator converges and the areas in the two-phase and superheat region are also satisfied.

B.3 Reciprocating compressor

Inlet conditions

$$T_{su} = 16.528 \text{ °C}$$

$$p_{su} = 4.206 \text{ MPa}$$

$$p_{ex} = 1.3775 \text{ MPa}$$

The inlet to the compressor is in the superheat region, thus the inlet properties are a function of the temperature and pressure.

Inlet specific volume

$$v_{su} = f(p_{su}, T_{su}) = 0.0501 \text{ m}^3\text{/kg}$$

Inlet enthalpy

$$h_{su} = f(p_{su}, T_{su}) = 258.167 \text{ kJ/kg}$$

Inlet entropy

$$s_{su} = f(p_{su}, T_{su}) = 0.9307 \text{ kJ/kg}$$

Make an assumption that the process is isentropic in order to obtain the outlet conditions, thus

$$s_{ex,s} = s_{su} = 0.937 \text{ kJ/kg}$$

Determine isentropic outlet conditions

Outlet temperature

$$T_{ex} = f(p_{ex}, s_{ex,s}) = 61.8085\ °C$$

Outlet enthalpy

$$h_{ex,s} = f(p_{ex}, s_{ex,s}) = 283.6555\ kJ/kg$$

Outlet specific volume

$$\nu_{ex} = f(p_{ex}, s_{ex,s}) = 0.0154\ m^3/kg$$

Isentropic work is given by

$$Ws = h_{ex,s} - h_{su} = 25.4883\ kJ/kg$$

Assume that the outlet enthalpy is equal to the isentropic enthalpy.

$$h_{ex} = h_{ex,s} = 283.6555\ kJ/kg$$

Efficiency is determined by

$$\eta = -0.073386\left(\frac{\nu_{su}}{\nu_{ex}}\right)^2 + 0.514421\left(\frac{\nu_{su}}{\nu_{ex}}\right) - 0.334602 = 0.5621$$

Volume flow is determined by

$$\dot{q} = -1.421386x10^{-4}\left(\frac{\nu_{su}}{\nu_{ex}}\right) + 7.772138x10^{-4} = 0.3153x10^{-3}\ m^3/s$$

Mass flow rate of the refrigerant is given by

$$m_r = \frac{\dot{q}}{v_{su}} = 0.006296\ kg/s$$

Compressor work on the refrigerant

$$Wcp = m_r\left(\frac{Ws}{\eta}\right) = 285.4675\ W$$

The change in outlet enthalpy is determined by

$$dh_{ex} = \frac{Wcp}{m_r} + h_{su} - h_{ex} = 19.8557\ kJ/kg$$

New outlet enthalpy is now calculated with

$$h_{ex} = h_{ex} + (\text{relaxation parameter}).dh_{ex}$$
$$= h_{ex} + 0.8(dh_{ex})$$
$$= 299.5401\ kJ/kg$$

The outlet conditions of the compressor can now be calculated with the pressure and the new enthalpy.

Outlet temperature

$T_{ex} = f(p_{ex}, h_{ex}) = 75.01$ °C

Outlet specific volume

$v_{ex} = f(p_{ex}, h_{ex}) = 0.0169$ m^3/kg

Outlet entropy

$s_{ex} = f(p_{ex}, h_{ex}) = 977.9298$ kJ/kg

The simulation is iterated until convergence of enthalpy is reached thus yielding the outlet condition of the compressor as shown in Appendix A.

B.4 Capillary tube

Dimensionless Correlation of Bittle et al. (1998)

Capillary tube geometry

$d_c = 0.001778$ m

$L = 1.5$ m

Supply conditions

$T_{su} = 48.076$ °C

$p_{in} = 1.3254$ MPa

$\Delta T_{sc} = 2.144$ °C

Enthalpy of the liquid at the inlet

$h_f = f(T_{su}) = 117.2703$ kJ/kg

Enthalpy of the vapour at the inlet

$h_g = f(T_{su}) = 270.195$ kJ/kg

Enthalpy at the inlet

$h_{fg} = h_g - h_f = 152.9247$ kJ/kg

Liquid specific volume at the inlet

$v_f = f(T_{su}) = 0.899 \times 10^{-3}$ m^3/kg

Vapour specific volume at the inlet

$$v_g = f(T_{su}) = 0.0158\ m^3/kg$$

Liquid viscosity at the inlet

$$\mu_f = f(T_{su}) = 0.1616x10^{-3}\ kg/(s.m)$$

Vapour viscosity at the inlet

$$\mu_g = f(T_{su}) = 13.6761x10^{-6}\ kg/(s.m)$$

Specific heat

$$c_p = f(T_{su}) = 1553.608\ J/kg.K$$

Dimensionless parameters

$$\Pi_1 = \frac{L_c}{d_c} \quad \text{(Geometry)}$$

$$= 843.6445$$

$$\Pi_2 = \frac{d_c{}^2.h_{fg}}{v_f{}^2.\mu_f{}^2} \quad \text{(Vaporisation)}$$

$$= 22.9088x10^{12}$$

$$\Pi_4 = \frac{d_c{}^2.P_{in}}{v_f.\mu_f{}^2} \quad \text{(Inlet pressure)}$$

$$= 178.5396x10^{9}$$

$$\Pi_5 = \frac{d_c{}^2.c_{pf}.\Delta T_{sc}}{v_f{}^2.\mu_f{}^2} \quad \text{(Subcool inlet condition)}$$

$$= 498.9895x10^{9}$$

$$\Pi_6 = \frac{v_g}{v_f} \quad \text{(Density)}$$

$$= 17.6013$$

$$\Pi_7 = \frac{\mu_f - \mu_g}{\mu_g} \quad \text{(Viscosity)}$$

$$= 10.8126$$

Determine the mass flow rate

$$\dot{m}_r = d_c.\mu_f.(1.893\Pi_4{}^{1.369}\Pi_1{}^{-0.484}\Pi_5{}^{0.019}\Pi_2{}^{-0.824}\Pi_6{}^{0.773}\Pi_7{}^{0.265})$$

$$= 0.007324\ kg/s$$

The mass flow rate determined by the capillary tube model can now be compared to the mass flow rate determined by the compressor model. In the complete heat pump cycle the routine is iterated until both mass flow rates converges to the same value.